Titre: Title:	Shaft straightness and concentricity in process correction
Auteur: Author:	Acher-Igal Abenhaim
Date:	2004
Type:	Mémoire ou thèse / Dissertation or Thesis
Référence: Citation:	Abenhaim, A.-I. (2004). Shaft straightness and concentricity in process correction [Master's thesis, École Polytechnique de Montréal]. PolyPublie. https://publications.polymtl.ca/7858/

UNIVERSITÉ DE MONTRÉAL

SHAFT STRAIGHTNESS AND CONCENTRICITY IN PROCESS CORRECTION

ACHER-IGAL ABENHAIM
DÉPARTEMENT DE GÉNIE MÉCANIQUE
ÉCOLE POLYTECHNIQUE DE MONTRÉAL

MÉMOIRE PRÉSENTÉ EN VUE DE L'OBTENTION
DU DIPLÔME DE MAÎTRISE ÈS SCIENCES APPLIQUÉES
(GÉNIE MÉCANIQUE)
DÉCEMBRE 2004

Your file Votre référence
ISBN: 978-0-494-19272-6
Our file Notre référence
ISBN: 978-0-494-19272-6

UNIVERSITÉ DE MONTRÉAL

ÉCOLE POLYTECHNIQUE DE MONTRÉAL

Ce mémoire intitulé:

SHAFT STRAIGHTNESS AND CONCENTRICITY IN PROCESS CORRECTION

présenté par: ABENHAIM Acher-Igal

en vue de l'obtention du diplôme de: Maîtrise ès sciences appliquées

a été dûment acceptée par le jury d'examen constitué de:

M. FORTIN Clément, Ph.D., président

M. BALAZINSKI Marek, Ph.D., membre et directeur de recherche

M. SASU Ioan, Ph.D., membre et codirecteur de recherche

M. MAYER René, Ph.D. membre

Acknowledgments

First I'd like to express my gratitude to my codirector Ioan Sasu from Pratt and Whitney Canada for the chance he gave me to participate in this project. I would like to thank him also for all of his inputs in the technical parts of the projects as well as solving all the other challenges I found along the way. Basically, this project wouldn't have been possible without his participation, passion and patience.

I would also like to thank my director Marek Balazinski for helping out throughout the project and for insuring that this experience was as educating as it was.

Special thanks to everybody from NRC and Pratt & Whitney Canada for all their help, especially to Claude Perron, Iraj Mantegh, Simon Larose from NRC for their partnership in most of this projects and to Glyn Richards, Isabelle Bacon and Nihad Ben Salah from PWC for their technical input in the project.

I am also very thankful to my colleagues, Roberto Grassi and Maruius Petean for all the good times and knowledge shared during our studies together.

Last but not least I'd like to thank my parents Lilianne and Henry, my brothers, my sister Ilana, my best friend Gregory Dahan and my girlfriend Cynthia Strich for all their patience, support and encouragements.

Résumé

Ce mémoire traite de la correction de la concentricité et de la rectitude des arbres de turbomoteurs produits par Pratt & Whitney Canada. Les objectifs du projet sont de réduire le coût de fabrication des arbres des turbomoteurs, en corrigeant les erreurs de concentricité et de rectitude. La réduction du coût résulte du soulagement des tolérances serrées sur les opérations coûteuses et de l'amélioration de la qualité.

Le redressage ajouté à la correction de concentricité déjà utilisée à PWC consiste en la solution étudiée pour corriger les erreurs de forme des arbres. Ce processus de redressage pourrait être facilement contrôlable et n'affectera pas les propriétés de l'arbre en s'assurant que l'arbre pourra supporter les charges nécessaires.

Le mémoire débute par la revue bibliographique dans laquelle sont exposés les différents principes et équipements existants capables de redresser les arbres. La section traitant de la pertinence du projet énonce les différents types d'erreurs de forme, leur provenance et les coûts qu'ils génèrent. De plus, les méthodes et principes du redressage par déformation plastique créé par presse et du redressage par contraintes résiduelles y sont expliqués.

Pour le redressage par presse, un modèle d'éléments finis a aidé au développement d'un prototype. Les essais effectués avec le CNRC sur le prototype sont en concordance avec les résultats du modèle d'éléments finis.

Pour le redressage par contrainte résiduelle, un premier équipement développé est le redressage par grenaillage ultrason. Les essais effectués avec le CNRC ont prouvés que la déflection permanente créée est suffisante pour redresser des arbres, que la circularité et la rugosité de la section grenaillée sont dégradées, et que le procédé est contrôlable,

parce qu'un arbre ayant un battement initial de 0.007", a été redressé à un battement en dessous de 0.001".

Une étude fut débutée sur un autre équipement de redressage par contraintes résiduelles, le redressage par brunissage. Pour le redressage par brunissage, un prototype aussi bien qu'un modèle d'éléments finis devrait être mis sur pied. Des essais semblables à ceux du redressage par presse et par grenaillage devraient être effectués.

Le procédé de redressage idéal serait une combinaison du redressage par presse et du redressage par grenaillage. Le redressage par presse pourrait être utilisé seulement en début du procédé en raison de la contrainte résiduelle en tension qu'il génère. Le redressage par grenaillage pourrait être employé sur l'arbre fini pour raffiner le redressage.

Abstract

This thesis treats the correction of concentricity and straightness errors of turbine engine shafts produced by Pratt & Whitney Canada. The objectives of the project are to reduce the manufacturing cost of the turbo shafts engine by correcting concentricity and straightness shape errors. The cost reduction results from relieving the tight tolerances on costly operation, as well as improving the quality.

The straightening added to the correction of concentricity already used at PWC consists of the solution studied to correct the shaft shape errors. This process could be easily controlled and will not affect the properties of the shaft and insure that it will be able to support the necessary loads.

The thesis begins with the bibliographical review in which are exposed the various principles and existing equipment able to straighten shafts. In the section stating the project relevance, the various types of errors of form are defined as well as their source and the costs which they generate. The methods and principles of the straightening by plastic deformation created by a press and of straightening by inducing residual stresses are explained.

For straightening by a press, a finite element model helped with the development of a prototype. The tests carried out at the CNRC on the prototype are in agreement with the finite element results.

For the straightening by residual stress, the first developed equipment is the straightening by ultrasound peening. Tests carried out at the CNRC proved that the permanent deflection created is sufficient to straighten shafts, that the circularity and the roughness of the peenend section are degraded and that the process is controllable because an initially eccentric shaft of 0.007" of runout was straightened to a runout below 0.001".

A study was begun on another equipment of straightening by residual stress, straightening by burnishing. For the straightening by burnishing, a prototype as well a finite element model should be developed. Tests similar to those done on the straightening by press and by peening should be carried out.

The optimum straightening process would be a combination of the straightening by a press and the straightening by peening. The straightening by a press could be used only at the beginning of the process because of the residual stress in tension that it generates. The straightening by peening could be employed on the finished shaft to refine the straightening.

Condensé en français

Introduction

La plupart des avions modernes sont propulsés par des turbomoteurs qui ont été développés pendant la deuxième guerre mondiale par Sir Frank Whittles et Dr. Hans Von Ohain. Il y a deux principaux types de turbomoteurs produits par Pratt et Whitney Canada (PWC) : les turbosoufflantes et les turbopropulseurs.

L'arbre est la pièce centrale du moteur couplant les turbines de basses pressions avec la soufflante, pour une turbosoufflante, ou le propulseur, pour un turbopropulseur. Par conséquent, l'arbre est soumis à de la torsion et ce à hautes vitesses de rotation et à des températures élevées. En raison de sa vitesse de rotation élevée, n'importe quelle masse non équilibrée peut créer des vibrations inacceptables et donc réduire les performances du moteur, augmenter le bruit et diminuer la vie des roulements.

Pour éviter d'avoir un arbre non équilibré, les mesures prises sont de réduire la tolérance sur l'épaisseur des parois et la tolérance de battement sur le diamètre extérieur. Ceci est équivalent à réduire la tolérance de rectitude sur les diamètres intérieurs et extérieurs ainsi que réduire la tolérance de concentricité entre ces diamètres. De plus, un processus d'équilibrage à grande vitesse est réalisé pour limiter l'effet du déséquilibre, car même en améliorant la fabrication, les arbres fléchissent à grande vitesse.

Auparavant, la fabrication de ces arbres a été optimisée pour rencontrer les tolérances géométriques en employant des têtes plus stables pour le foret. Puisque la tolérance sur l'épaisseur de la paroi devient de plus en plus réduite, la compagnie est confrontée à trouver de nouvelles solutions. Une solution consiste en l'ajout d'une cellule de correction de ces erreurs dans le procédé de fabrication des arbres.

Une première étape de correction, déjà dans le procédé de PWC, est de corriger l'excentricité du trou en rectifiant les références extérieures pour les aligner avec une droite des moindres carrés passant par le centre du trou des sections mesurées. La deuxième étape, qui est au cœur de ce mémoire, consiste en la correction de la rectitude de l'arbre en le redressant par pliage. Deux méthodes sont proposées pour plier les arbres : la flexion en trois points ou le formage par grenaillage.

Pour comprendre et prévoir l'effet du redressage sur les propriétés de l'arbre, un modèle d'éléments finis a été développé pour le redressage par flexion et une recherche intensive sur le processus de grenaillage a été faite. Une recherche sur les équipements existants a donné un bon point de départ pour le développement du prototype d'équipement de redressage par presse et du prototype d'équipement de redressage par grenaillage. Ces prototypes ont été utilisés dans les expériences faites au CNRC.

Revue bibliographique

Les sites Nasa Glenn Research Center [1] et Pratt & Whitney U.S. [2] donnent une bonne vue d'ensemble du fonctionnement des turbomoteurs. La turbosoufflante et le turbopropulseur qui représentent 82 % des moteurs produits à PWC y sont brièvement expliqués.

Pour la turbosoufflante, le processus de propulsion commence par la soufflante à l'avant du moteur qui absorbe un grand volume d'air et le sépare dans deux jets. Le premier, en général 85 % du volume d'air total, est orienté vers le canal de dérivation annulaire et constitue l'essentiel de la poussée. Le reste est comprimé et envoyé dans la chambre de combustion. Les gaz font tourner le premier étage de turbine qui mène le compresseur, ainsi que le second qui mène la soufflante. Les gaz chauds s'échappent ensuite par la tuyère d'éjection. Le turbopropulseur incorpore les mêmes concepts de base et technologie que la turbosoufflante avec l'hélice qui remplace la soufflante.

Un vaste nombre d'articles sur les différents types de forage de trous profonds indiquent que le forage, utilisé par PWC, est bien la méthode la plus appropriée pour faire des trous longs de faibles diamètres. P. Rudd et L. Hetherington [3] expliquent les différents types de processus de forage de trous profonds. J.-H. Chin, C.-T. Hsieh et de L.-W. LEE [4] ont établi un modèle qui étudie le comportement dynamique de l'arbre pendant le forage de trous profonds. Cet article montre comment les efforts en bout d'outil créent des erreurs de formes proportionnelles à la profondeur du trou.

Une étude effectuée sur les équipements existants a indiqué comment le marché international a attaqué la correction des erreurs de forme et comment leurs équipements fonctionnent. Après cette vaste recherche sur les équipements existants utilisés pour redresser les arbres, les résultats montrent que deux types d'équipements sont employés sur le marché : redressage par rouleaux et redressage par presse.

Le redressage par rouleaux est surtout employé pour des pièces de volume élevé avec un diamètre extérieur presque constant. Le redressage par presse est plus approprié pour le redressage des arbres de turbine à gaz. Les compagnies Eitel Presses, Galdabini, Savage Industries et Kokusai ont développé des équipements de redressage par presse. Leur fonctionnement est simple (Figure I): l'arbre (1) est maintenu entre les centres (2), le battement est mesuré (3) pour déterminer le point le plus élevé. Ce point est tourné vers le haut et la presse (4) force l'arbre contre les appuis (5) et le libère. Ce processus continue jusqu'à ce que le battement soit selon les spécifications désirées.

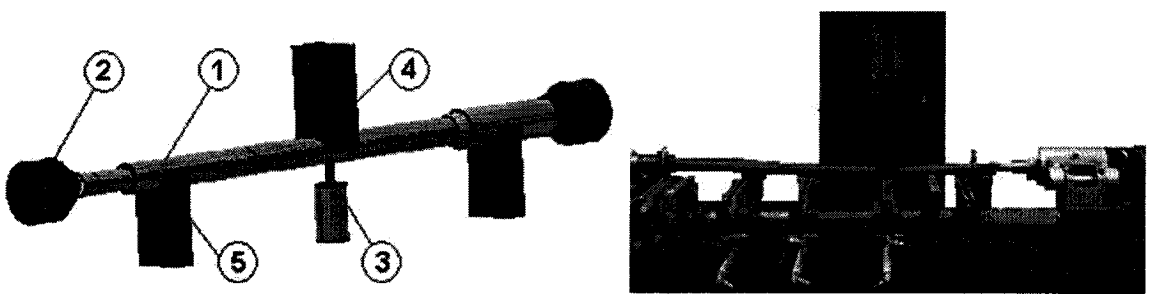

Figure I Redressage par presse de Eitel Presses [9]

Un système de commande de redressage optimisé pour le diamètre extérieur des arbres a été développé par S.-C. Kim et S.-C. Chung (2000) [10]. La déflexion permanente est calculée pendant le chargement à l'aide de la courbe de la déflexion en fonction de la charge. Un contrôleur calcule les commandes de redressage optimales par l'analyse de l'ordre de la courbure à corriger, ainsi que de la valeur et direction de la déflexion maximum. Ces commandes qui sont le point de redressage, la direction, la déflexion permanente et les conditions de support sont choisies avec l'utilisation des rapports de déflexion. Ce rapport de déflexion qui est calculé en quelques points est la déflexion du point divisé par la déflexion du point de redressage. Quatre-vingt barres de support ont été mesurées et redressées en dedans de 30 μm de tolérance de rectitude.

Jack Champaigne (2001) [29] et K. Lida [25] décrivent la formation de la région déformée par le grenaillage et le profil typique de la contrainte résiduelle en compression. H. O. Fuchs et E. R. Hutchinson [28] et George Leghorn (1957) [31], expliquent la notation d'intensité d'Almen qui consiste en une mesure de l'arc créée par le grenaillage d'une bande d'acier normalisée. H. O. Fuchs et E. R. Hutchinson [28] donnent une méthode pour calculer la force sur la surface en fonction de la mesure d'arc d'Almen. S. Kittel, W. Linnemann, F. Wustefeld, R. Kopp [26] ont construit un équipement de formage par grenaillage pour du métal en feuille.

Paul S. Prevéy[23] a développé un procédé de brunissage (Figure II) générant une couche de contrainte résiduelle en compression avec un minimum de déformation plastique.

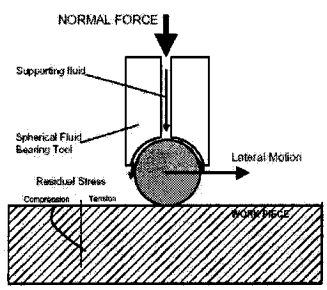

Figure II brunissage [23]

Objectives et pertinence

Les objectifs de ce projet sont :

1) réduire le coût de fabrication d'arbres des turbomoteurs en éliminant les rejets causés par les erreurs de concentricité et de rectitude, ainsi qu'en augmentant les tolérances serrées sur les opérations coûteuses comme le perçage et le meulage.

2) améliorer la qualité en ayant un contrôle sur la rectitude des arbres.

L'hypothèse est que le processus de redressage ajouté à la correction de concentricité déjà utilisée à PWC réduirait les coûts de fabrication et améliorera la qualité des arbres des turbomoteurs. Ce processus de redressage pourrait être facilement contrôlable et n'affectera pas les propriétés de l'arbre en s'assurant que l'arbre pourra supporter les charges nécessaires.

Types d'erreurs de forme

Il y a trois types d'erreurs de forme qui peuvent être identifiées. La concentricité et les erreurs de rectitude sont principalement vues dans le processus de forage et l'erreur de battement serait créée par le tournage, le meulage ou par le procédé de relaxation de contraintes.

La concentricité d'un trou est le diamètre d'un cylindre, centré sur l'axe de rotation, dans lequel l'axe du trou est contenu. L'erreur de concentricité est actuellement corrigé chez Pratt et Whitney Canada en rectifiant les références extérieures pour les aligner avec une droite des moindres carrés passant par le centre du trou des sections mesurées.

La rectitude d'un trou est le diamètre du cylindre dans lequel l'axe du trou est contenu et le battement est la variation mesurée par un capteur posé sur la surface du diamètre à mesurer, pendant un tour autour de l'axe de rotation. Ces types d'erreur ne sont pas actuellement corrigés chez PWC, et sont au cœur de ce projet.

Cause d'erreurs de forme

Le processus de fabrication employé pour faire le diamètre intérieur est le forage. Il est très difficile de forer des pièces avec un grand rapport longueur/diamètre parce que le bout de l'outil n'est pas restreint. Ceci cause la force d'usinage de déplacer le bout de l'outil et de créer des erreurs d'excentricité et de rectitude.

Même après les opérations de forage, une erreur de forme peut se produire pendant le meulage ou le tournage du diamètre extérieur. Pendant les opérations de tournage, l'arbre est soumis aux forces de machinage et pourrait donc se déformer. De plus, ces opérations d'usinage laisse des contraintes résiduelles sur la surface et peuvent déformer l'arbre.

Étude de capabilité de procédé

Puisque la certification des processus devient importante chez PWC, la première étape du projet était d'étudier les possibilités de la fabrication des arbres. Cette étude est basée sur les méthodes de calcul d'un index de capabilité pour les tolérances géométriques et dimensionnelles (GD&T) exposées par les deux articles suivants et calculées par Minitab [7]. D. P. Karl, J. Morisette et W. Taam [5] proposent d'employer Cpk (Équation I) d'une distribution de Wiebul parce qu'il y a seulement une limite supérieure et que les valeurs sont toujours positives. M. Pillet, S. Rochon, et E. Duclos [6] proposent l'utilisation d'une généralisation de l'index de C_{PM} (Équation II) pour la distribution unilatérale.

$$C_{pk} = C_{pu} = \frac{USL - X_{0.50}}{X_{0.99875} - X_{0.50}}$$

Équation I

$$C_{pm} = \frac{USL - T}{\frac{toler}{2} \times \sqrt{\frac{\sum_{i=1}^{n}(X_i - T)^2}{n-1}}}$$

Équation II

Où:

USL = Limite de spécification supérieure
$X_{0.05}$ = 50ième percentile
$X_{0.99875}$ = 99.875ième percentile
T = Valeur cible
Toler = Tolérance sigma, Minitab utilise 6

En utilisant les index de capabilité proposés, Cpk et C_{PM}, une étude de capabilité de procédé a été faite sur la forme des arbres complexes produits par PWC entre 1999 et 2003. La dimension étudiée est le battement mesuré par ultrasons, au fond du trou foré. Les résultats (Table I), en dessous de la limite de 1.33, montrent qu'il y a des problèmes de qualité, et ce, surtout pour le PW500 pour lequel les index sont environ 0.5.

Tableau I Étude de capabilité de procédé sur la forme des arbres complexes

	jt15	pw100	pw150	pw308	pw500
Cpm	1.04	1.25			
Cpk		1.18			

Cp > 1.33
1 < Cp < 1.33
Cp < 1

Coûts des erreurs de forme

Plusieurs coûts de fabrication peuvent être associés aux erreurs de forme. Le plus évident est celui généré par les rejets. Un autre est le coût de fabrication pour obtenir les tolérances très serrées demandées par le dessin.

Pendant les dernières années, de l'argent a été investi pour améliorer la rectitude des axes en améliorant le processus de fabrication. Le foret a été amélioré en investissant dans la conception de têtes de foret plus stables. De plus, l'utilisation de la correction de concentricité a amélioré de manière significative la concentricité entre les diamètres extérieurs et intérieurs. Le meulage, qui est une opération coûteuse, est également une forme de correction des erreurs de battements du diamètre extérieur. Finalement l'équilibrage à haute vitesse permet de réduire la déflexion créée par la masse excentrique que génèrent les erreurs de forme.

Redressage : méthodes et principes

La différence majeure entre le processus de fabrication des arbres chez PWC (Figure IIIa) et ceux de sa compétition (Figure IIIb), est que le redressage utilisé par la compétition à plusieurs étapes du procédé et ce pour un total de six fois. Le procédé proposé illustré à la Figure IIIc, consiste à tirer profit des deux procédés, le recentrage et le redressage.

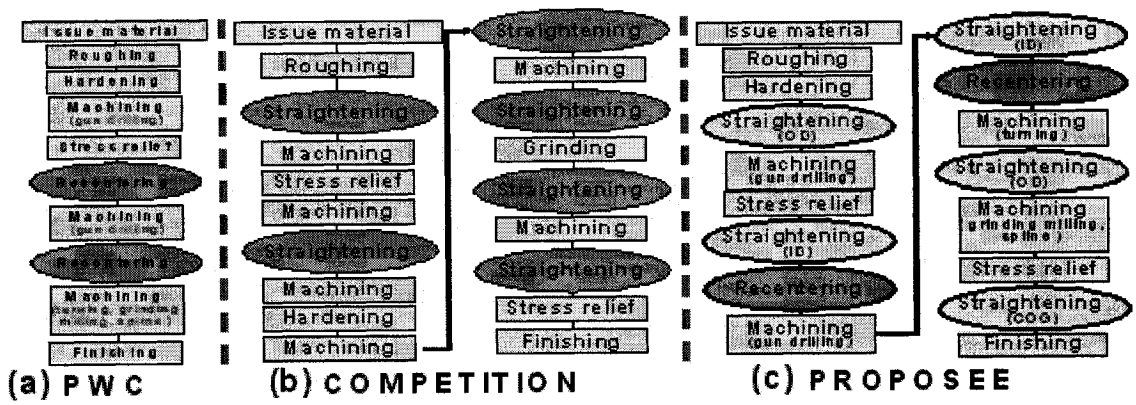

Figure III (a)Procédé de fabrication de PWC, (b) compétition, (c) proposée.

Le processus de recentrage a été inclus dans le processus de PWC à la fin des années 90. Le processus consiste en :

(a) Mesurer l'excentricité de diamètre interne de l'arbre par rapport au diamètre externe.

(b) Une ligne des moindres carrés est calculée à travers les excentricités mesurées.

(c) Le programme renvoie la position de nouvelles références d'usinage pour que l'axe du diamètre externe (OD) coïncide avec la ligne calculée en (b)

(d) L'OD est alors usiné pour suivre la ligne des moindres carrés .

Le résultat final est que l'axe de l'OD coïncide avec la ligne des moindres carrés. Ceci réduit donc l'excentricité entre le diamètre interne et externe.

Le procédé proposé utilise le recentrage ainsi que les trois différents redressages suivants:

1- Le redressage du diamètre extérieur (OD) utilisé après le dégrossissage, permet d'enlever plus de matériel à l'opération de dégrossissage puisque moins de matériel doit être laissé pour le processus de recentrage. Utilisé avant le meulage, il permet de soulager le processus de meulage parce que le battement du diamètre extérieur sera plus près de sa tolérance.

2- Le redressage du diamètre intérieur (ID) est employé ainsi que le recentrage pour s'assurer que les diamètres sont concentriques.

3- Le redressage du centre de gravité (COG) est employé à la fin de la fabrication de l'arbre pour s'assurer que le centre de gravité de chaque section mesurée est sur l'axe de rotation de l'arbre.

Principe du redressage par déformation plastique induite par flexion

Pour le redressage par déformation plastique induite par flexion, la pièce est soutenue entre 2 points et une pression (P) est appliquée en un troisième point. Pour créer une déflexion permanente et donc plastifier l'arbre, la contrainte ($\sigma_{a,b}$) doit être plus élevé que la limite d'élasticité (Se) (à ne pas être confondu avec la limite d'écoulement Sy à laquelle il y aurait déjà 0.2 % d'élongation plastique). La région plastifiée de l'arbre est bornée par les courbes des Équations III et IV et la région plastifiée est illustrée à la Figure IV.

$$Se = \sigma_a = \frac{P \times b \times x \times y}{2 \times L \times I} \qquad 0 < x < a \qquad \textit{Équation III}$$

$$Se = \sigma_b = \frac{P \times a \times (L - x) \times y}{2 \times L \times I} \qquad a < x < L \qquad \textit{Équation IV}$$

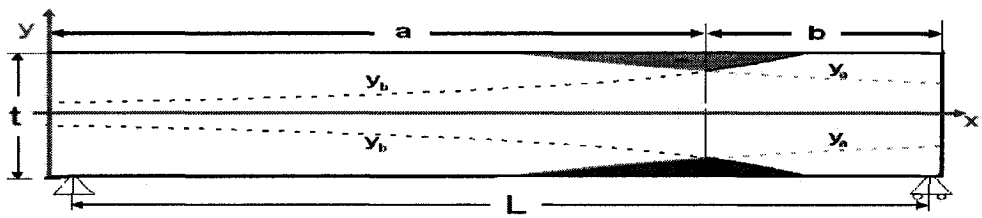

Figure IV Région plastifiée par la flexion 3 points

Principe du redressage par contraintes résiduelles induites par grenaillage

Le grenaillage crée une contrainte résiduelle en compression sur une couche mince à la surface de la région grenaillée. Cette contrainte résiduelle crée un moment fléchissant qui fléchit l'arbre pour lui donner une déflexion permanente. La Figure V illustre les contraintes résiduelles pour un arbre redressé par grenaillage.

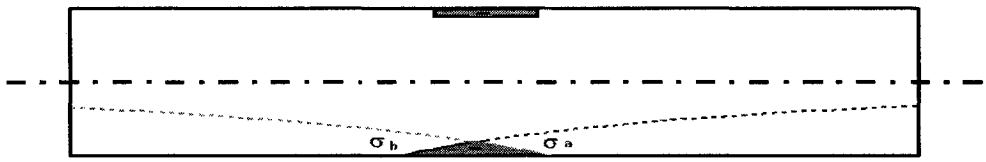

Figure V Contraintes résiduelles générées après le redressage par grenaillages

L'avantage évident du redressage par grenaillage est qu'il ne génère que des contraintes résiduelles en compression tandis que le redressage par flexion génère des contraintes résiduelles en traction, ce qui affaiblit l'arbre.

Analyse et amélioration d'équipement de redressage d'arbres par presse

Pour pouvoir optimiser les équipements existants, un modèle éléments finis a été développé pour simuler le processus de redressage par presse.

La pièce modélisée est un arbre de turbomoteur après que son deuxième trou a été foré. Les appuis (Figure VIa) sont modélisés par des surfaces de contact attachées à un point centré sur l'axe de l'arbre et la presse est modelée par une force linéaire (Figure VIb) appliquée sur les noeuds dans la direction X et Y pour simuler une charge normale à la surface. Le matériel est le CPW245 dont le modèle vient de la base de données de PWC.

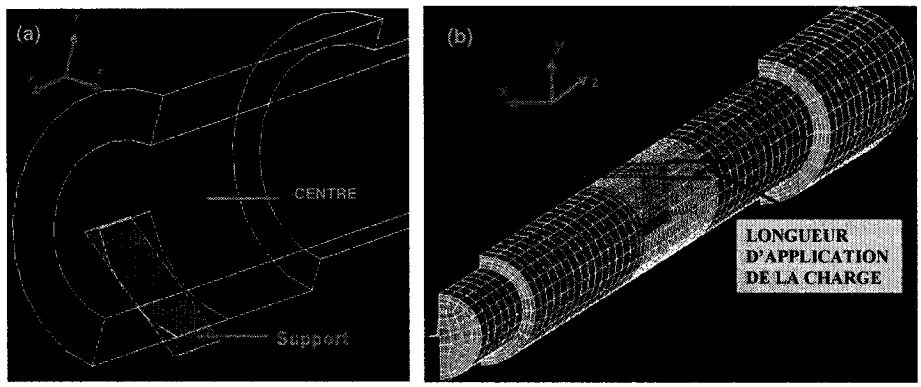

Figure VI Modélisation a)des appuis, b) de la presse

Pour choisir la taille optimale des éléments, une étude de convergence du maillage a été effectuée. En élasticité, le modèle d'éléments finis est comparé à un résultat théorique obtenu par la méthode de moment d'aire. La valeur théorique obtenue est de 0.3854" pour la déflexion et de 62000 Psi pour la contrainte axiale.

Les résultats de l'étude de convergence montrent qu'augmenter le nombre d'éléments de :

- la circonférence réduit la déflexion
- la profondeur n'affecte pas la déflexion
- la longueur augmente la déflexion

Le type d'éléments choisis est le SOLID185 (du programme ANSYS 6.1) à 8 nœuds car il donne des résultats aussi précis que l'élément SOLID95 à 20 nœuds et nécessite approximativement 10 fois moins de temps de calcul.

Les simulations faites avec des longueurs de charge variant de 0.5 a 5 pouces montrent qu'une longueur de 3.5 pouces est idéale pour le prototype parce que l'effet de la longueur sur la déformation plastique commençait à stabiliser et une longueur de plus de 3.5 pouces réduirait le nombre de régions sur l'arbre où une charge pourrait être appliquée.

D'autres simulations ont été faites avec trois modèles différents, chacune avec une forme initiale différente d'excentricité et amplitude. Les trois modèles ont été chargés de la même manière : signifiant que le point de départ de lecture, les conditions de support et la force de chargement sont identiques.

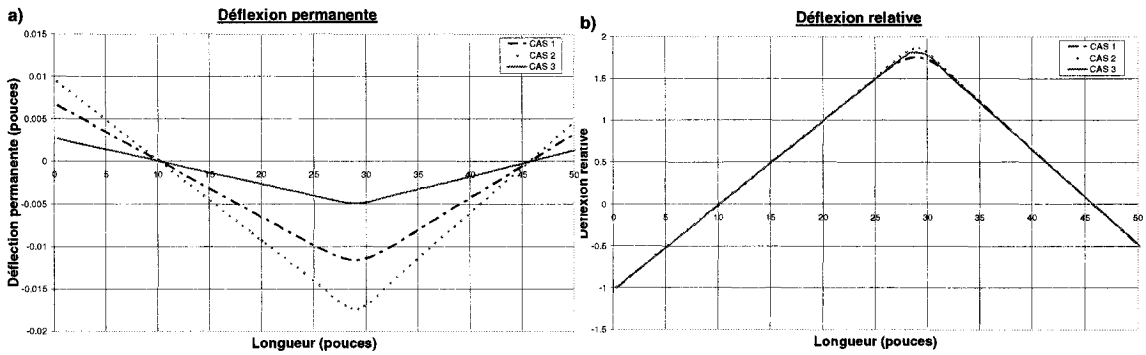

Figure VII a)Déflexion permanente, b) Déflexion relative

La Figure VIIa montre que la déflexion permanente pour chaque modèle varie tandis que la Figure VIIb montre que la déflexion relative est quasi identique. La déflexion relative étant le rapport de la déflexion du point de mesure relative à la déflexion d'un point choisi, pour ce cas à 20 pouces.

Conception du prototype de redressage par presse

La Figure VIII illustre le fonctionnement du prototype de redressage par presse.

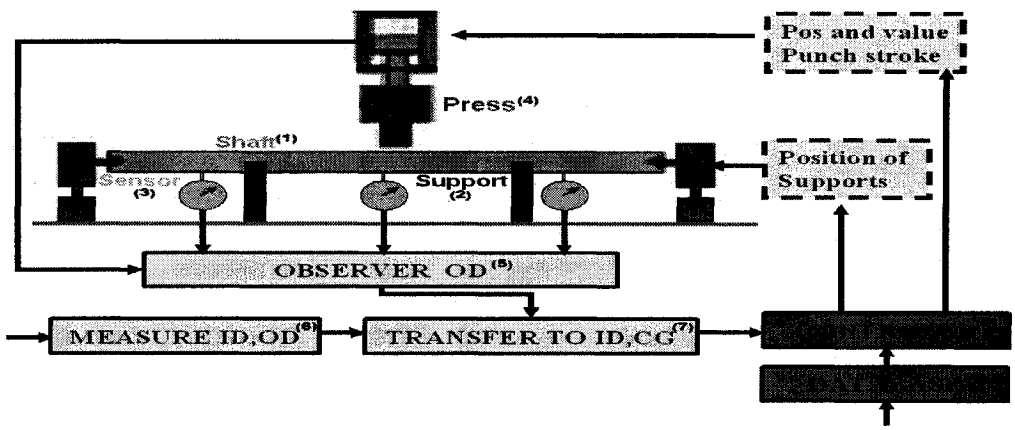

Figure VIII Fonctionnement du prototype de redressage par presse

L'arbre (1) est placé sur deux appuis (2) dans une position qui est fonction des mesures initiales (6). L'observateur (5) mesure le déplacement du diamètre extérieur en fonction de la charge à l'aide de capteurs (3) placés le long de l'axe et d'un capteur de force sur la presse (4). La forme finale désirée est transférée (7) en fonction de la forme du diamètre extérieur. Le contrôleur (9) sélectionne de la base de données (10) le meilleur ensemble de commandes de redressage afin d'obtenir la forme finale désirée.

La presse utilisée pour les expériences est une machine de soudage par friction du CNRC qui nous donne l'avantage de commander le déplacement.

Les appuis ont été conçus avec une surface cylindrique de 0.102 m de diamètre, en contact avec la table, pour que l'arbre soit le moins retenu en rotation et évite ainsi d'avoir des zones de concentration de contraintes. Le centre de ce cylindre est sur l'axe de l'arbre, de sorte que n'importe quelle mesure prise corresponde directement à la déflexion plutôt qu'au mouvement de corps rigide.

Les capteurs utilisés pour mesurer la déflexion sont fixes et ont une résolution entre 0.0001"et 0.0005".

L'observateur calcule la déflexion permanente en traçant la courbe de la déflexion en fonction de la charge. La déflexion permanente est donc facilement évaluée puisque le déchargement va suivre la même pente que le chargement élastique.

La mesure du diamètre intérieur est faite à l'aide du système de mesures ultrasonique Saupal de PWC.

La base de données est créée en utilisant 10 différentes configurations, de la position de la charge et des appuis. Chaque position a été soigneusement choisie de sorte que la seule section plastifiée soit celle qui est chargée.

La déflexion relative (CR(X)) calculée, basée sur la méthode de S.-C. Kim et S.-C. Chung (2000) [8], est la déflexion au point X (D(X)) divisé par la déflexion d'un point de référence (Dref1), choisis à 36" (Figure IX).

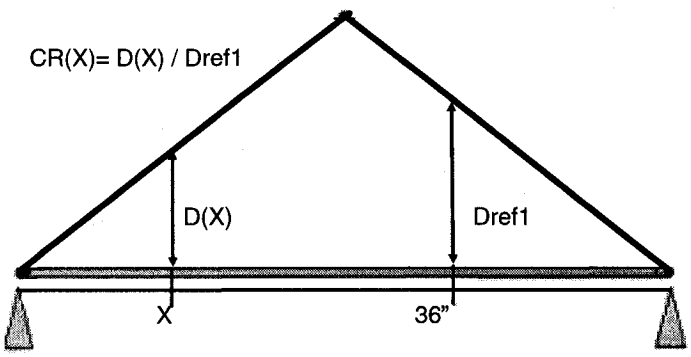

Figure IX Déflexion relative

L'avantage d'employer la déflexion relative est que la déflexion permanente créée à n'importe quelle position "x" le long de l'axe peut être calculée (Équation V) en fonction de la déflexion permanente du point de référence, indépendamment des propriétés géométriques ou du matériau de l'arbre.

$$D(X) = CR_1(X) * Dref_1 \qquad \textit{Équation V}$$

La déflexion permanente créée en "X1" par une série de différentes configurations de redressage (1 à n) est définie par l'Équation VI.

$$[CR_1(X_1) \quad CR_2(X_1) \quad \ldots \quad CR_{n-1}(X_1) \quad CR_n(X_1)] \times \begin{bmatrix} Dref_1 \\ Dref_2 \\ \ldots \\ Dref_{n-1} \\ Dref_n \end{bmatrix} = [D(X1)] \qquad \textit{Équation VI}$$

Pour plusieurs points de mesures X1 à Xm, la déflexion permanente est donnée par l'Équation VII.

$$\begin{bmatrix} CR_1(X_1) & CR_2(X_1) & \dots & CR_{n-1}(X_1) & CR_n(X_1) \\ CR_1(X_2) & CR_2(X_2) & \dots & CR_{n-1}(X_2) & CR_n(X_2) \\ \dots & \dots & \dots & \dots & \dots \\ CR_1(X_m) & CR_2(X_m) & \dots & CR_{n-1}(X_m) & CR_n(X_m) \end{bmatrix} \times \begin{bmatrix} Dref1 \\ Dref2 \\ \dots \\ Drefn-1 \\ Drefn \end{bmatrix} = \begin{bmatrix} D(X_1) \\ D(X_2) \\ \\ D(X_m) \end{bmatrix}$$

$$CR\ (X) \qquad x \quad Drefn \quad = \quad D(X) \qquad \textit{Équation VII}$$

Le contrôleur choisit les paramètres de redressage optimaux. Ces paramètres sont les positions de chaque appui, la position du chargement et la déflexion permanente nécessaire. Ceci est fait en remplacent dans l'Équation VII la matrice D(X) par la matrice des excentricités initiales E(X), et de résoudre l'Équation VIII pour trouver les valeurs optimales à employer pour Dref, en utilisant la configuration représentée par CR (X).

$$Drefn \quad = \quad inverse\ (CR\ (X)) \ * \ E(X) \qquad \textit{Équation VIII}$$

La matrice de déflexion permanente Drefn est résolue pour chaque combinaison possible de configuration CR pour 1 à 5 points de redressage. La configuration retenue est celle avec l'excentricité résiduelle (E(X) - CR(X) * Drefn) minimale tout en ayant une matrice de déflexion permanente Drefn acceptable.

Des essais ont été fais au CNRC avec le prototype décrit plus haut pour évaluer la précision du modèle d'éléments finis, et valider le prototype. Lors de l'essai employé pour valider le modèle d'éléments finis, l'arbre est chargé plastiquement de 14000 livres à 31", et les appuis sont à 6" et à 56". Les pourcentages d'erreur donnés au tableau I sont par rapport aux résultats expérimentaux pour un modèle d'éléments finis de même déflexion permanente maximale de 0.028".

Tableau II Pourcentage d'erreur du modèle éléments finis sur les résultats expérimentaux

	Déflexion	Déformation 16.35"	Déformation 31"	Déformation 49"	Charge
CHARGE	-3.6	-10.2	2.6	-14.6	-14.0
DÉCHARGE	-2.0	N/A	52.1 %	N/A	N/A

Le modèle d'éléments finis surestime l'élongation plastique maximum par plus de 50%. Puisque la contrainte résiduelle est directement proportionnelle à l'élongation plastique, nous pourrions conclure que la contrainte résiduelle est également surestimée par la même quantité. Ces deux observations signifient que le modèle d'éléments finis donnera seulement des résultats plus élevés que la réalité, ce qui rend son utilisation valide.

Développement d'un équipement de redressage d'arbres par grenaillage

Les équipements de grenaillage sur le marché sont principalement employés pour augmenter la résistance en fatigue des pièces en induisant une contrainte résiduelle de compression en surface. Le grenaillage à écrouissage a été également employé comme procédé de formage par S. Kittel, W. Linnemann, F. Wustefeld, R. Kopp [26] pour courber des plaques minces.

Puisque la conception du prototype de redressage par grenaillage est presque identique à celle décrite pour le redressage par presse, seules les différences seront décrites. Pour le redressage des arbres de turbomoteur, le grenaillage est produit par un pistolet ultrason de Sonats appartenant au CNRC. Cet outil de grenaillage fonctionne en faisant osciller des cylindres par une membrane excitée par ultrasons. Cet outil est choisi car il donne un meilleur contrôle de la région grenailler. La vitesse des cylindres est ajustable en modifiant la fréquence d'excitation de la membrane. Le seul inconvénient est que le pistolet est contrôlé manuellement et donc la vitesse de contact varie puisqu'elle dépend de la distance entre le pistolet et la pièce.

Le contrôle est plus simple puisque la déflexion permanente est directement mesurée. La seule difficulté est que les vibrations provoquées par grenaillage forcent l'arrêt pour prendre la mesure. La déflexion permanente est obtenue en faisant varier l'aire de la région grenaillée.

La base de données se compose également de rapports de déflexion mais pour des configurations dont la position des appuis est toujours aux extrémités de l'arbre. La déflexion permanente maximum serait seulement limitée par la quantité d'effort résiduel que le procédé est capable d'induire à la surface. La quantification de ses limites, qui ferait partie d'une étude ultérieure, nécessiterait une vaste quantité d'expériences.

Les essais effectués au CNRC ont pour objectif de :

(a) vérifier si la contrainte résiduelle appliquée par grenaillage est suffisante pour redresser un arbre excentrique. Un premier arbre a été grenaillé sur une région de 5" x 1.5". Les résultats ont prouvés que la contrainte résiduelle appliquée par grenaillage est suffisante puisqu'une déflexion permanente de 0.012" a été atteinte, sur deux plans perpendiculaires donnant un déflexion permanente totale de 0.016" entre les deux plans.

(b) Évaluer l'effet du grenaillage sur la circularité et la rugosité de l'arbre. La circularité mesurée montre une élévation de 0.0015" de la surface grenaillée et bien que la rugosité moyenne est de 16 µPouce la surface grenaillée comporte des variations de 0.002".

(c) Vérifier si la déflexion permanente créée par ce procédé est contrôlable. Un arbre ayant son centre de gravité excentrique de 0.0035", fut redressé en utilisant le procédé de grenaillage. Le procédé étant contrôlable l'excentricité finale était de moins de 0.0005".

Etude sur la méthode de redressage par brunissage

La méthode de redressage par brunissage est semblable à celle par grenaillage. La seule différence est dans la méthode utilisée pour introduire les contraintes résiduelles. La méthode utilisée emploie le processus de brunissage, développé par Paul S. Prevey, qui permet d'obtenir une couche de contrainte résiduelle en compression avec un minimum de déformation plastique. La contrainte résiduelle est introduite à l'aide d'une sphère, libre en rotation, qui est roulée le long de la surface. La force avec laquelle la sphère est pressée contre la surface est assez grande pour déformer plastiquement une couche extérieure de matériel et ainsi générer une contrainte résiduelle en compression. Cette

contrainte résiduelle créera, de la même manière que pour le grenaillage, un moment de flexion qui sera employé pour redresser l'arbre.

Les avantages de cette méthode sont :

(a) La sphère peut être contrôlée par une machine-outil à commande numérique donnant un contrôle sur la région bruni ainsi que l'intensité de brunissage. De plus le passage entre la région brunie et le reste de la pièce peut être progressif, réduisant ainsi les discontinuités dans la surface de la pièce.

(b) La rugosité de la surface brunie se voit améliorée.

(c) Comme la déformation plastique est minimale les contraintes résistent à la relaxation thermique, lorsqu'elles sont exposées à de hautes températures.

Un concept de prototype permettant de redresser les arbres en brunissant simultanément les diamètres intérieurs et extérieurs est illustré à la figure X.

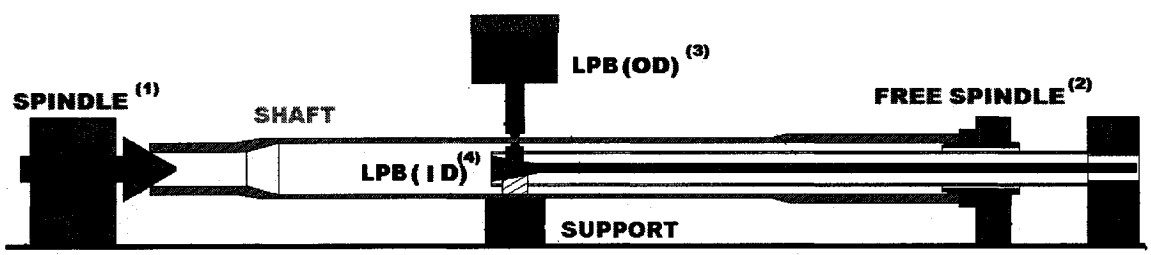

Figure X Concept d'un équipement de redressage par brunissage

Conclusion

Pour le redressage par presse, le modèle d'éléments finis a aidé pour comprendre le phénomène et pour développer le prototype. Les essais avec le prototype conçu étaient en concordance avec le FEM.

Les résultats des expériences de redressage par grenaillage montrent qu'il:
(a) crée assez de déflection permanente pour redresser des arbres,
(b) augmente la rugosité et altère la circularité,
(c) est contrôlable parce qu'un arbre initialement excentrique de 0.007" de battement a été redressé à un battement en dessous de 0.001".

Le redressage par brunissage est presque identique au redressage par grenaillage. La seule différence est que la contrainte résiduelle serait introduite simultanément en brunissant la surface intérieure et extérieure de l'arbre.

Une combinaison du redressage par presse et du redressage par grenaillage donnerait les meilleurs résultats. Le redressage par presse pourrait être utilisée seulement en début du procédé en raison de la contrainte résiduelle en tension qu'il génère. Le redressage par grenaillage pourrait être employé sur l'arbre fini pour raffiner le redressage.

Pour le redressage par presse, la presse pourrait être améliorée en employant un matériel déformable entre l'arbre et la presse ou en ajoutant à la presse des composants qui pourraient s'ajuster au recourbement de l'arbre.

Les arbres redressés par presse vont être utilisés pour comprendre l'effet du traitement thermique et de l'usinage de la région plastique. Ces résultats seront utiles pour comprendre comment intégrer le redressage par presse dans le processus de fabrication de PWC.

Pour le redressage par grenaillage, les améliorations sont:

- grenailler la surface intérieure,
- ajouter un contrôleur « fuzzy» pour choisir les paramètres,
- se limiter aux régions où la température est assez basse afin d'éviter la relaxation de la contrainte résiduelle.

Pour le redressage par brunissage, un prototype aussi bien qu'un modèle d'éléments finis devraient être mis sur pied. Des essais semblables à ceux du redressage par presse et par grenaillage devraient être effectués.

Table of contents

List of figures

List of tables

List of abbreviations

OD	- Outer Diameter
ID	- Inner Diameter
PWC	- Pratt & Whitney Canada
BTA	- Boring and Trepanning Association
TIR	- Total Indicator Reading
COG	- Center Of Gravity
USL	- Upper Specification Limit
$X_{0.05}$	- The 50 percentile for the specified distribution
$X_{0.99875}$	- The 99.875 percentile for the specified distribution
T	- Target value
Toler	- Sigma tolerance
SS	- Surface Stress
CSMAX	- Maximum Compressive Stress
d	- Depth of the compressive stress
TS MAX	- Maximum Tensile Stress
E	- Elastic modulus
I	- Inertia
M	- Bending Moment
h	- Arc Height
c	- Cord
M_a, M_b	- Bending moment in section a and b respectively
P	- Applied load
a, b	- Distance between load and supports
L	- Distance between supports
x	- Distance from 1st support where the bending moment is evaluated
σ_a, σ_b	- Stress in section a and b respectively

y - Height from center at which the bending moment is evaluated

$\left[A_{under}\frac{M}{EI}\right]_0^L$ - Area under the area moment curve between x= L and 0.

$\bar{X}_L$ - Centroïd of the area moment curve between x= L and 0.

$\left[A_{under}\frac{M}{EI}\right]_0^{L/2}$ - Area under the area moment curve between x= L/2 and 0.

$\bar{\bar{X}}_{L/2}$ - Centroïd of the area moment curve between x= L/2 and 0

$\delta_{L/2}$ - Deflection at L/2

Ndiv Circ - Number of element over the circumference

ndiv thick - Number of elements in the thickness

Uy - Deflection

LPB - Low Plasticity Burnishing

LVDT - Linear Variable Differential Transformers

GD&T - Geometric Dimensional and Tolerances

Introduction

Most modern passenger and military aircraft are powered by gas turbine engines. This engine also called the jet engine was developed during World War II by Sir Frank Whittles and Dr. Hans Von Ohain. There are two main types of gas turbine engines manufactured by Pratt & Whitney Canada (PWC): the turbofans and the turboprops. For the turbofan 90 % of the thrust is created by the fan that accelerates a large volume of air and 10 % of the thrust is created by the hot exhaust gas which passes through the nozzle. For the turboprop, all the thrust is created by the propeller that accelerates a large volume of air. For both the air temperature and pressure are elevated when passing through the compressors, fuel then is added and the mixture is burned. The hot air whirls the high speed turbines which rotates the compressors and the fan or the propeller.

The shaft is the center part of the motor coupling the high speed turbines with the compressors and the fan, for a turbofan, or the propeller, for a turboprop. Therefore the shaft is submitted to torsion at high rotational speeds and temperatures. Due to its high rotational speed, any unbalanced mass could create unacceptable vibrations and therefore reduce the motor performance, increase the noise and reduce the life of the bearings.

To avoid having an unbalanced, shaft the wall thickness tolerance and the runout tolerance on the outer diameter (OD) were reduced. These tolerances are equivalent to a straightness tolerance on the inner diameter (ID) and OD as well as a concentricity tolerance between the ID and OD. Since even by controlling the manufacturing of the shaft there is still unbalance, a high speed balancing process is carried out to limit its effect.

The manufacturing of those shafts by PWC is mostly done by turning and gun drilling of an initially solid bar. In the past years, the manufacturing of those long shafts was optimized to meet the geometric tolerances by using a more stable head for the gun drill.

Since the tolerance on the shaft wall thickness just keeps getting tighter and that the optimization of the gun drill process is attaining its limits, the company requires new solutions; one of which consists of doing an in process correction of those errors.

The eccentricity of the hole is already corrected at PWC by best fitting a line through the measured points and grinding the outside reference to follow this line

The correction of the straightness of the shaft by bending is at the center of this thesis. Two ways of bending the shafts were proposed: three point bending by a press and bending by peening.

To be able to understand and predict the effect that straightening will have on the material properties of the shaft, a finite element model was developed for the press straightening and an exhaustive research on the peening process was also done.

Subsequently a research on the existing equipments initiated for the development of a prototype that was used in the experiments done with NRC, to prove that the two methods were controllable and predictable.

Chapter I: Bibliographic revue

1.1 The shaft in gas turbine engines

The Nasa Glenn Research Center [1] and Pratt & Whitney U.S. [2] websites give a good overview of how turbine engines work. The turbofan and turboprop which represent 82 % of the engines produced at PWC are explained below.

For a turbofan engine, there are six major components in that engine (Figure 1.1). The propulsion process begins with the fan at the front of the engine which draws in a large volume of air that separates into two streams. The larger stream, typically about 85 % of the total, is called the bypass air. The smaller stream typically about 15% of the total volume, is called primary air. Because of its huge volume, bypass air only needs to accelerate a small amount to produce an enormous thrust (90% of total), and has the added benefit of keeping the engine cooler, quieter and more fuel efficient.

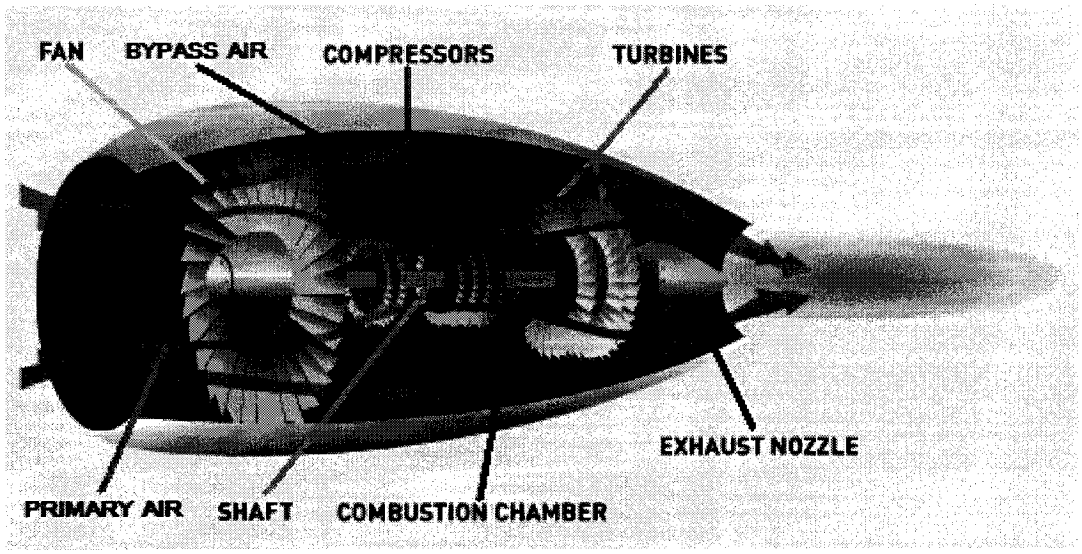

Figure 1.1 Turbofan [2]

The primary air enters the compressors that rises significantly both its temperature and pressure. When compression is complete, the air now 30 times higher in pressure and 1100 °F hotter is forced through a combustor, where fuel is added and burned. The air temperature soars even higher and reaches beyond 2000 °F. The hot air then blasts through the blades of the turbines. The whirling turbines drive the shafts that in turn drive both compressors and the fan at the front of the engine. After passing through the turbines, the hot air is forced through the exhaust opening at the back of the engine. The narrowing walls of the exhaust nozzle forces the air, which combined with its acceleration, also drives the engine forward.

The turboprop engine (Figure 1.2) incorporates the same basic concepts and technology as the turbofan engine with the propeller replacing the fan.

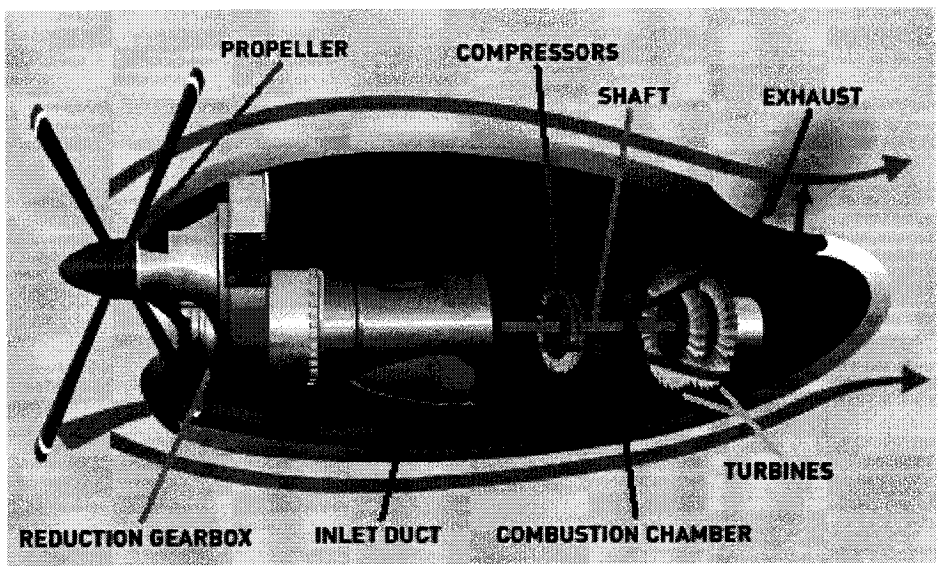

Figure 1.2 Turboprop [2]

Air entering the turboprop engine through the inlet duct, flows through the compressors that rises significantly both its temperature and pressure. The air leaving the compressor, now typically 30 times higher in pressure and 1000 °F hotter, enters the combustion chamber where fuel is injected and mixed with the air. Spark plugs called igniters ignite

the fuel/air mixture to initially start the combustion, which then becomes continuous. The temperature of the burning gas mixture soars even higher, reaching well beyond 3000 °F. The hot gas then blasts through the blades of the turbines. The whirling turbines are coupled to, and thus rotate, the compressors and propeller in the front of the engine. After passing through the turbines the hot gas exits through the exhaust opening at the back of the engine. The whirling turbines drive the propeller through the reduction gearbox. The propeller provides the primary thrust and rotates at a typical 1000 to 1200 rpm, up to 15 times slower than the turbines.

1.2 Manufacturing of shafts

The shafts manufacturing is primarily done by operations such as turning, gun drilling and grinding. The operation that affects the most the precision of the hole shape is the gun drilling. A vast number of studies were found on the three types of deep hole drilling which are boring and trepanning association (BTA), ejector drilling and gun drilling. Gun drilling is used at PWC for the manufacturing of deep holes.

P. Rudd and L. Hetherington [3] explain the three types of deep hole drilling process. J.-H. Chin, C.-T. Hsieh and L.-W. Lee [4] established a model and investigated the shafts dynamic behaviour during deep hole drilling. Figure 1.3 shows a schematic of the boundary conditions at the tool head.

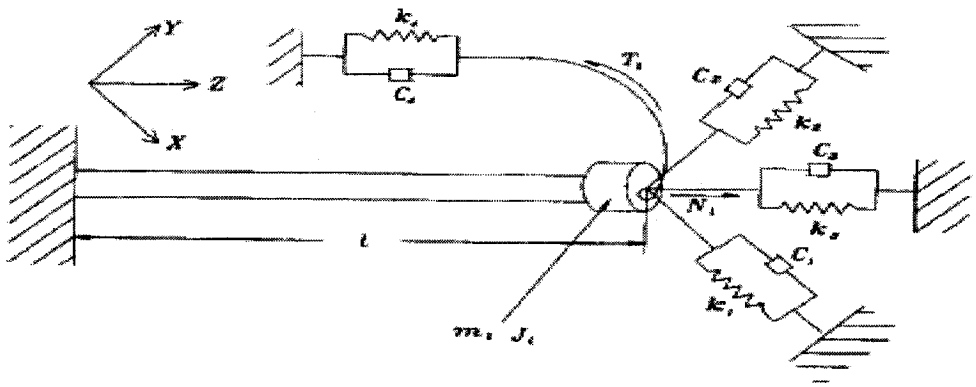

Figure 1.3 Boundary condition on the tool head [4]

These studies show that the deeper the hole, the more the moment on the tool head because the moment on the tool head is equal to the force times the distance (depth). The moment results in a deflection of the tool which generates shape errors.

1.3 Press straightening

A study made on existing equipment revealed how the international market addressed the correction of shape errors and how their equipment work. After this vast research of existing equipment used for straightening, the results showed that two types of equipments are used in the market: roll straightening and press straightening.

The companies Benex Corp [8], Universal Tool & Engineering, Bronx/taylor-wilson, and Meeco developed roll straightening equipments. The roll straightening equipment works by passing the shafts through a series of roller placed in a manner that the shafts outer diameter (OD) is forced through a straight line and therefore each runout point of the part will be bent to fit the centerline defined by the cross rolls (Figure 1.4) .

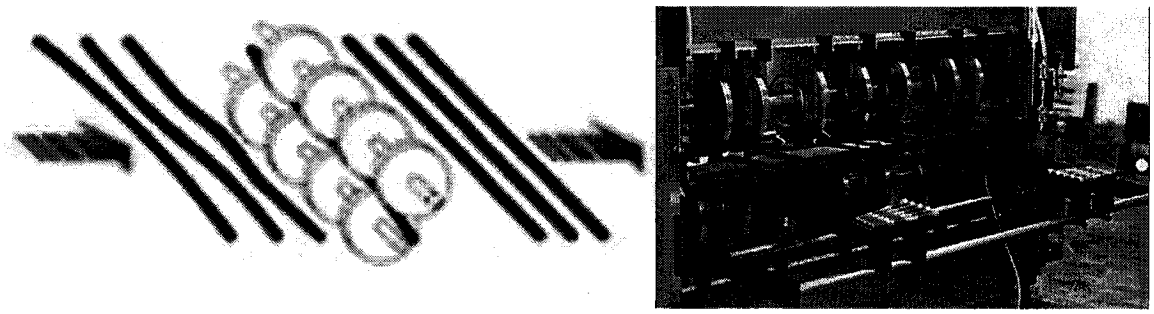

Figure 1.4 Roll straightening from Benex Corp [8]

This process is mostly used for high volume parts with an almost constant OD. Since this process is only capable of correcting the OD it was put aside for the rest of this study.

The companies Eitel Presses, Galdabini, Savage Industries and Kokusai developed press straightening equipments very close to the one we need to design but their straightening process is too unpredictable and could damage the shaft. For these press straightening equipment (Figure 1.5), the part (1) is clamped between centers (2) or on rollers and rotated. Its total indicator reading (TIR) is measured with a sensor (3) to determine the high point location. The high point is turned up and a ram/punch (4) flexes plastically the part against the supports (5) and releases it. The TIR is then re-measured and this process continues until the TIR is within specification.

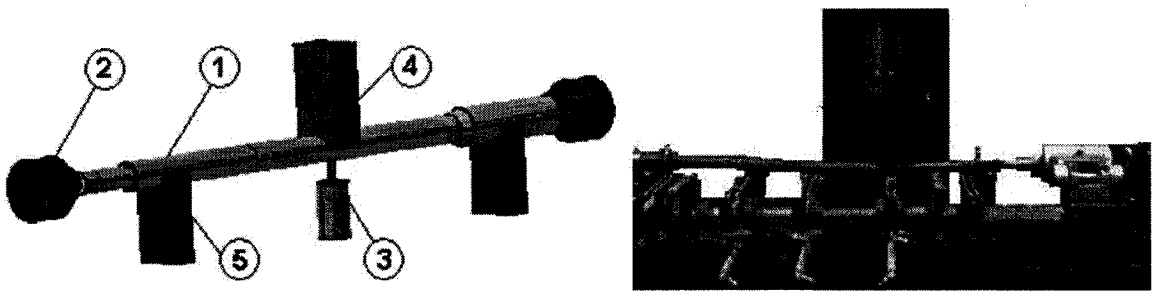

Figure 1.5 Press straightening from Eitel Presses [9]

Although press straightening is mainly used in the automotive industry for OD correction; Savage Industries, Galdabini and Kokusai, already worked on inside diameter (ID) straightening of gun barrels. Table 1.1 summarizes the capabilities and cost of the press straightening equipments.

Table 1.1 Press equipments capabilities

	Power (tons)	*price (US K$)*	*Accuracy (TIR)*
Eitel Presses	*40 to 250*	*165-200*	*0,005 " per feet*
Kokusai	*1-150*	*225*	*0.000005 TIR*
Galdabini	*NA*	*250 OD 350 ID*	*0,001 " per feet*
Savage Industries	*1-500*	*160-250*	*0.001 TIR*

The only inconvenience with current equipment is since they are used on automotive parts which are over-dimensioned the process is not optimized to minimize the number of straightening cycles and to make sure that the part still meets the engineering demands, such as the maximal allowable tensile residual stress.

An optimized multi-step straightening control system of the outer diameter of shafts was developed by S.-C. Kim and S.-C. Chung (2000) [10]. Their straightening system shown in Figure 1.6 is capable of correcting the outer diameter of shafts by three point bending.

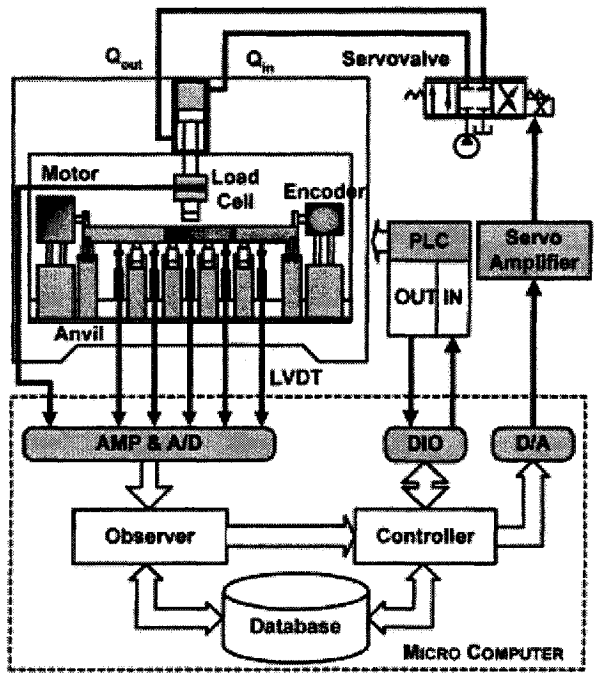

Figure 1.6 Multi step straightening control system [10]

The main components of this system are listed below:

- Springback observer
- Hydraulic punch stroke control system
- Database
- A multi step straightening operation controller
- Fuzzy self-learning controller

During the loading, a spring-back observer is used to estimate the permanent deflection. A load deflection curve is plotted (Figure 1.7) by using the real-time measurement of load F and deflection δ, acquired respectively by a load cell and a linear variable differential transformers (LVDT).

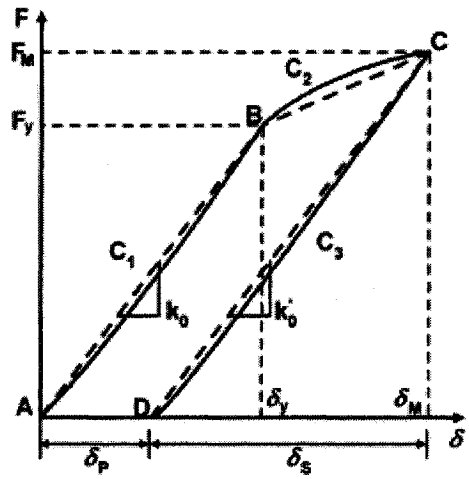

Figure 1.7 Load–deflection model of three-point bending for shafts [10]

During the loading process the elastic modulus is estimated and the permanent deflection amount is estimated by using Equation 1.1.

$$\delta_p = \delta_m - \frac{F_m}{K_0} \qquad \textit{Equation 1.1}$$

where:

δ_p=Permanent deflection

δ_m = Loaded deflection.

F_m= Load.

K_o= Slope during loading (estimate of the elastic modulus).

The hydraulic punch stroke control system is designed to take real-time controls of the permanent deflection of shafts.

A multi-step straightening controller computes the optimal straightening commands through the analysis of the shafts deflection pattern (Figure 1.8), maximum deflection and deflection direction. These commands are the straightening point, direction, permanent deflection and supporting conditions and are chosen with the use of change ratios.

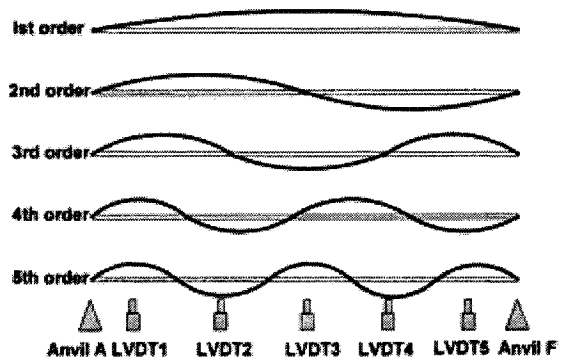

Figure 1.8 Deflection patterns [10]

Change ratios (Figure 1.9) are calculated, in Equation 1.2, for each measuring point as being its displacement (d_i) divided by the displacement of the straightening point, which is equal to the permanent deflection (δ_p).

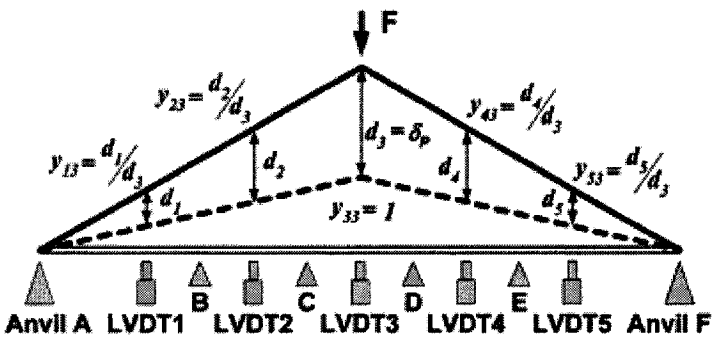

Figure 1.9 Change ratios when the shaft is supported on anvil A and F [10]

$$Y_{ip} = \frac{d_i}{\delta_p} \qquad \textit{Equation 1.2}$$

Y_{ip} = Change ratios at point i

d_i = displacement of point i

δ_p = permanent deflection = displacement of the straightening point.

A fuzzy self-learning controller is used to optimize the straightening commands by estimating the change ratios.

The straightening point is the maximum deflection point (δ_1) and the straightening direction (θ) is calculated by Equation 1.3. The database contains the straightening limits of the equipment and the change ratios for various supporting conditions and straightening points.

$$\theta = \theta_1 + \frac{\theta_2 - \theta_1}{2}\left(\frac{\delta_2}{\delta_1}\right)^2$$

Equation 1.3

where:

δ_1, δ_2 = 1st and 2nd maximum deflection respectively

θ_1, θ_2 = angles at δ_1, δ_2 respectively

θ = straightening direction

The 80 rack bars shown in Figure 1.10 were measured and straightened within a 30 μm of straightness tolerance.

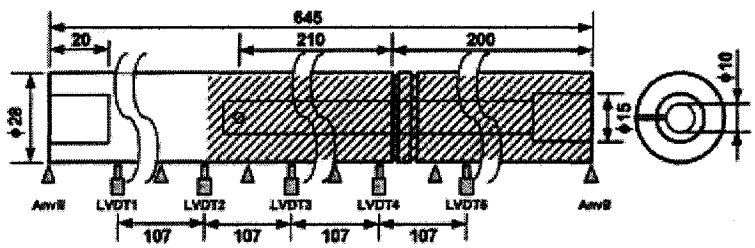

Figure 1.10 Rack bar dimensions [10]

The results in table 1.2 show that the 79 out of tolerance bars were straightened with an average number of cycles of 3 and an average straightening time of 19.9 seconds.

Table 1.2 Straightening of rack bars results [10]

Number of straightening cycle	1	2	3	4	5	6	7	Average
Number of items	13	15	25	16	7	2	1	3.0 cycles
Average time required for straightening	7	13	20	27	33	38	45	19.9 s

The inconvenience with the press straightening method is that it induces undesirable residual tensile stress on the surface of the part at the straightening point. This is the reason why the peen straightening process is also considered.

1.4 Peen straightening

For the straightening by peening, an extensive research was done to better understand the ability of peening to bend a shaft. Table 1.3 gives an overview of the subjects treated by each of the consulted articles.

Table 1.3 Overview of peening article's subjects

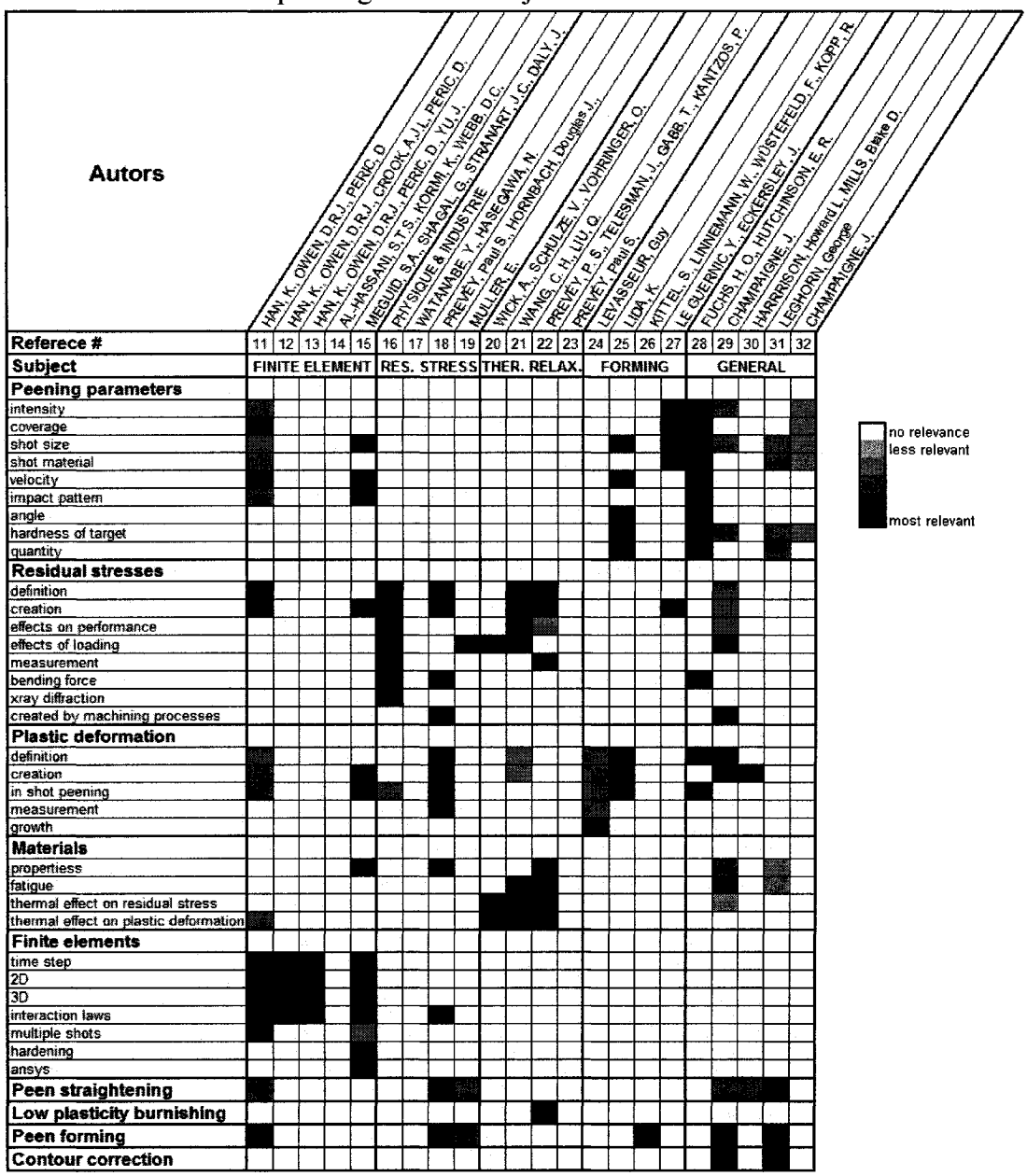

Jack Champaigne (2001) [29] and K. Lida [25] describe the formation of the plastic dimple (Figure 1.11) created by shot peening and the typical residual compressive stress profile (Figure 1.12).

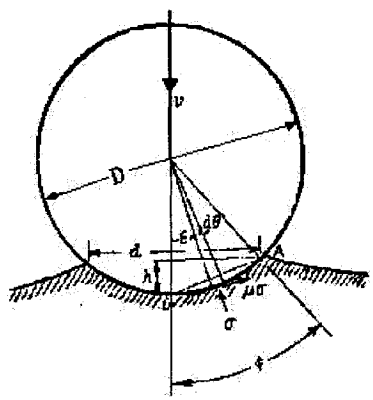

Figure 1.11 Plastic dimple created by shot peening [25]

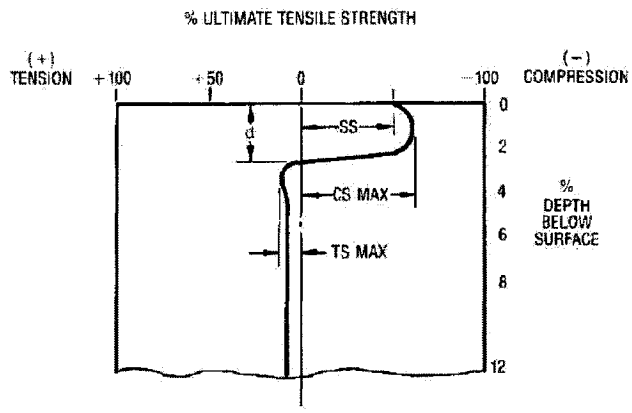

Figure 1.12 Typical residual compressive stress profile [29]

In Figure 1.12:

SS = Surface Stress.

CS MAX = Maximum Compressive Stress.

d = Depth of the compressive stress.

TS MAX = Maximum Tensile Stress.

H. O. Fuchs and E. R. Hutchinson [28] and George Leghorn (1957) [31], explain the Almen intensity notation which consists of measuring the arc height created by shot peening on a standardized steel strip .

H. O. Fuchs and E. R. Hutchinson [28] give a method to approximate the force at the surface in function of the Almen strip arc height. He uses Equation 1.4 of the elastic bending moment

$$M = \frac{8EIh}{c^2} \qquad \textit{Equation 1.4}$$

and

$$F = \frac{2M}{t} \qquad \textit{Equation 1.5}$$

which gives for an Almen strip

$$F = 66000 \times h \ lb \qquad \textit{Equation 1.6}$$

where :

E = Elastic modulus

I = Inertia

M = Bending moment

h = Arc height

c = Cord

S. Kittel, W. Linnemann, F. Wustefeld, R. Kopp [26] constructed a peen forming tool and its control system (Figure 1.13) which was tested to peen form a sheet metal (Figure 1.14).

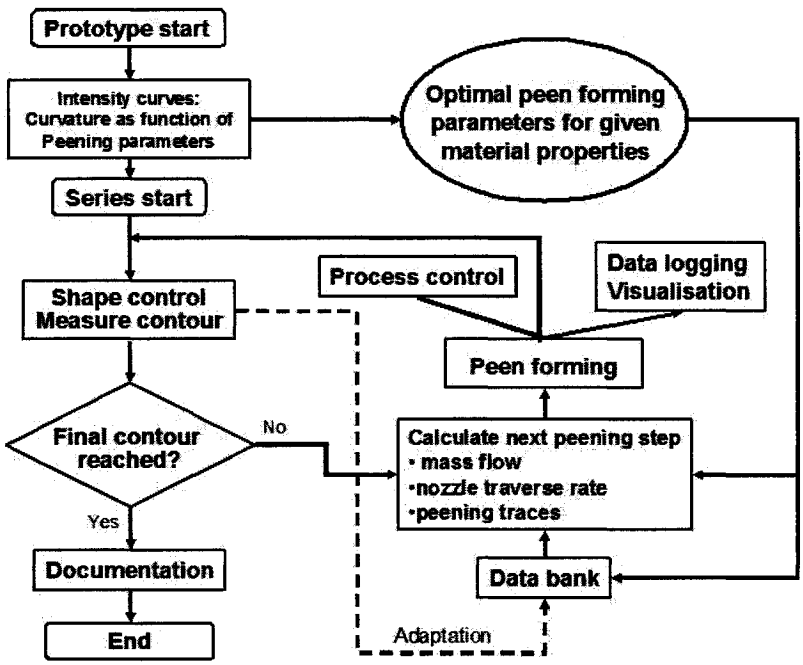

Figure 1.13 Flow chart for controlled peen forming [26]

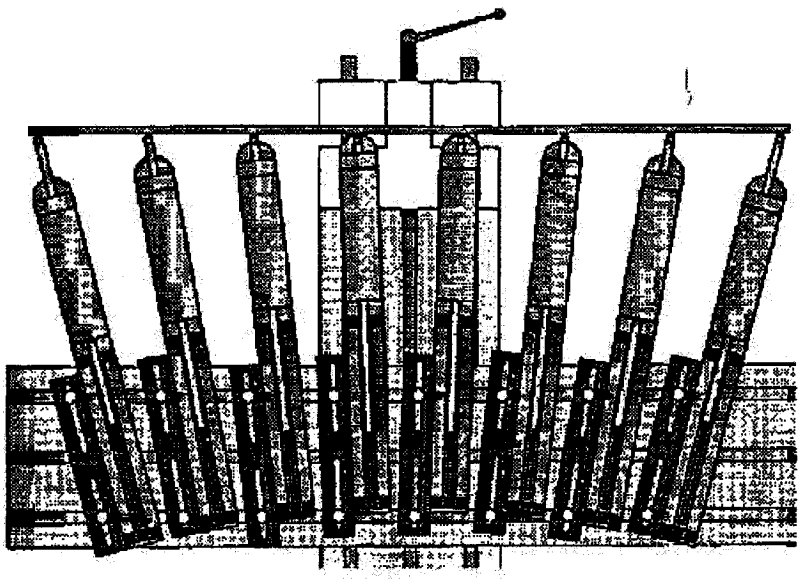

Figure 1.14 Peen forming setup [26]

This sheet metal of dimensions of 500 mm x 500 mm by 2.99 mm thick was curved to a radius of 1,000 mm and 2.500 mm by applying the process shown in Figure 1.13 and splitting the sheet in 7 areas (Figure 1.15).

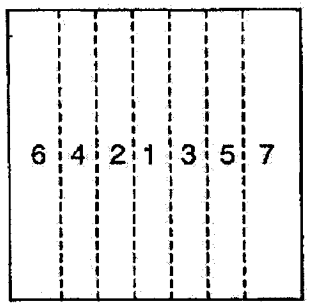

Figure 1.15 Splitted sheet [26]

K. Han, D.R.J. Owen and D. Peric (2001) [11], developed an efficient finite element model of shot peening capable of simulating the peen forming process. They compute the residual stress/strain profile under particular peening conditions by modeling a small scale sample model (Figure 1.16). Then they apply this profile to the peened section of the full scale model (Figure 1.17) to obtain the final deformation and stress distribution using an implicit static analysis.

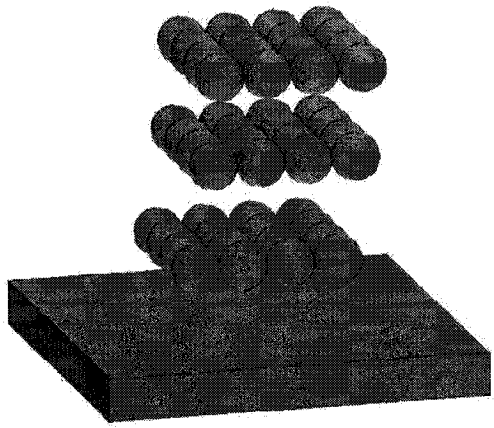

Figure 1.16 Small scale sample model [11]

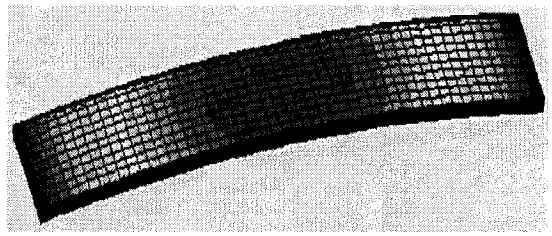

Figure 1.17 Final deformation of an Almen strip [11]

The control of peening parameters to change the shape of a part was mainly motivated by its applications in peen forming aircraft wings. The same methodology or equipments could be used for straightening.

George Leghorn (1957) [31] states that: " Automobile axle shafts can be straightened out by peening after heat treating with life increases of more than a hundred fold."

Jack Champaigne (2001) [29] in his overview of shot peening writes:
"Just as it is possible to create a desired curvature and shape to components by shot peening, it is also possible to correct the shape and form of parts as well. The shot peening process avoids the unfavourable (tensile) residual stresses produced by other straightening methods and instead produces favourable (compressive) residual stresses. Many companies have correctively peened a great variety of parts such as shafts, tubes, rings, gears, axles, crankshafts, jet engine discs and wing spar extrusions and forgings. Carburized ring gears as large as 48 inches (122 cm) diameter, which were out of round as much as 0.125 inch (3.17mm) have been corrected to within 0.003 inch (.076mm)."
He also points that both sides of a peen-formed piece have compressive stress, since the curvature created by peening will create a compressive stress in the unpeened side.

1.5 Low Plasticity Burnishing

Paul S. Prevéy (2000) [23] shows that for Inconel 718, a nickel-alloy omnipresent in aircraft engines, that low plasticity burnishing (Figure 1.18) is a more stable process because residual stresses are less affected by temperature changes. He compares the residual stresses of gravity peening, laser shock peening (LSP) and low plasticity burnishing (LPB) before and after being exposed to high temperatures . For a shot peened piece exposed to temperatures between 500 and 670 *C, 50 % of the residual stress are lost after only minutes compared with only 15 % for a LPB piece.

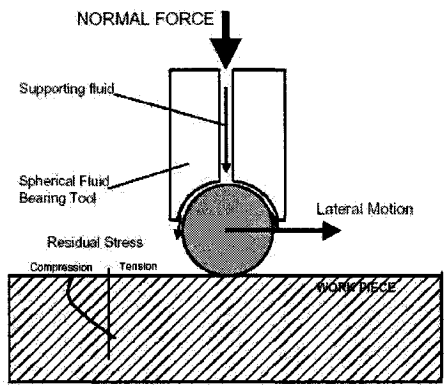

Figure 1.18 Low plasticity Burnishing [23]

1.6 Conclusion

For straightening by bending, studies and equipments show that it is a process frequently used for cylindrical parts having a high length over radius ratio. What is missing in these researches is the effect it has on the shaft's resistance and the straightening process isn't optimized to minimize the negative effects on the shaft's resistance.

For peen straightening the closest thing found to peen straightening is peen forming of aircraft wings.

Chapter II Project relevance

The project relevance starts by exposing the objectives and hypothesis. Then, the types of shape errors that need corrections are defined as well as their source and cost in the manufacturing of shafts.

2.1 Project description

2.1.1 Objectives and hypothesis

The objectives of this project are to:

1) reduce the manufacturing cost of turbine engine shafts by:
   - Eliminating the scraps due to concentricity and straightness shape errors.
   - Relieving the tight tolerances on costly operation like gun drilling and grinding.

2) improve the quality by having a control on the straightness of the shafts.

A straightening process added to the concentricity correction already used at PWC would reduce the manufacturing costs and improve the quality of complex shafts. This straightness process should be easily controllable and should not affect the properties of the shaft by meeting the engineering demands and making sure that the shaft will be able to undertake the necessary loads.

2.2 Shape errors

There are three types of shape errors that can be identified. The concentricity and the straightness errors are primarily seen in the gun drilling process and the runout error would be a result of turning, grinding or after a stress relief.

2.2.1 Concentricity error

The concentricity error (Figure 2.1) consists of the center line of the hole making an angle with the centre line of the outside diameter.

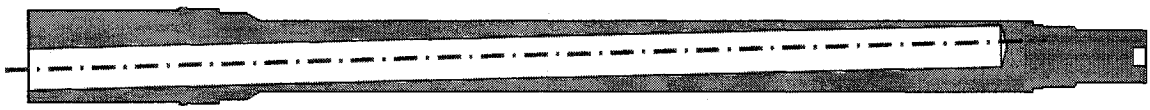

Figure 2.1 Illustration of a concentricity error

The concentricity of a hole (Figure 2.2) is the diameter of a cylinder, centered on the reference axis (Centerline OD), within which the centerline of the hole (Centerline ID) is contained.

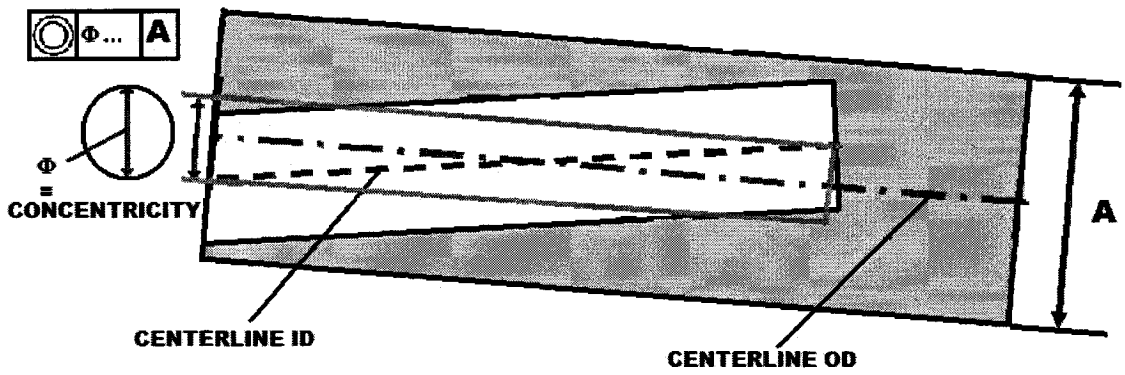

Figure 2.2 Measurement of concentricity

This type of error is currently corrected at Pratt & Whitney Canada by measuring the inner diameter at certain sections, best fitting a line and then readjusting the outside reference to follow this line.

2.2.2 Straightness error

The straightness error (Figure 2.3) consists of the center line of the hole having a second or higher order shape.

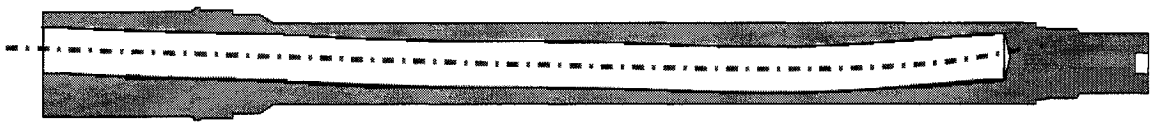

Figure 2.3 Illustration of a straightness error

The straightness of a hole (Figure 2.4) is the diameter of the cylinder within which the centerline of the hole is contained.

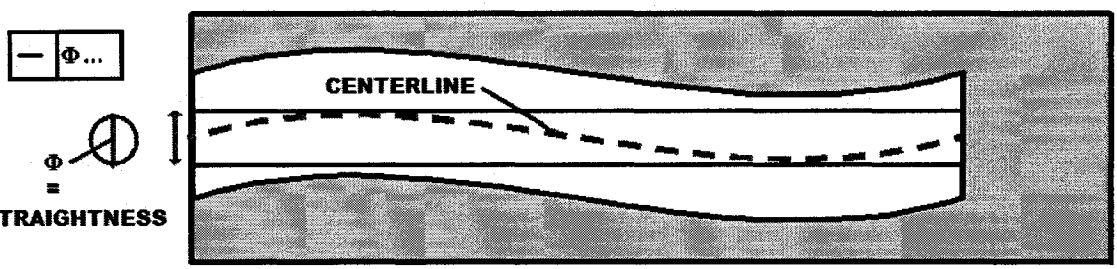

Figure 2.4 Measurement of straightness

This type of error is not currently corrected at Pratt & Whitney Canada and represents the core of this project.

2.2.3 Runout error

If the wall thickness is constant there may still be a runout error (Figure 2.5), because although the exterior center line coincides with the interior center line, this line may not coincide with the axis of rotation of the shaft.

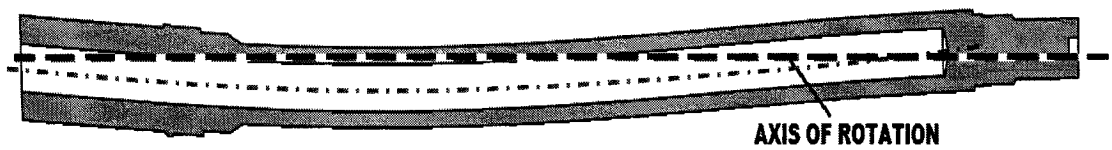

Figure 2.5 Illustration of a runout error

The runout of the OD at a given section (Figure 2.6) is the variation measured by the gage during a full rotation of the shaft as he is supported at its reference location (A and B in Figure 2.6), usually at bearing locations. The runout is also equal to twice the distance (E in Figure 2.6) between the axis of rotation and the center of the measured section.

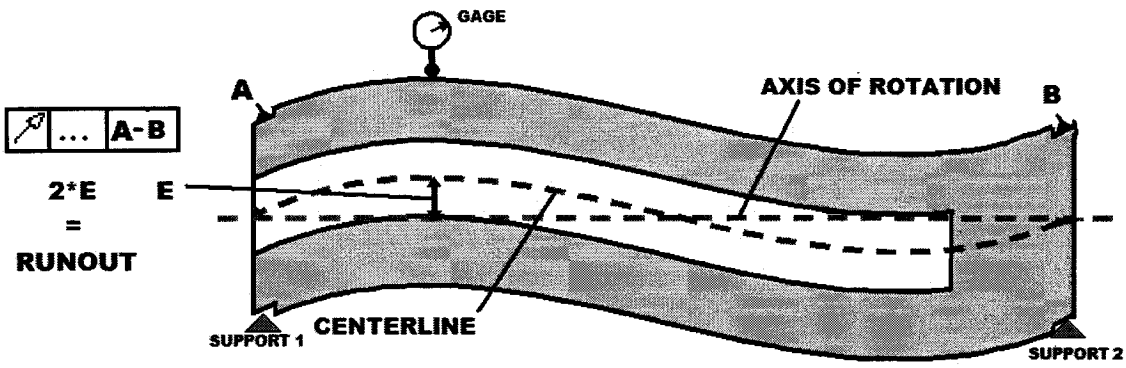

Figure 2.6 Measurement of runout

2.3 Cause of shape errors

2.3.1 Gun drilling

The actual manufacturing process used to make the inner diameter is gun drilling (Figure 2.7). The gun drilling of parts with a large length/diameter ratio are very hard to machine because the tip of the tool is unrestrained. This allows the machining force to displace the tip of the tool and create eccentricity and straightness errors.

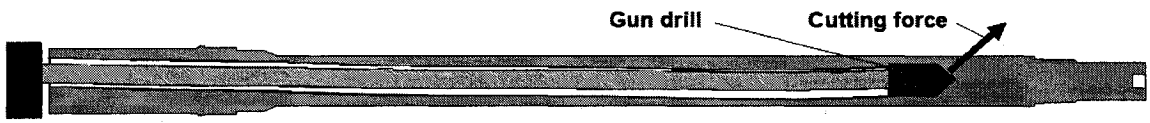

Figure 2.7 Cutting force during gun drilling

2.3.2 Outer diameter grinding or turning

Even after the gun drilling operations, an error could occur during the grinding or turning of the outer diameter. During the turning operations the shaft is submitted to forces and therefore could deform itself and this machining operation leaves residual stress at the surface that could also deform the shaft.

2.4 Process capability evaluation of shafts runout

The first step of the project was to understand the actual capability of the manufacturing of the shafts. This study will be based on the methods of calculating a capability index for geometric dimensional and tolerances (GD&T) exposed by the two following articles and calculated by Minitab [7].

D. P. Karl, J. Morisette and W. Taam [5] propose to use C_{pk} of a Wiebul distribution because there is only an upper limit and that the values are always positive. This C_{pk} is effectively a C_{pu} which is calculated taking in consideration only the upper limit using Equation 2.1.

$$C_{pk} = C_{pu} = \frac{USL - X_{0.50}}{X_{0.99875} - X_{0.50}} \qquad \textit{Equation } 2.1$$

Where:

USL = Upper specification limit.

$X_{0.05}$ = The 50 percentile for the specified distribution.

$X_{0.99875}$ = The 99.875 percentile for the specified distribution.

The values showed are calculated using Minitab [7] for which C_{pu} is calculated (called P_{pu} by Matlab in Figure 2.8).

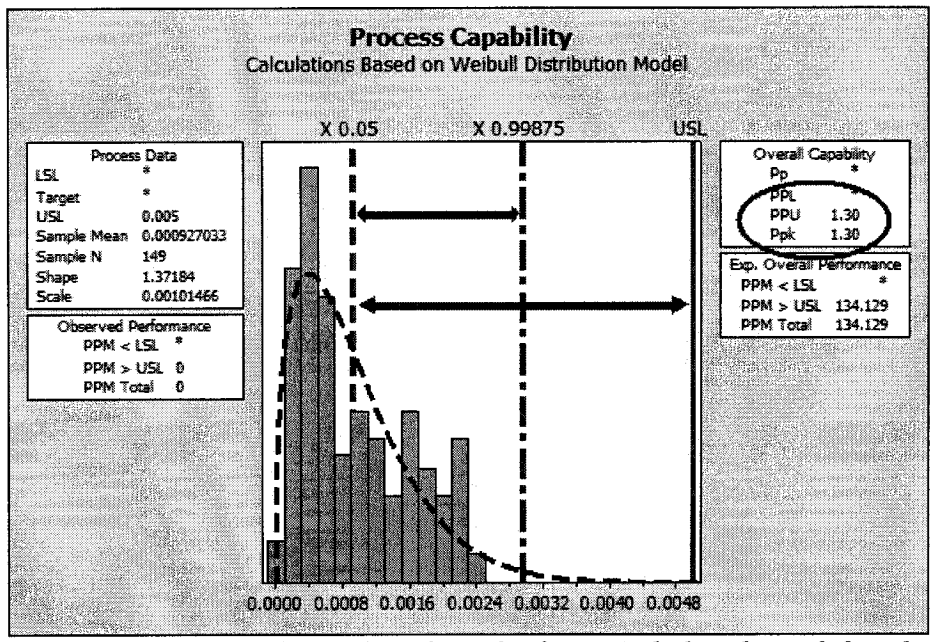

Figure 2.8 Example of Minitab graph and results for a Weibul unilateral distribution.

M. Pillet, S. Rochon, and E. Duclos [6] propose the use of a generalization of the C_{pm} index for unilateral distribution. Using different examples of C_{pm} calculations and interpretations for unilateral distributions they show its advantage over the C_{pk} index.
The C_{pm} index (Equation 2.2) is calculated by Minitab [7] with Taguchi's loss function.

$$C_{pm} = \frac{USL - T}{\frac{toler}{2} \times \sqrt{\frac{\sum_{i=1}^{n}(X_i - T)^2}{n-1}}}$$

Equation 2.3

Where:

USL = Upper specification limit.

T = Target value

Toler = Sigma tolerance, Minitab uses 6

C_{pk} and C_{pm} will be used to evaluate PWC turbine shafts manufacturing process. As a rule, a process that is in control has a $C_p > 1.33$.

The study was done on all shafts of the turboprop and turbofan engines produced by PWC between 1999 and 2003. The dimension studied is the deepest measured runout of the drilled hole. As you could observe in table 2.2 major quality problems are present during the manufacturing of turbofan and turboprop engines.

Table 2.1 Process capability study of complex shafts manufacturing

	jt15	pw100	pw150	pw308	pw500
Cpm	1.04	1.25			
Cpk		1.18			

Cp > 1.33
1 < Cp < 1.33
Cp < 1

We could also observe in Figure 2.9 that there wasn't any appreciable evolution of the measured runout through the past five years for the PW150 shaft, for which we have the most data.

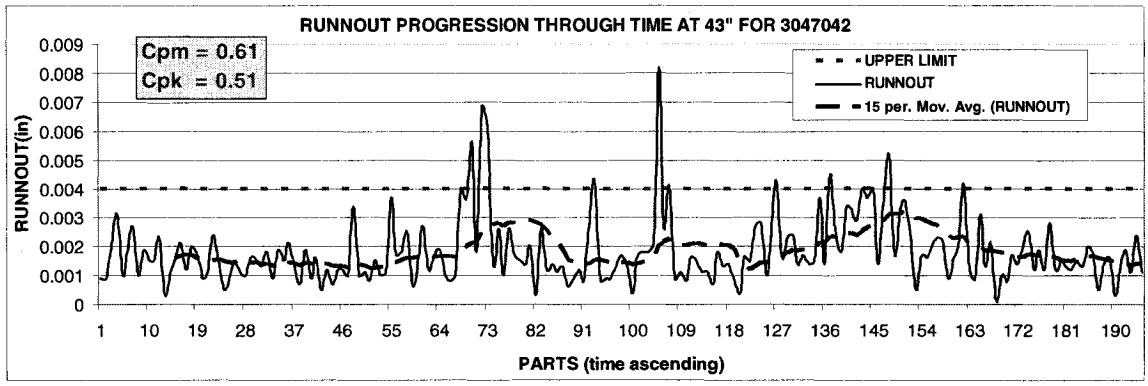

Figure 2.9 Runout in function of ascending time for the PW150 engines

Figure 2.10 shows the runout capability index as a function of the depth for the PW308 shaft, which is used through this thesis to evaluate and understand the press straightening method. As presumed in Chapter 2.3.1 the deeper the measure is taken the worst is the runout.

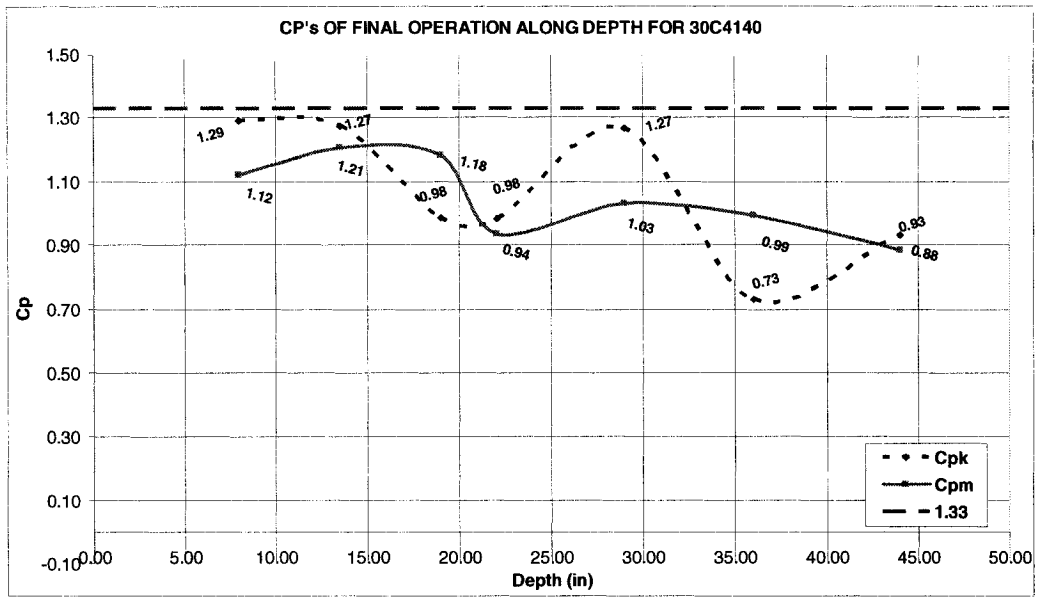

Figure 2.10 Capability index evaluated along the depth

Figure 2.11 shows the effect of the recentering done at PWC. We can see that when recentered, the runout is more uniformly distributed over the shafts length, therefore reducing the runout at the end of the hole where it is the hardest to stay inside the tolerance.

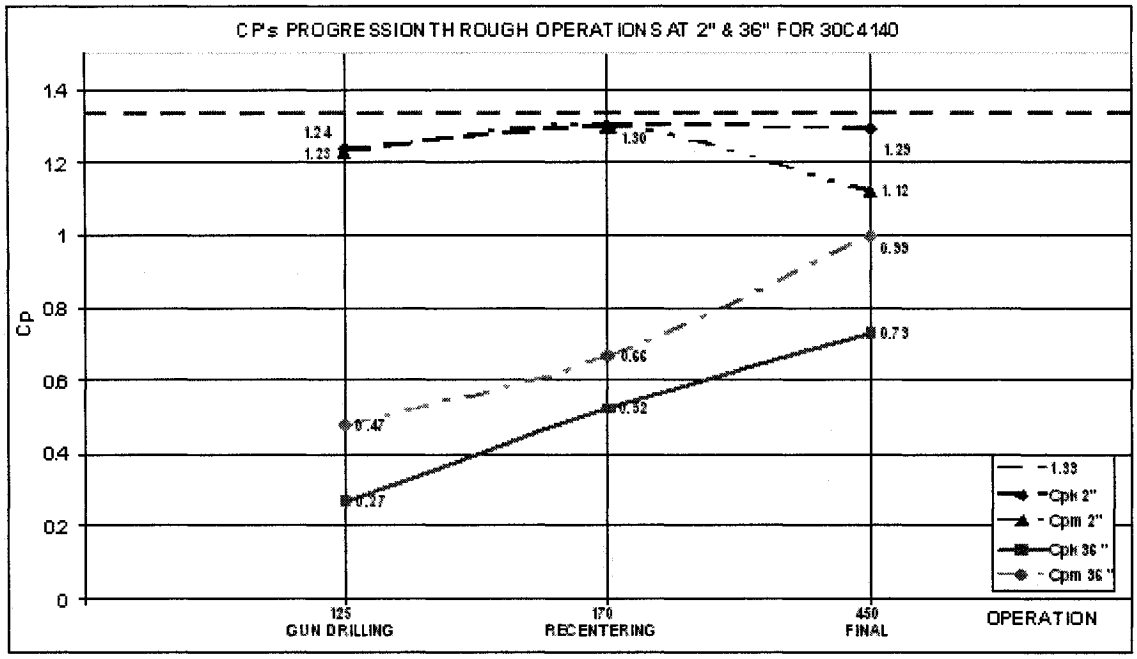

Figure 2.11 Capability index progression through operations, evaluated at 2" and 36"

Straightening equipments combined with concentricity correction should give a high control of the final shape of shafts. This would ideally allow PWC to produce shaft's for which the capability index would be way over the 1.33 limit.

2.5 *Costs associated to shape errors*

There are many costs associated with shape errors. The most obvious is the fact that shape errors create scraps. The cost off the scrap depends on the operation at which the error is detected. Another cost of shape errors could be associated to the manufacturing cost to obtain the tolerances that we wanted to achieve. In the past years, money was invested to improve the straightness of the shafts by improving the manufacturing process. The gun drilling of holes was improved by investing in the design of more stable drill heads. Then the use of concentricity correction improved significantly the concentricity between the outer and inner diameters. Grinding which is a costly operation is also mostly used to correct the outer diameter runout and straightness errors.

Figure 2.12 shows how straightening equipments could produce shafts more then within tolerance and therefore give the possibility of relieving the tolerances for gun drilling and reducing the amount of material to be removed during the grinding operations. The first line shows the different operations and their generated errors (Err). On the right is shown how these errors add up for an uncorrected process (Err uncor) and a corrected one (Err cor). The uncorrected one generates a total error that is out of tolerance by ΔErr_{OT} and the corrected one generates a total error within tolerance which gives a ΔErr_{res} that can be used to relieve other processes.

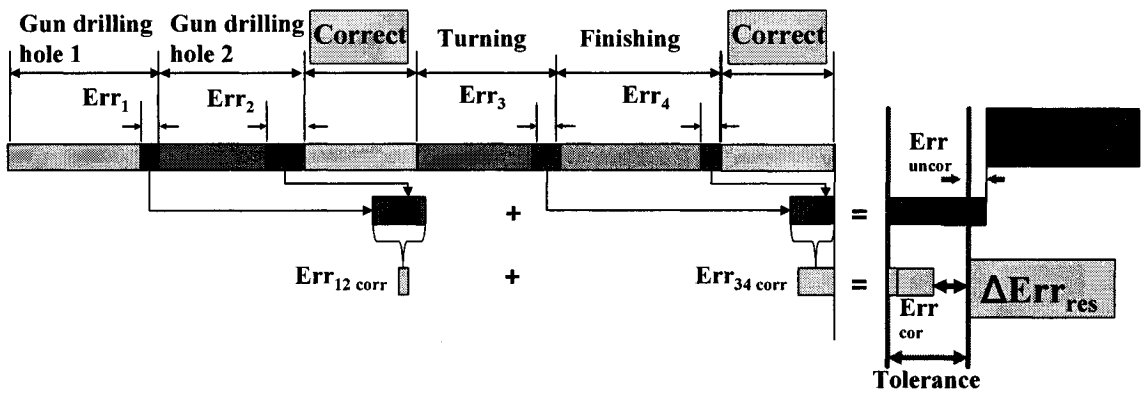

Figure 2.12 Effect of having an in process straightening correction

We could also include in the cost of having shape errors the cost of doing the high speed balancing operation, which compensates for the imbalance created by the shape errors. Straightness and concentricity errors create an imbalance of mass because the center of gravity of each section does not lie on the center of rotation of the shaft. When the shaft is rotating at high speeds, this imbalance creates non uniform centrifugal forces and therefore deflects the shaft (Figure 2.13). Since the components of the motor are fairly close to each other (~0.1 in) a high speed balancing process is done on the finished shafts to counterbalance this deflection.

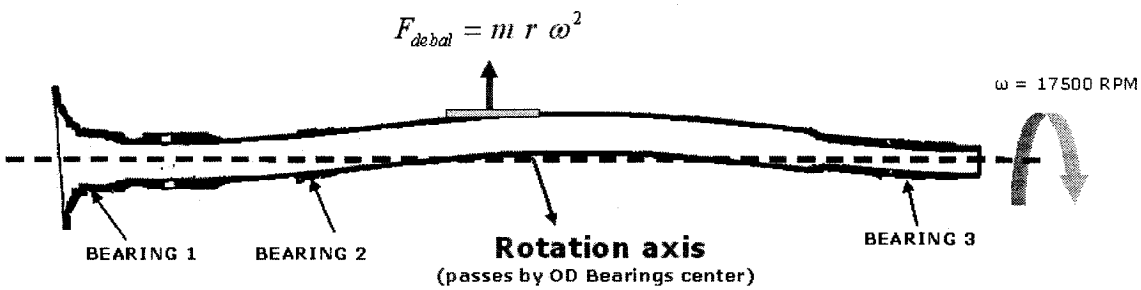

Figure 2.13 High speed balancing

For this reason, it would be advantageous to straighten the shaft and make the center of gravity of each section correspond with the center of rotation of the shaft. This would on one hand make the shafts easier to balance and reduce the shafts vibration.

Chapter III: Straightening methods and principles

3.1 Manufacturing of shafts

3.1.1 PWC's shaft manufacturing process

The actual process used by PWC to manufacture shafts is shown in Figure 3.1

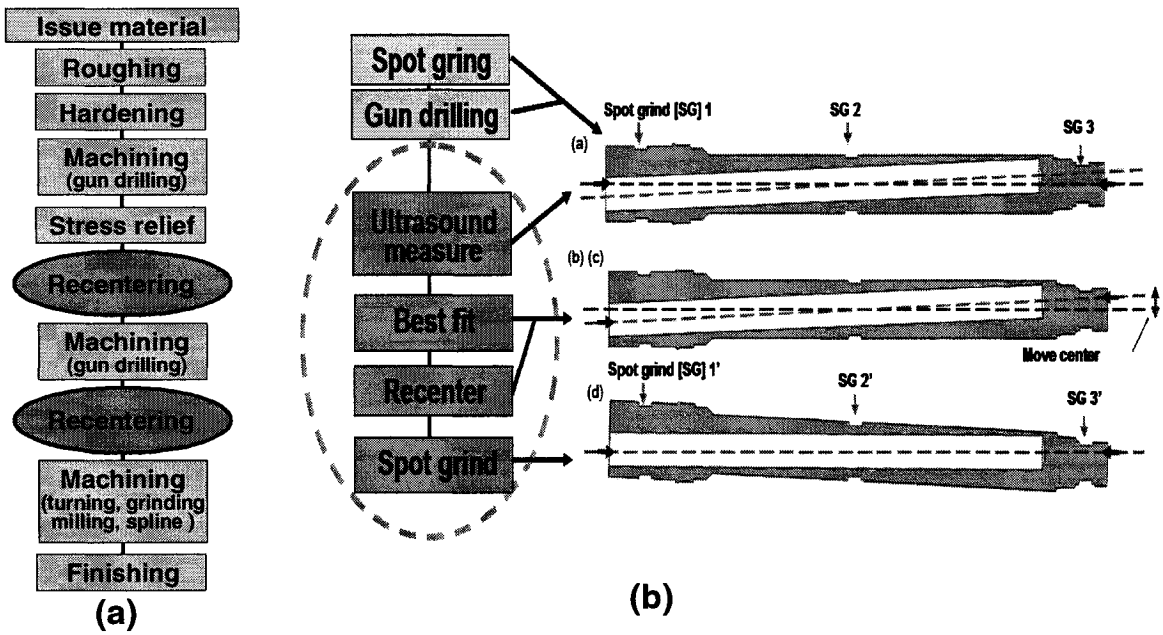

Figure 3.1 (a) PWC shaft manufacturing process (b) Recentering process

The recentering process (Figure 3.1b) was included in the PWC process in the end of the 1990's to help manufacture concentric shafts. The recentering process consists in:
(a) Measuring the shaft's eccentricity at reference spot grinded positions along the length.

The shaft is placed on an ultrasound measuring machine (Figure 3.2). The ultrasonic probe measures the wall thickness at every 10 degrees for each of the spot grinded reference section. Since this reference sections are grinded the OD of all the sections is considered perfectly cylindrical. Using the wall thickness measures the equipment

returns, for each of the reference sections, the eccentricity of the ID in respect to the centerline of the OD.

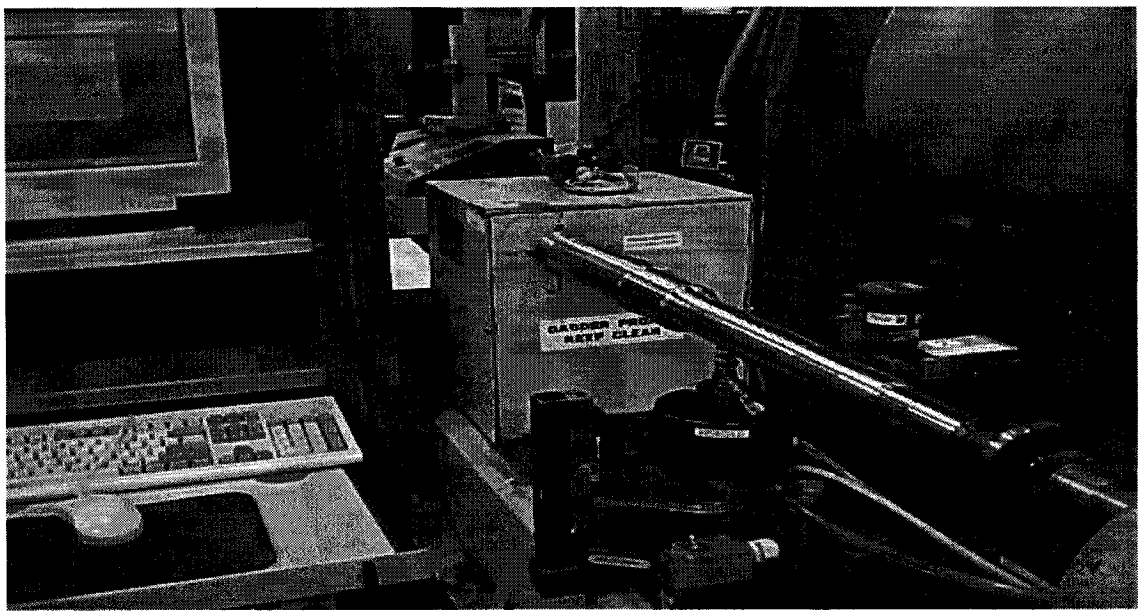

Figure 3.2 ultrasound measuring machine

Figure 3.3 shows the eccentricity of each measured section along the length.

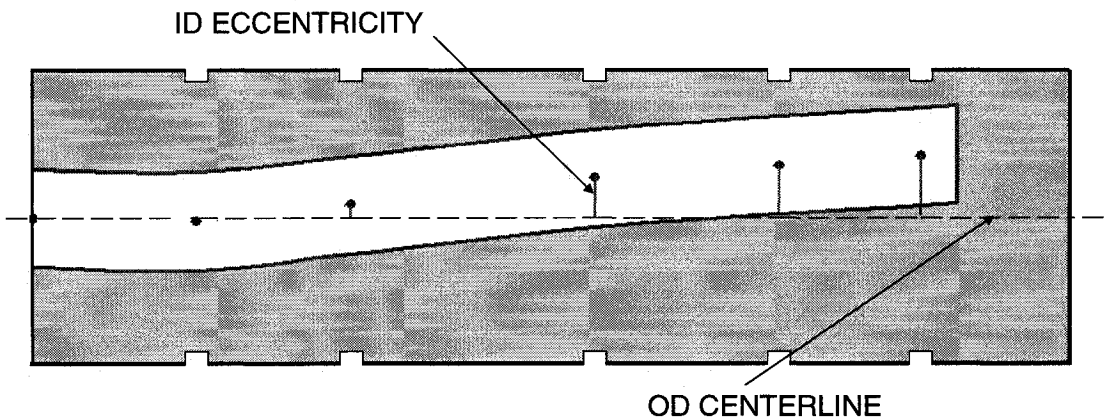

Figure 3.3 ID eccentricities measured along the length

(b) A best fit line is calculated through the measured eccentricities (Figure 3.4).

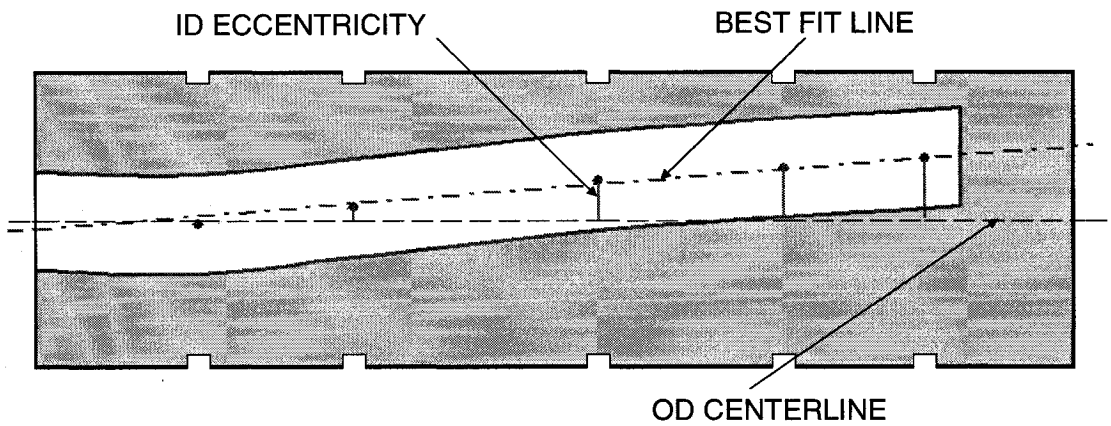

Figure 3.4 Best fit line going through the measured ID eccentricities

(c) The program then returns the amount of offset for the OD centerline to coincide with the ID best fit line (Figure 3.5).

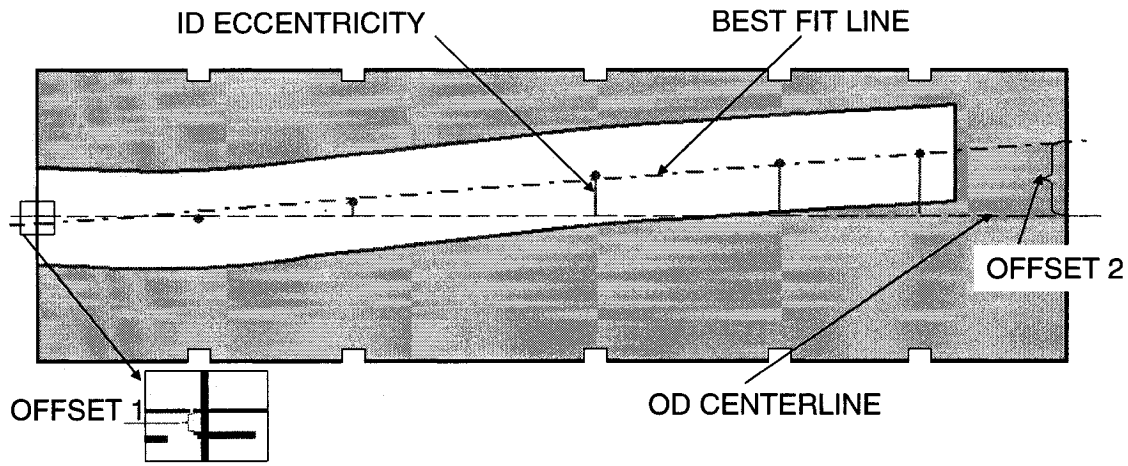

Figure 3.5 Offset between the ID best fit line and the OD centerline

(d) The OD is then machined to follow the ID best fit line by using the calculate offset in step (c) (Figure 3.6).

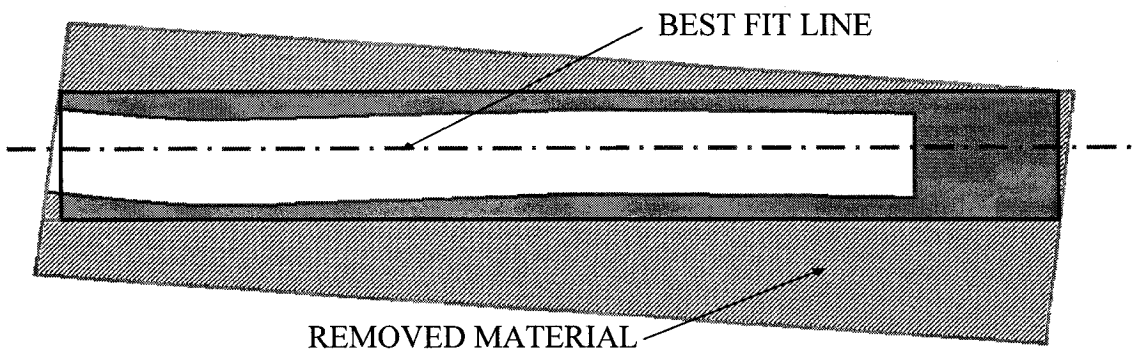

Figure 3.6 Machining of the OD to follow the ID best fit line

(e) The final result is an OD centerline that follows the ID best fit line, therefore minimizing the ID eccentricity in respect to the OD (Figure 3.7).

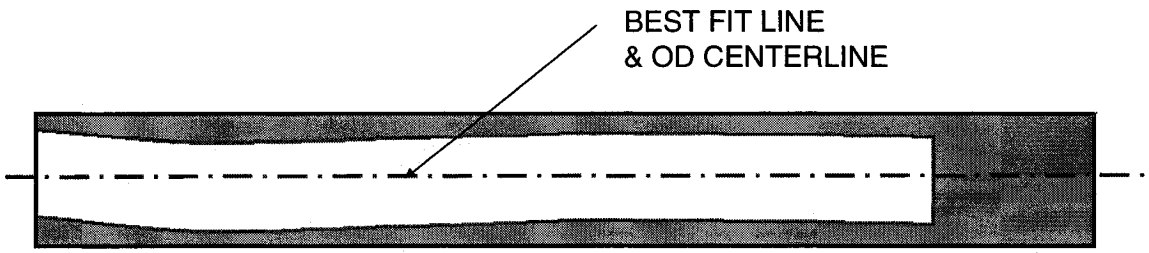

Figure 3.7 Final result of the recentering process

The recentering method therefore permits a correction of the eccentricity of the hole by ensuring that the ID best fit line coincides with the OD centerline. But this method isn't capable of correcting a banana shaped hole because the best fit line would already coincide with the OD centerline (Figure 3.8).

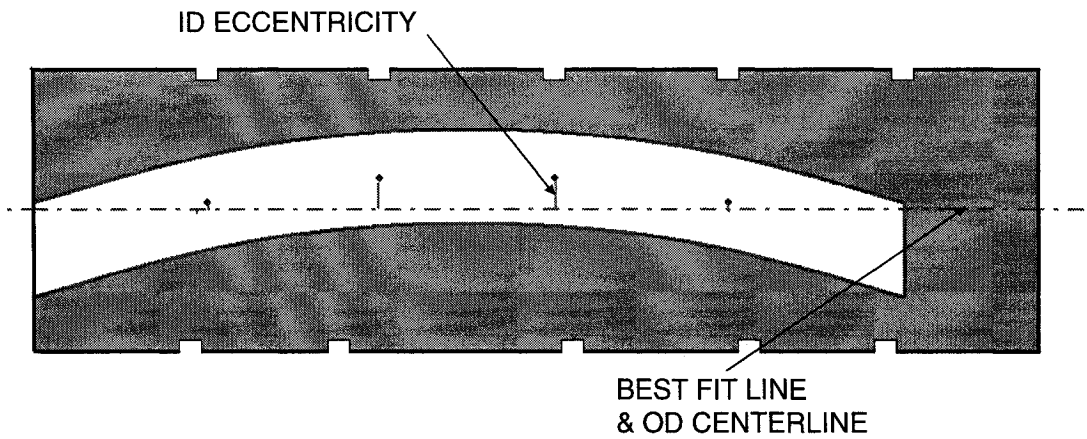

Figure 3.8 Banana shape hole uncorrectable by the recentering process

3.1.2 Competitor's shaft manufacturing process

The process shown below is that of a PWC supplier.

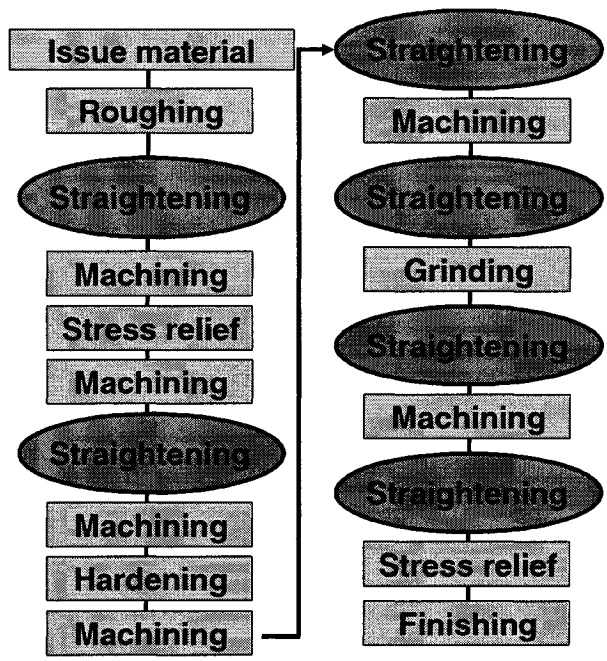

Figure 3.9 Competitor's shaft manufacturing process

As Figure 3.9 shows, the supplier straightens the shaft after almost every manufacturing operation and finishes it by a stress relief.

3.1.3 Proposed process

The process shown in Figure 3.10 represents how straightening could be introduced to the PWC process.

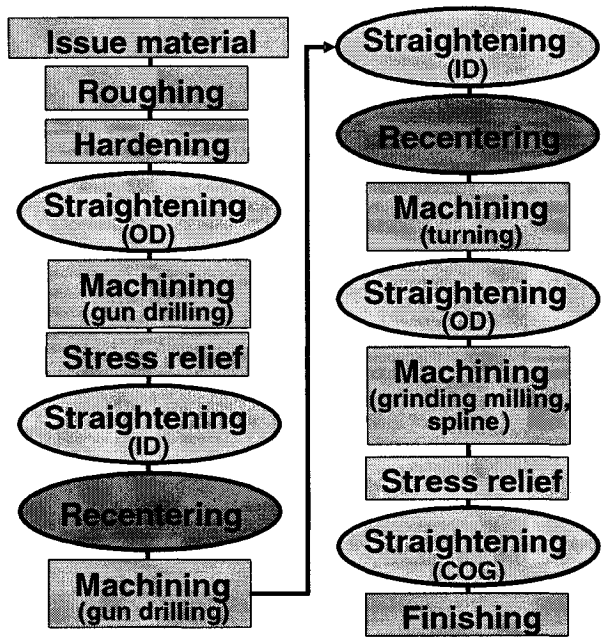

Figure 3.10 Proposed shaft manufacturing process

In this process a distinction was made between three types of straightening process:

1- Straightening of the outer diameter (OD) used after the roughing, allows removing more material at the roughing operation since less material needs to be left for the recentering process. When used before the grinding, straightening permits to relieve the grinding process because the OD's runout will be closer to its tolerance.

2- Straightening of the inner diameter (ID) is used together with the recentering to ensure that the ID and OD are concentric.

3- Straightening of the center of gravity (COG) is used at the end of the manufacturing of the shaft to ensure that the COG of each measured section is on the axis or rotation of the shaft.

3.2 Straightening principles

The two studied solutions are based on two close but different principles that are exposed in the following sections.

3.2.1 Plastic deformation by bending

The press straightening principle is based on a three point plastic bending (Figure 3.11). The part is supported at 2 points and a force is applied at a third point. This force is applied until the shaft starts to deform plastically and then the force is released.

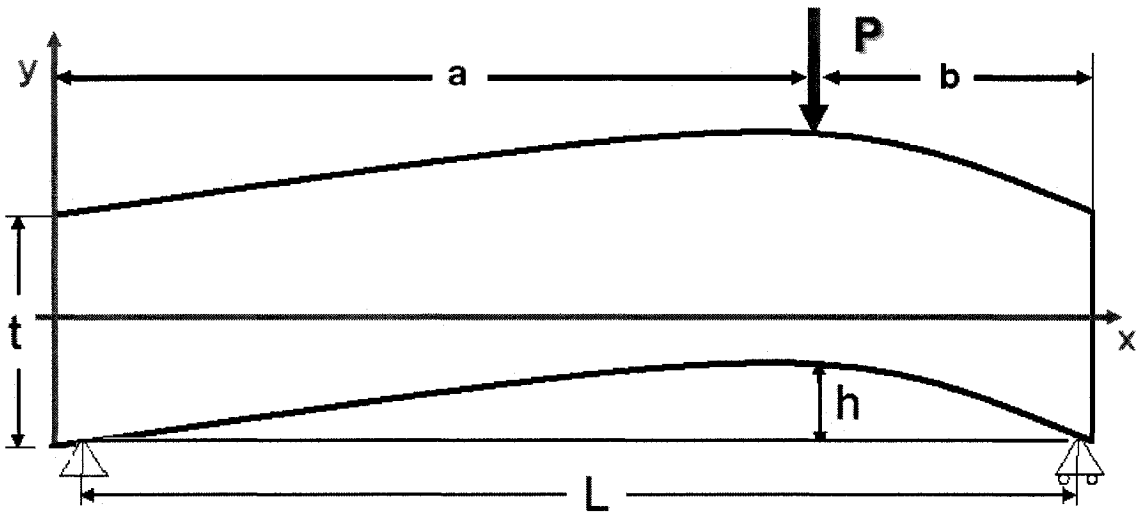

Figure 3.11 Three point bending principle for press straightening

The loading unloading cycle as well as the final deflection is represented in Figure 3.12.

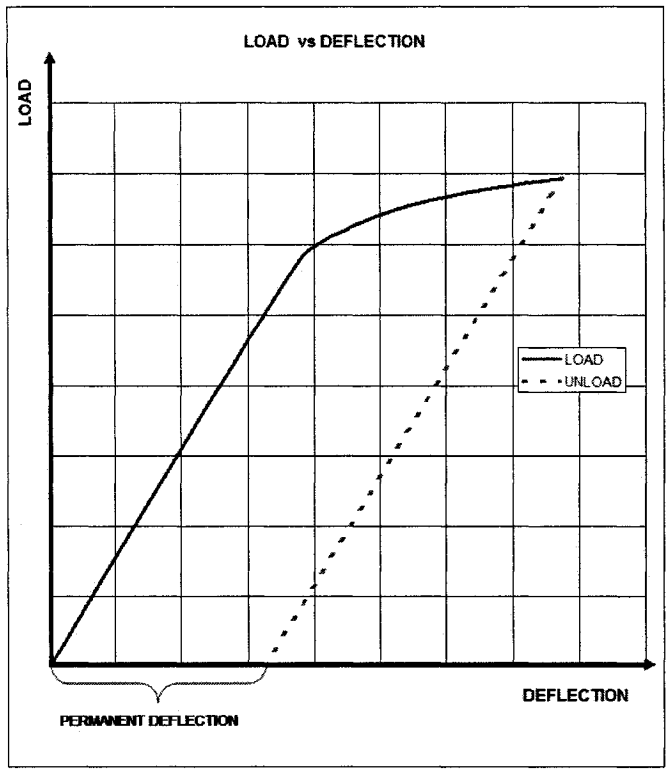

Figure 3.12 Load vs deflection for 3 point bending

When loading a part of constant Young modulus and inertia, the momentum along the length is calculated by Equations 3.1 and 3.2.

$$M_a = \frac{P \times b \times x}{L} \qquad for\ 0 < x < a \qquad \textit{Equation } 3.1$$

$$M_b = \frac{P \times a \times (L - x)}{L} \qquad for\ a < x < L \qquad \textit{Equation } 3.2$$

Where:

M_a, M_b = Bending moment in section a and b respectively (lb x in).

P = Applied load (lb)

a, b = Distance between load and supports (in)

L = Distance between supports (in)

x = Distance from 1st support at which the bending moment is evaluated (in)

The stress along the length is calculated by equations 3.3 and 3.4.

$$\sigma_a = \frac{P \times b \times x \times y}{L \times I} \qquad for\ 0 < x < a \qquad Equation\ 3.3$$

$$\sigma_b = \frac{P \times a \times (L-x) \times y}{L \times I} \qquad for\ a < x < L \qquad Equation\ 3.4$$

Where:

σ_a, σ_b = Stress (psi)

I = Inertia (in^4)

y = Height from center at which the bending moment is evaluated (in)

To reach plasticity, the stress must be higher than the elastic limit Se, which should not be confused with the yield strength Sy (stress for which you would already have 0.2 % of plastic deformation).

$$\sigma = Se \qquad Equation\ 3.5$$

Replacing σ_a, σ_b of equation 3.3 and 3.4 in 3.5, it is possible to draw the curves bordering the plastically deformed region of equations 3.6, 3.7.

$$y_a = \frac{L \times I \times Se}{P \times b} \times \frac{1}{x} \qquad for\ 0 < x < a \qquad Equation\ 3.6$$

$$y_b = \frac{L \times I \times Se}{P \times a} \times \frac{1}{(L-x)} \qquad for\ a < x < L \qquad Equation\ 3.7$$

This gives a plastically deformed region of the shape shown in Figure 3.13.

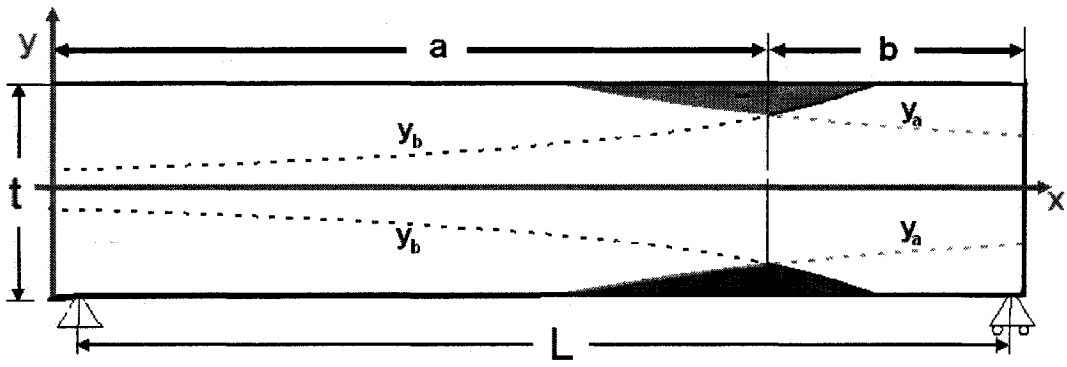

Figure 3.13 Shape of plastically deformed region by 3 point bending

To better understand what happens to the material during the loading and unloading a spring model is showed in Figure 3.14.

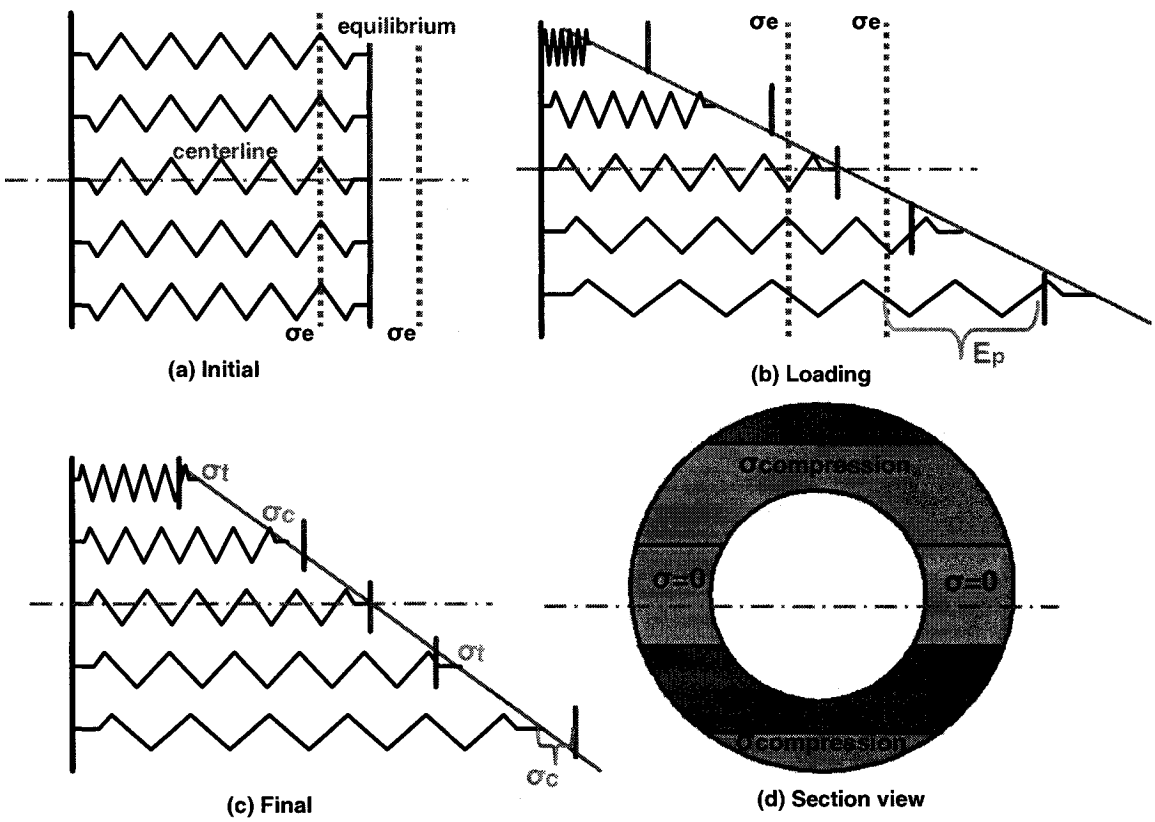

Figure 3.14 Spring model illustrating stress induced by 3 point bending

The spring are initially at equilibrium Figure 3.14a and when the load is applied on the top the upper spring get compressed and the lower ones stretch Figure 3.14b. The loading results in plastic deformation of the springs which implies that the equilibrium position is displaced. When the load is released the springs go to an equilibrium position Figure 3.14c. At this position a tensile (σ_t) and compressive (σ_c) residual stress is generated. For the plastically loaded section of the shaft, the residual stress configuration is shown in Figure 3.14d.

3.2.2 Residual stress by peening

With peening, a thin layer of residual stress can be created on the surface of the shaft. This residual stress is equivalent to a force applied at the peened surface along the axial direction (Figure 3.15). This creates a moment equal to the force times the distance of the peened surface from the centerline of the part. The bending moment creates a curvature on the shaft and therefore a permanent deflection that bends the shaft

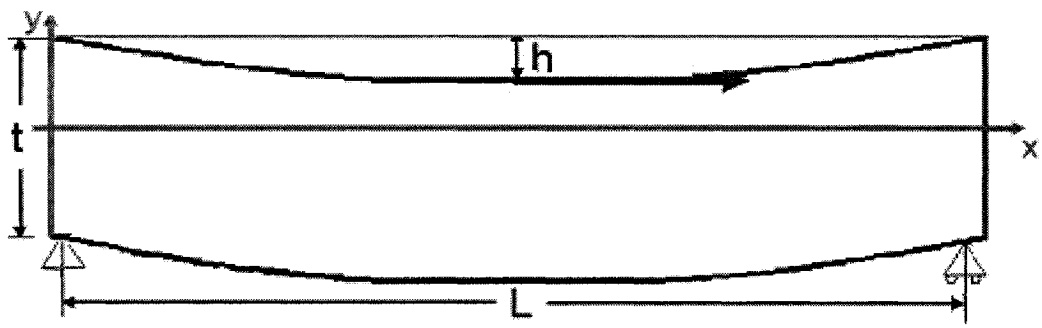

Figure 3.15 Principle of straightening using residual stress created by peening.

A peened shaft will have residual stress profile similar to the one showed in Figure 3.16. The upper part represents the residual compressive stress created by the peening. The lower part represents the compressive residual stress created by the bending of the part.

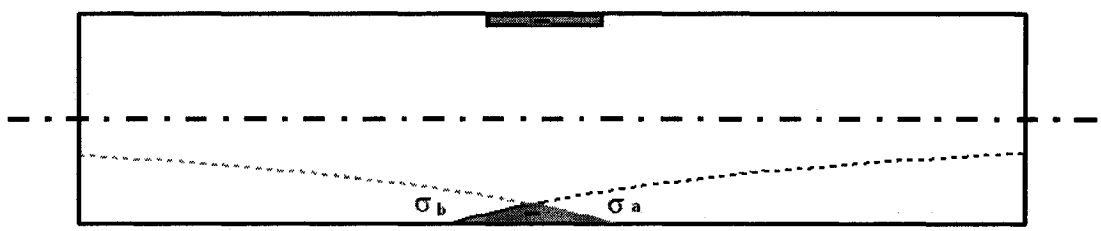

Figure 3.16 Residual stress created when straightening by peening.

The obvious advantage of peen straightening over press straightening is that press straightening induces undesirable tension residual stress but peen straightening only creates compressive residual stress that should improve the fatigue life of the shaft.

Chapter IV

Analysis and improvement of a precision press straightening equipment for turbine engine shafts

Since the existing press straightening equipments are mainly used for automotive parts which are over-dimensioned, the straightening process is not optimized. For turbine engine shaft we need to minimize the number of straightening points and insure that the part still meets the engineering specifications.

To be able to optimize the existing press equipment, a finite element model was developed to simulate the press straightening process. Before simulating different press configuration the finite element model was first validated.

4.1 Finite Element Modeling

4.1.1 Part

The part modeled is a PW308 shaft after its second hole was drilled. The shaft is modeled as a cylinder with three outer steps and two holes as in Figure 4.1.

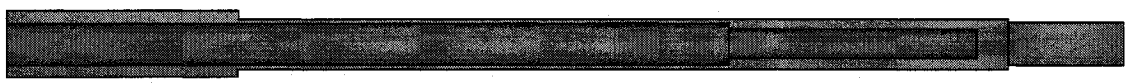

Figure 4.1 Solid model of the shaft

To model the actual shaft, the measures of eccentricity of the inner diameter (ID) relative to the outer diameter (OD) were used to model the holes by removing a volume created via the extrusion of a circle trough the centerline. The centerline was modeled by a Bspline passing through the measured points on the shaft.

4.1.2 Machine

The supports (Figure 4.2a) are modeled by contact surfaces attached to a point on the center of the shaft. The press is modeled by a linear force (Figure 4.2b) applied on the nodes in the direction X and Y to simulate a load normal to the shaft surface.

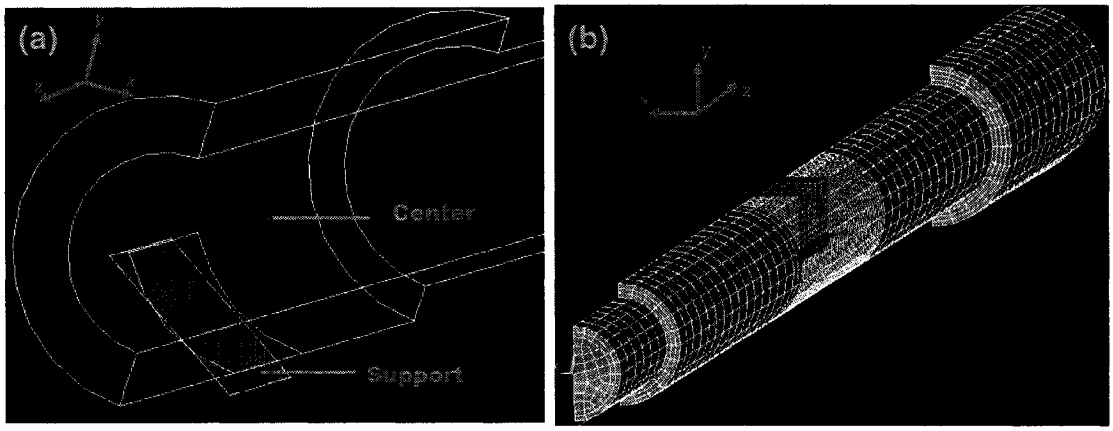

Figure 4.2 Support (a) and force (b) finite element modeling

4.1.3 Material

The material is CPW 245 (Figure 4.3) and its data comes from the PWC database, used at 70 degrees Fahrenheit. It is a nonlinear material model with isotropic hardening.

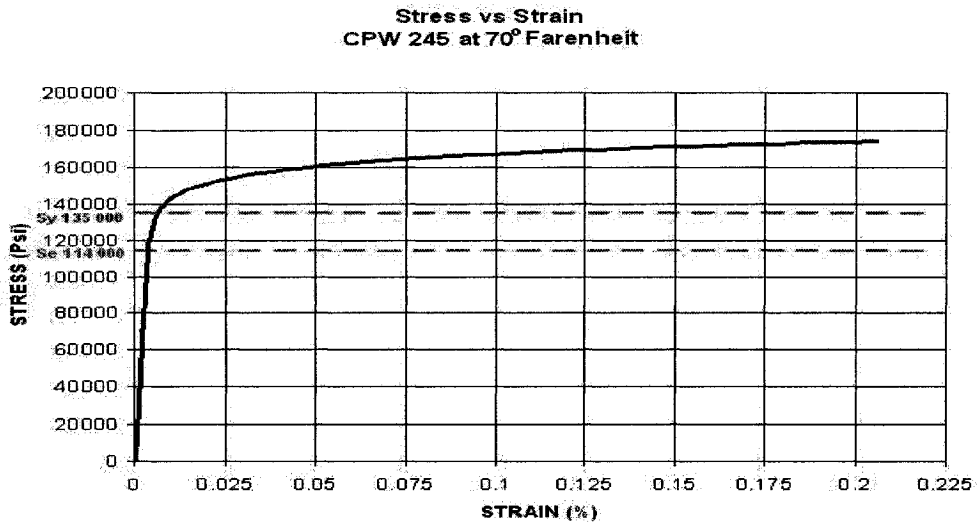

Figure 4.3 Stress vs Strain curve for CPW245 at 70° F

4.2 Model validation

4.2.1 Mesh convergence

To choose the optimal size of the elements used to model the shaft, a mesh convergence study was carried out. The finite element model results where compared with a theoretical result obtained by the area moment method explained by A. BAZERGUI [33]. The results were for a semi finished PW308 engine shaft after the second gun drill with the supports at the two edges and with the force applied in the middle (Figure 4.4).

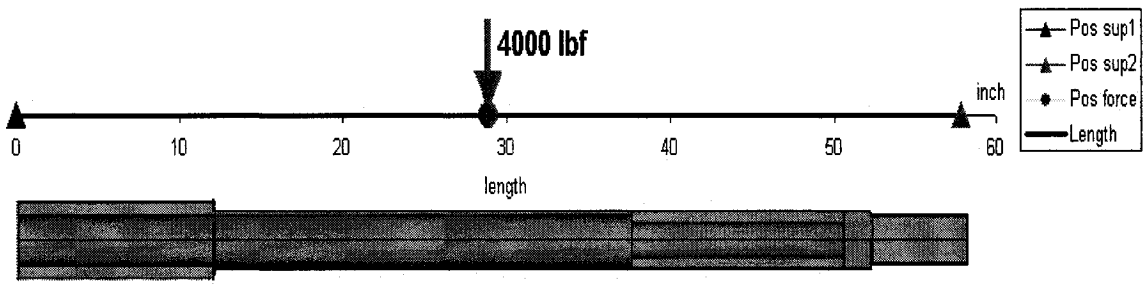

Figure 4.4 Configuration used for the finite element mesh convergence study

4.2.1.1 Theoretical value

Since the shaft's section varies, the deflection under the loading was evaluate by the area moment method with an elastic material with modulus = 0.307E+08 Psi. The shaft is divided in 5 sections of constant inertia (Figure 4.5) and a curve of M/EI is drawn (Figure 4.6).

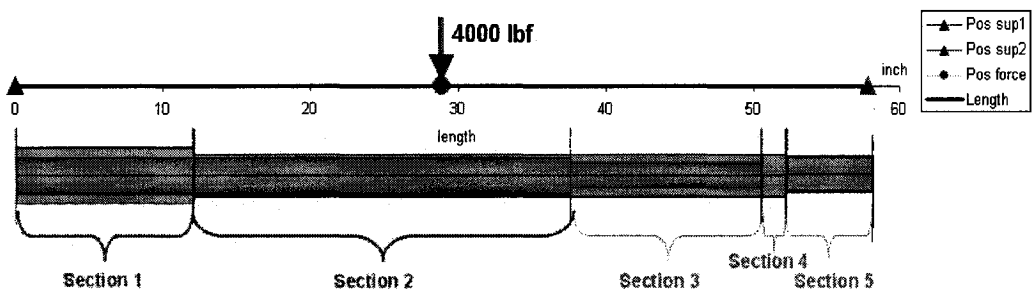

Figure 4.5 Split shaft in sections of constant inertia

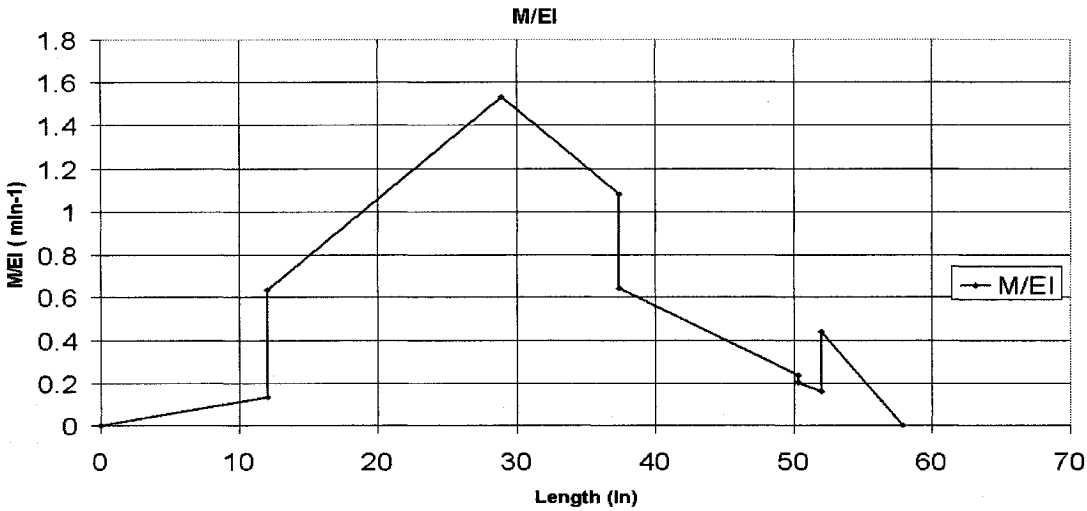

Figure 4.6 Area moment graph

Where:

M = Bending moment (lb x in)

E = Elastic modulus (psi)

I = Inertia (in^4)

Then the deflection is calculated at L/2 with Equation 4.1 of area moment.

$$\delta_{L/2} = \left[A_{under}\frac{M}{EI}\right]_0^{L} \times \bar{X}_L \times \frac{L}{L/2} - \left[A_{under}\frac{M}{EI}\right]_0^{L/2} \times \bar{X}_{L/2}$$

Equation 4.1

Where:

$\left[A_{under}\frac{M}{EI}\right]_0^{L}$ = Area under the area moment curve between x= L and 0 (in^{-1})

$\bar{X}_L$ = Centroïd of the area moment curve between x= L and 0 (in)

$\left[A_{under}\frac{M}{EI}\right]_0^{L/2}$ = Area under the area moment curve between x= L/2 and 0 (in^{-1})

$\bar{X}_{L/2}$ = Centroïd of the area moment curve between x= L/2 and 0 (in)

$\delta_{L/2}$ = Deflection at L/2 (in)

Figure 4.7 shows a graphical representation of the area moment equation.

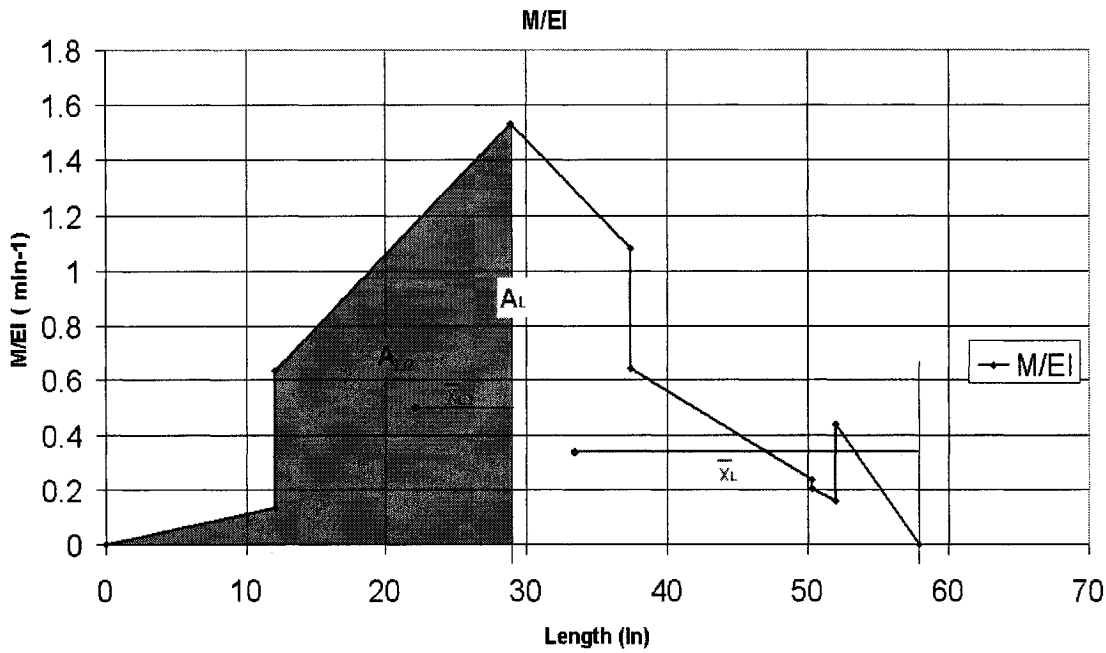

Figure 4.8 Graphical representation of the area moment equation

Solving equation 4.1 gives

$$\delta_{L/2} = A_L \times \overline{X}_L \times \frac{L}{L/2} - A_{L/2} \times \overline{X}_{L/2} = 0.3854 \text{ Inch}$$

Equation 4.2

For the axial stress Sz we have

$$\sigma_{L/2} = \frac{M_{L/2} \times OD_{L/2}}{2 \times I_{L/2}} = 62000 \text{ Psi}$$

Equation 4.3

4.2.2 Finite element results

The program used to do the finite element model (Figure 4.9) is ANSYS 6.1. To examine the convergence of the mesh, three mesh parameters were modified: the number of elements over the circumference (Ndiv Circ), the number of elements in the thickness (ndiv thick) and the size of element along the length (length).

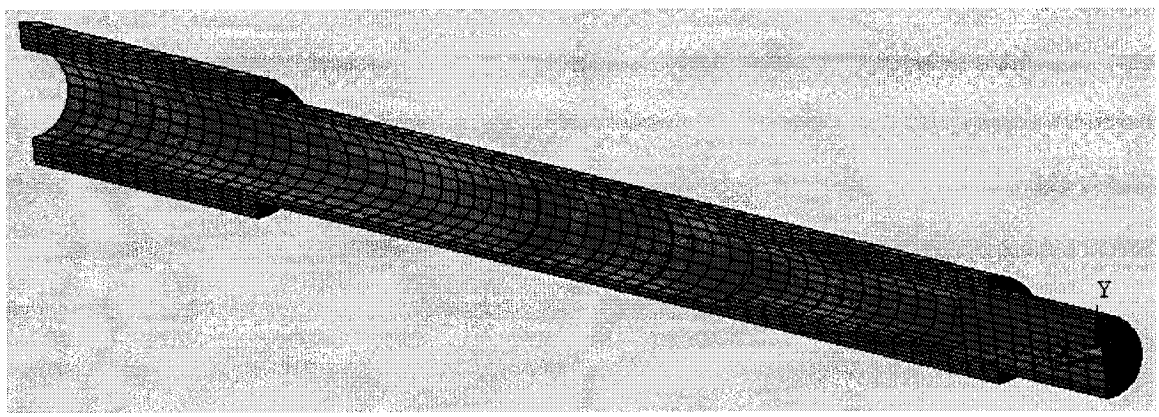

Figure 4.9 Meshed shaft

The study was made on three different type of mesh:

- SOLID45 is defined by eight nodes having three degrees of freedom: translations in the nodal x, y, and z directions.

- SOLID95 is a higher order version of the SOLID45 and is defined by twenty nodes having three degrees of freedom: translations in the nodal x, y, and z directions.

- SOLID185 is defined by eight nodes having three degrees of freedom at each node: translations in the nodal x, y, and z directions. It uses the selective reduced integration method to prevent from mesh locking and is the recommended type of element for use in nonlinear analysis in the ANSYS documentation.

4.2.3 Results when the shaft is under elastic loading

The analyzed results for each type of mesh are: time of calculation, displacement and axial stress of the lowest point at L/2. The results are summarized in Table 1.1

Table 4.1 Result summary of the Finite Element Model, elastically loaded

			SOLID 95			SOLID 185			SOLID 45		
ndiv circ	ndiv thick	ndiv length	time (s)	deflection Uy(In)	stress Sz(psi)	time (s)	deflection Uy(In)	stress Sz(psi)	time (s)	deflection Uy(In)	stress Sz(psi)
6	2	4	46	0.3895	55704	10	0.4264	62337	10	0.4261	60702
6	2	2	18	0.3893	55528	4	0.4196	61878	7	0.4255	60859
6	2	1	10	0.3889	55402	3	0.3972	59910	2	0.4237	61191
6	4	4	134	0.3896	55637	19	0.4269	62472	18	0.4263	60667
6	4	4	68	0.3893	55487	9	0.4200	62040	11	0.4257	60803
6	4	1	35	0.3889	55396	4	0.3975	60117	5	0.4239	61134
6	8	2	174	0.3893	55478	21	0.4201	62123	20	0.4257	60762
12	4	2	256	0.3893	54733	25	0.3906	57212	25	0.3977	56403
12	4	1	103	0.3888	54728	13	0.3698	55330	13	0.3965	56923
24	4	1	398	0.3888	54683	33	0.3570	54444	33	0.3900	55357
variation (% of min)				0.2	1.6		19.6	14.7		9.3	10.5

Table 4.1 shows that the SOLID95 gives very stable results (the deflection is within 0.2% and the stress is within 1.9 %, of the minimum value) and a displacement within 1% of the theoretical values. The inconvenient of using SOLID95 elements is that it's time consuming.

We can also see that for mesh types SOLID185 and SOLID45, using Ndiv Circ = 6 doesn't give good results because the area is underestimated (Figure 4.10). This is not the case for mesh type SOLID95 because it is uses 20 nodded elements that represent more closely the area.

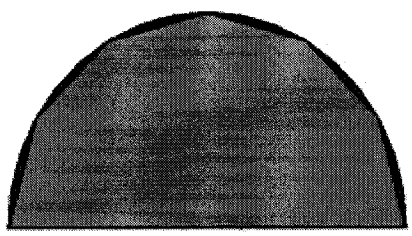

Figure 4.10 Area of the meshed shaft with Ndiv Circ =6

In Figure 4.11 to Figure 4.13 is illustrated the effect of modifying the number of division of the circumference and thickness as well as the length.

As stated above for mesh types SOLID185 and SOLID45, the effect of increasing Ndiv Circ is to rigidify the section because of the increase in effective area. Therefore increasing Ndiv Circ reduces the deflection (Uy) (Figure 4.11). But for mesh types SOLID95 the effect is negligible since it already represent closely the area with Ndiv Circ = 6.

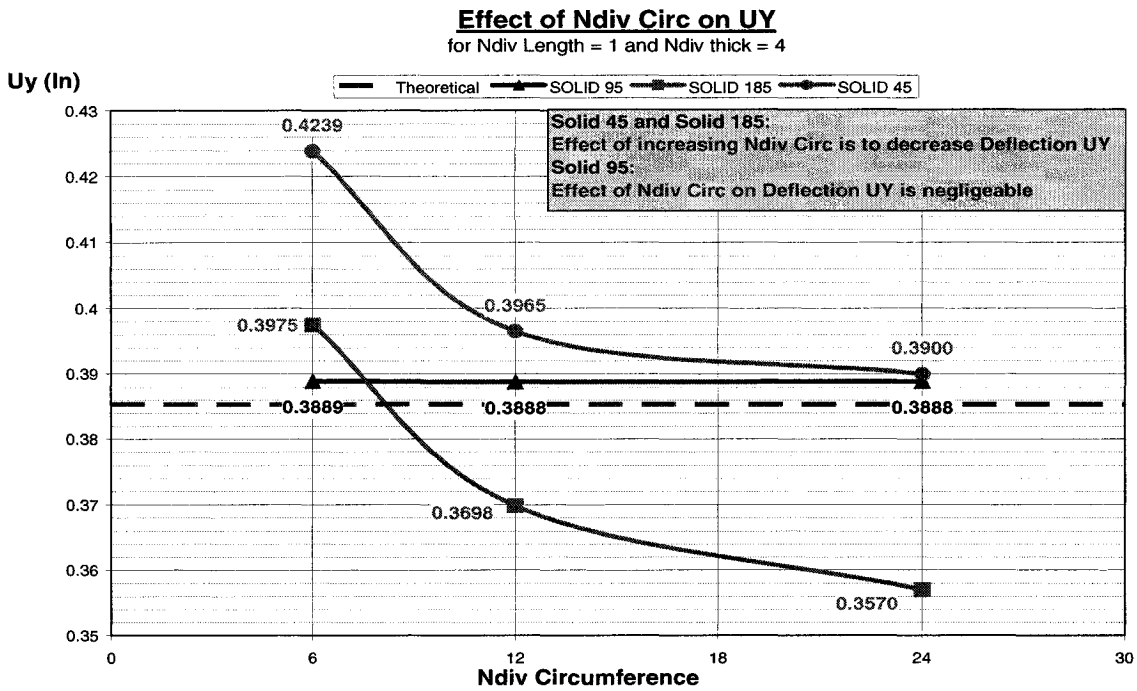

Figure 4.11 Circumference's number of divisions (Ndiv Circ) effect on deflection (Uy)

Figure 4.12 shows that increasing ndiv thick doesn't affect the deflection (Uy).

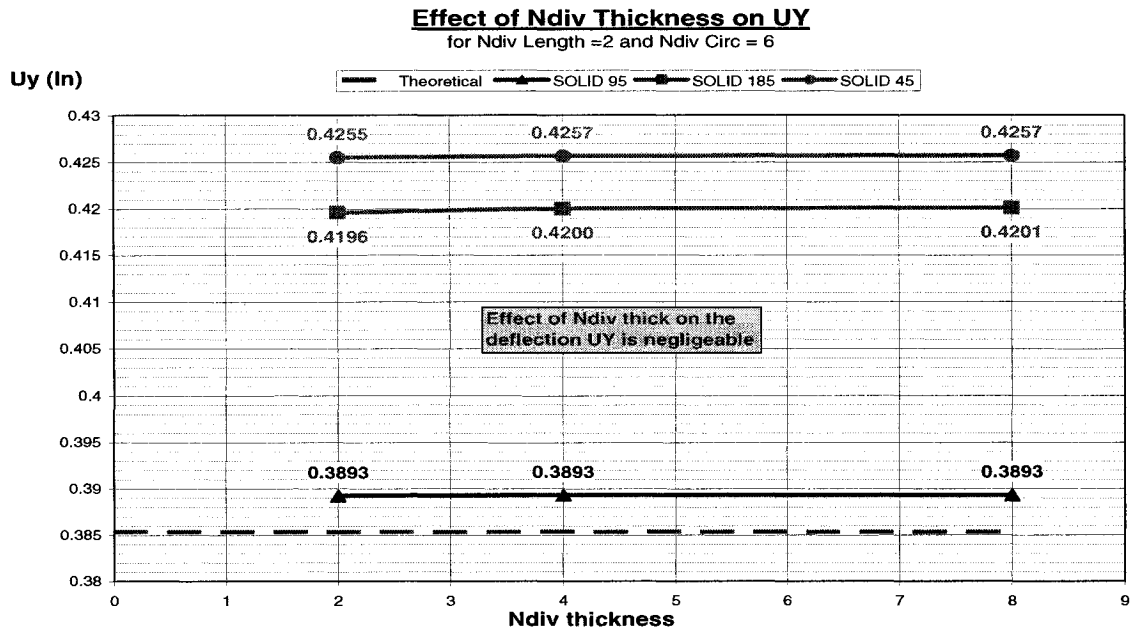

Figure 4.12 Thickness number of divisions (Ndiv thick) effect on deflection (Uy)

Figure 4.13 shows that the effect of diminishing the length is to increase the (Uy)

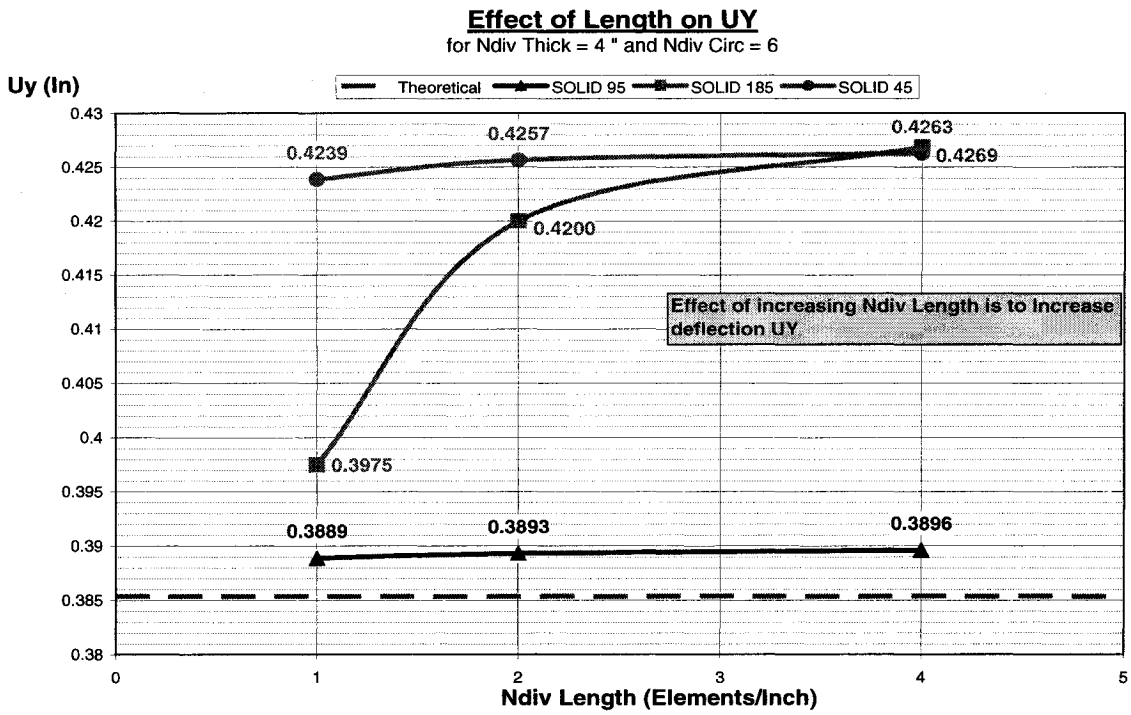

Figure 4.13 Length's effect on deflection (Uy)

4.2.4 Results when the shaft is under plastic loading

Plastic results were done using the same model but applying a load of 10000 lbf .
The results are tabulated in Table 4.2.

Table 4.2 Result summary of the Finite Element Model, plastically loaded

			SOLID 95				SOLID 185				SOLID 45			
ndiv circ	ndiv thick	ndiv length	time (s)	deflection Uy(In)	stress Sz(psi)	stress/in (ksi/in)	time (s)	deflection Uy(In)	stress Sz(psi)	stress/in (ksi/in)	time (s)	deflection Uy(In)	stress Sz(psi)	stress/in (ksi/in)
6	2	4	1521	0.0309	18273	591	123	0.0631	19438	308	150	0.0687	21083	307
6	2	2	805	0.0297	18233	614	62	0.0568	18623	328	76	0.0678	20868	308
6	2	1	265	0.0294	18101	616	31	0.0393	15618	403	39	0.0654	20828	319
6	4	4	-	-	-	-	308	0.0633	21128	334	373	0.0688	22529	328
6	4	2	2015	0.0298	18893	633	141	0.0570	20256	355	173	0.0678	22283	329
6	4	1	771	0.0294	18764	638	66	0.0395	17311	439	81	0.0654	22235	340
6	8	2	6047	0.0299	19236	644	334	0.0571	21082	369	395	0.0678	23005	339
12	4	2	9555	0.0314	18707	595	427	0.0311	17074	550	471	0.0368	18824	511
12	4	1	4022	0.0301	18646	620	194	0.0214	14225	666	216	0.0355	18043	508
24	4	1	-	-	-	-	558	0.0199	14266	716	627	0.0307	17416	567
variation (% of min)				7.0	6.3	8.9		217.9	48.5	132.3		123.8	32.1	84.7

Table 4.2 shows that the variation of the deflection and stress using SOLID95 is still within 10 % of the minimal value, but for SOLID185 and SOLID45 the variation goes up to 218%. These errors for SOLID45 and SOLID185 are probably due to the same reasons as stated in the elastic analysis. The SOLID95, although giving reliable results won't be retained because of its excessive computation time. The stress for the SOLID185 is always higher than the SOLID45 and both give good results for Ndiv Circ higher than 6. SOLID185 will be used for the rest of the study because its higher stress will be acting as a bonus security factor.

Then a study using a fine mesh under the loading zone for the SOLID185 elements is done to look for an efficient meshing that gives results close to the ones from the SOLID95 finest mesh which result are of Uy = 0.0314 Inch and Sz = 18707 Psi.

The results in Table 4.3 show that the fine mesh works well in elastic but still has variations in plastic loading. The last two columns give the percentage of error considering the SOLID95 finest mesh, described above, as the comparison value.

Table 4.3 Result summary fine meshing using type SOLID185

					Elastic		Plastic					Error (%)	
ndiv circ	ndiv thick	ndiv length	ndiv thick fine	ndiv length fine	deflection Uy(in)	Stress Sz(psi)	deflection Uy(in)	Stress Sz(psi)	permanent deflection Uy(in)	Residual Stress Sz(psi)	stress/in (ksi/in)	permanent deflection Uy	Residual Stress Sz
12	2	1	2	1	0.3758	56346	0.96324	123870	0.02496	13962	559	-20.5	-25.4
			8	2	0.3791	57147	0.9769	123600	0.0304	17643	588	-3.3	-4.6
			16	4	0.3804	57344	0.9828	123440	0.0330	18698	573	5.0	1.0
12	2	2	2	2	0.3916	57424	1.0097	125140	0.0318	15687	494	1.2	-16.1
			8	2	0.3917	57146	1.0096	123580	0.0317	17864	563	1.0	-4.5
			16	4	0.3929	57348	1.0156	123430	0.0344	18922	551	9.4	1.1
12	4	2	4	2	0.3919	57242	1.0102	124130	0.0317	17113	540	1.0	-6.5
			8	2	0.3919	57149	1.0103	123580	0.0317	17857	563	1.1	-4.5
			16	4	0.3932	57350	1.0103	123580	0.0317	17857	563	1.1	-4.5
24	2	2	2	2	0.3844	56000	0.9885	122200	0.0282	15214	539	-10.2	-18.7
			8	2	0.3845	55422	0.9883	119910	0.0279	17372	623	-11.2	-7.1
			16	4	0.3857	55547	0.9939	119450	0.0303	18481	610	-3.5	-1.2

The configuration pointed by the arrow (Table 4.3) gives accurate results compared to the SOLID95 element and requires approximately 10 times less calculation time. Therefore it is this configuration that is going to be used throughout this study because it also has a high residual stress/deflection ratio (= 588), that means that the residual stress is higher for a same permanent deflection. For a future study that requires high precision, the use of SOLID95 element types is recommended.

4.3 Simulation of press straightening

A series a simulation were launched using the finite element model. These simulations were used to get a better understanding of the phenomenon behind the press straightening method, then to find the optimal parameters to design the prototype and finally as a verification of the controller.

4.3.1 Effect of modifying the length of force application

One of the most important parameter to take into consideration when designing a press straightening machine is on what length is the part going to be loaded.

Analysis where launched with length (Figure 4.14) varying from 0.5 to 5 inch.

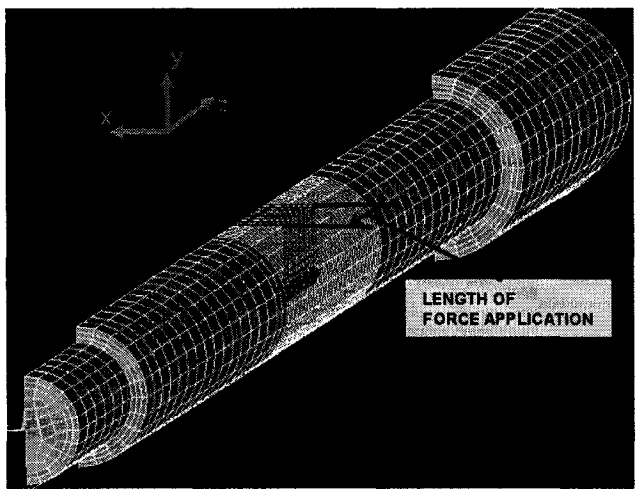

Figure 4.14 Length of force application

It was observed that for the same final deflection, the plastic deformation reduces as the length increases (Figure 4.15). A length of 3.5 inch was chosen for the prototype because the effect of the length on the plastic deformation was starting to stabilize and that length higher than 3.5 inch will reduce the number of regions on the shaft where a load could be applied.

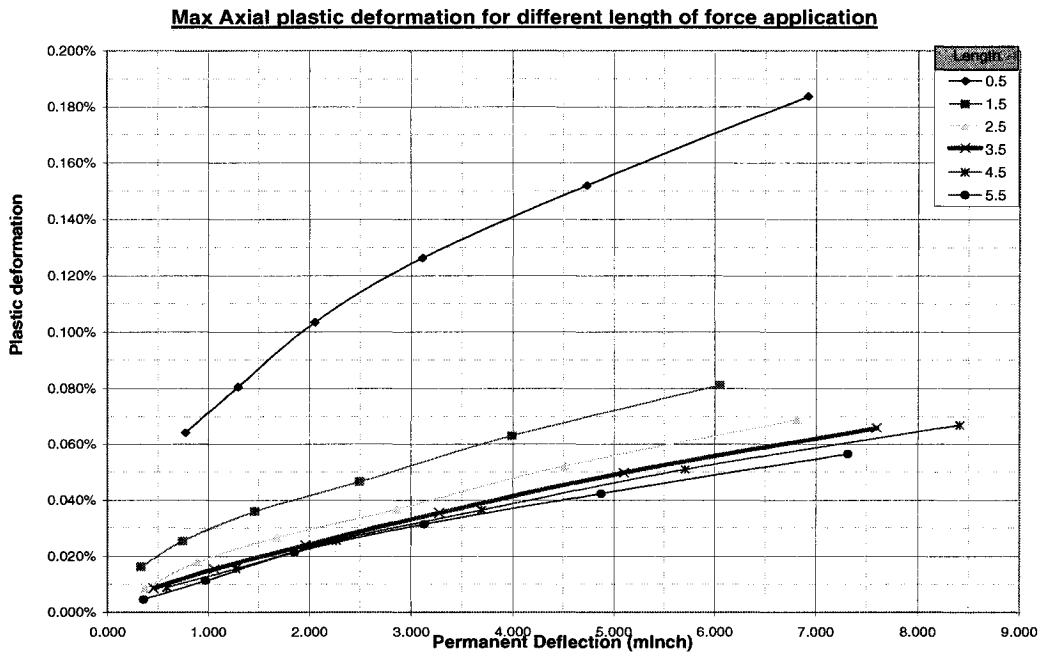

Figure 4.15 Plastic deformation for different length of force application

4.3.2 Effect of the force application contact shape

Another important parameter is the shape of the force application. Studies where done for a round shape with different depth, this showed that a round surface with a depth of at least 0.2 inch was the best option.

There is place for further studies to optimise the shape and material of the punch used for applying the load.

4.3.3 Effect of the initial eccentricity

An important study was to find out what are the effects of modifying the shape and amplitude of the initial eccentricity. For this study, simulations where done with three different models, each with a different initial eccentricity shape and amplitude (Figure 4.16).

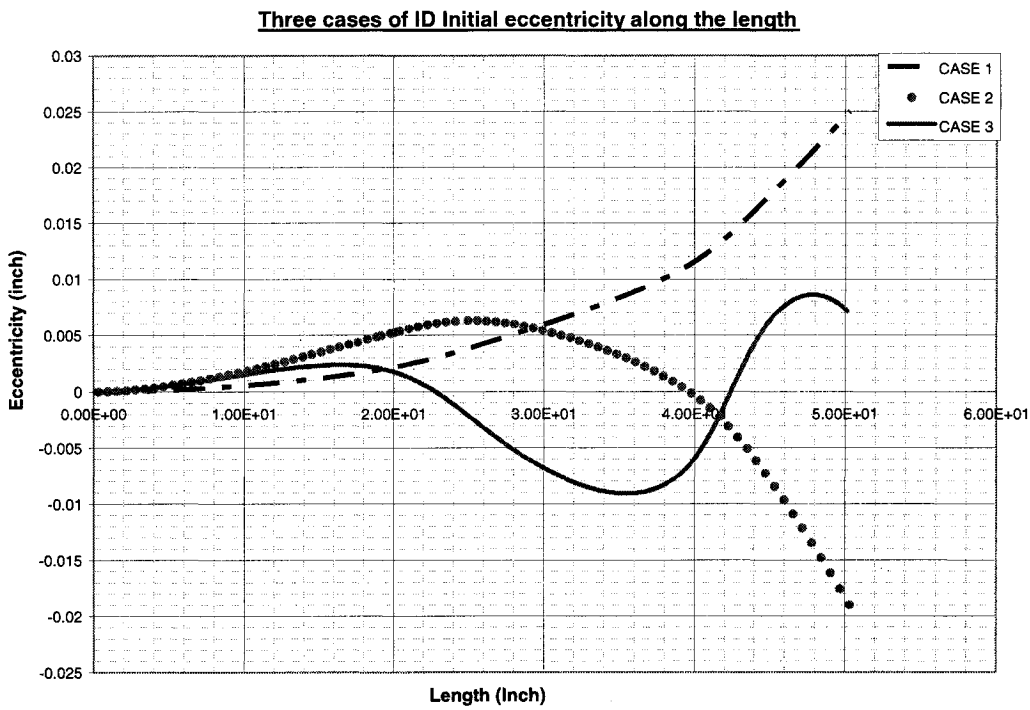

Figure 4.16 Three cases of ID Initial eccentricity

Figure 4.17 shows the permanent deflection for each model after being loaded in the same manner: meaning that the loading point, supporting conditions and loading force are the same.

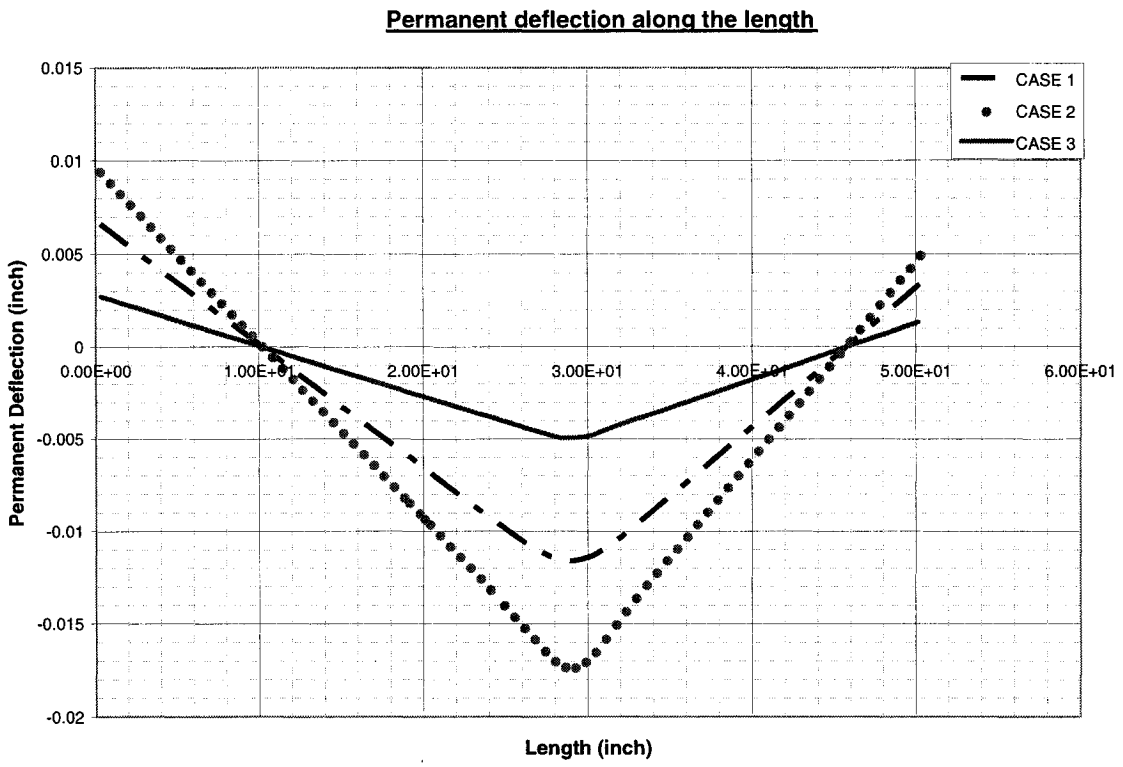

Figure 4.17 Permanent deflection along the length

Figure 4.18 shows the change ratios, which are defined as the permanent deflection at position X divided by the permanent deflection at X = 20 Inch.

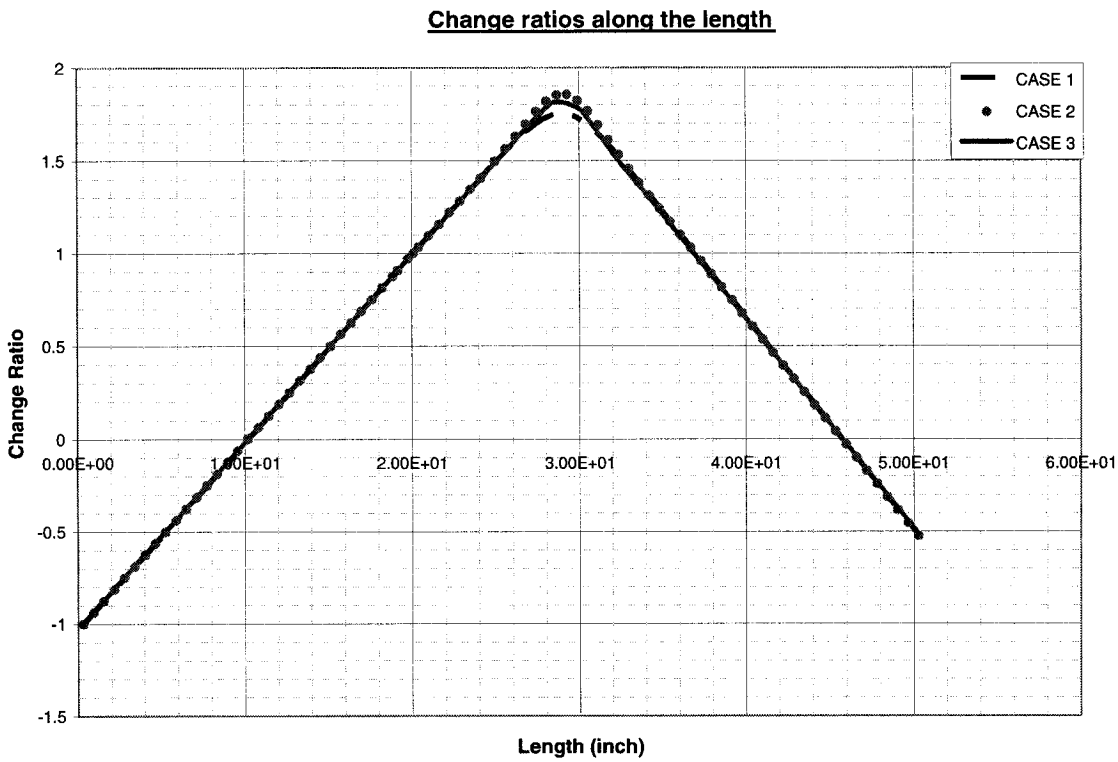

Figure 4.18 Change ratios along the length

The results show that although the maximum permanent deflection varied (Figure 4.17), the shape of the permanent deflection remained. By shape we mean that the change ratios (Figure 4.18), deflection of a point in respect to the loading point, are identical. The only variations are near the loading point and are of less than 5 % for the cases studied.

4.4 Design of prototype

4.4.1 Design scheme of the press straightening prototype

The diagram in Figure 4.19 illustrates how the press straightening prototype was designed to operate.

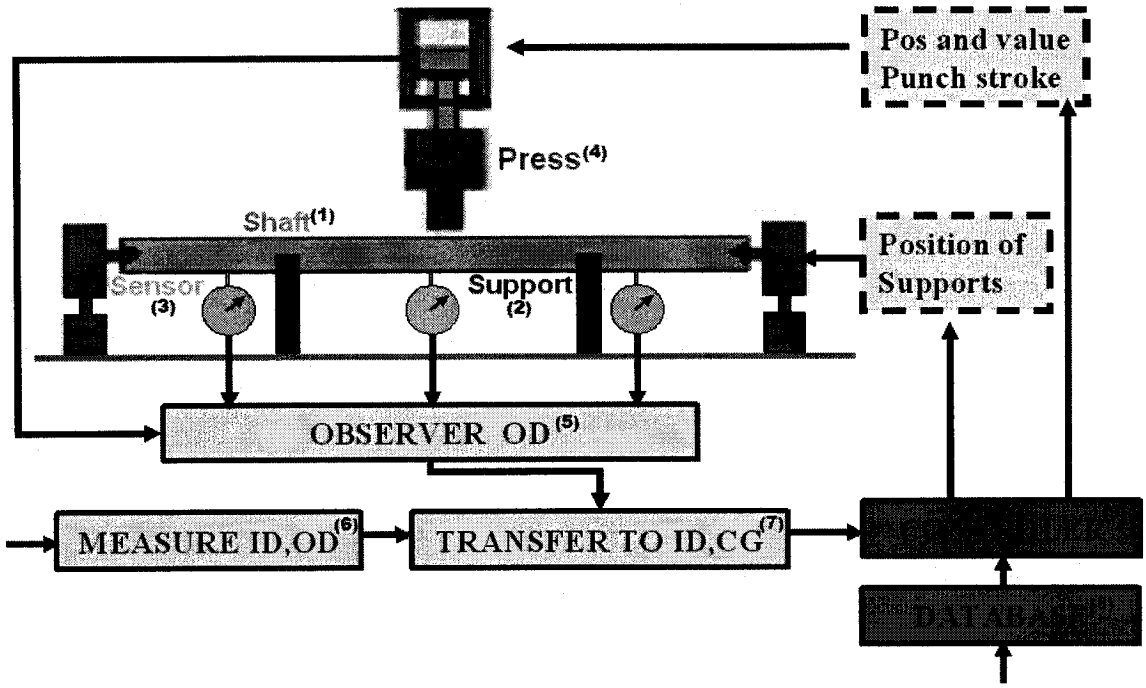

Figure 4.19 Design scheme of the press straightening prototype

The shaft (1) is placed on two supports (2) after the initial position of the inner (ID) and outer diameters (OD) are measured (6). The observer (5) measures the displacement of the OD in function of the load using sensors (3) placed along the shaft and a load cell on the press (4). Since the simplest is to control the shape of the OD, depending of the straightening desired (OD, ID or CG) the final desired shape is transferred (7) as a function of the shape of the OD. The controller (9) picks from the database (10) the best set of straightening commands to get the desired OD shape. All the components of the system are described below.

4.4.2 Press

The press used for the experiments is a stir welding machine from NRC (Figure 4.20). This equipment has the advantage of controlling the vertical displacements of the press.

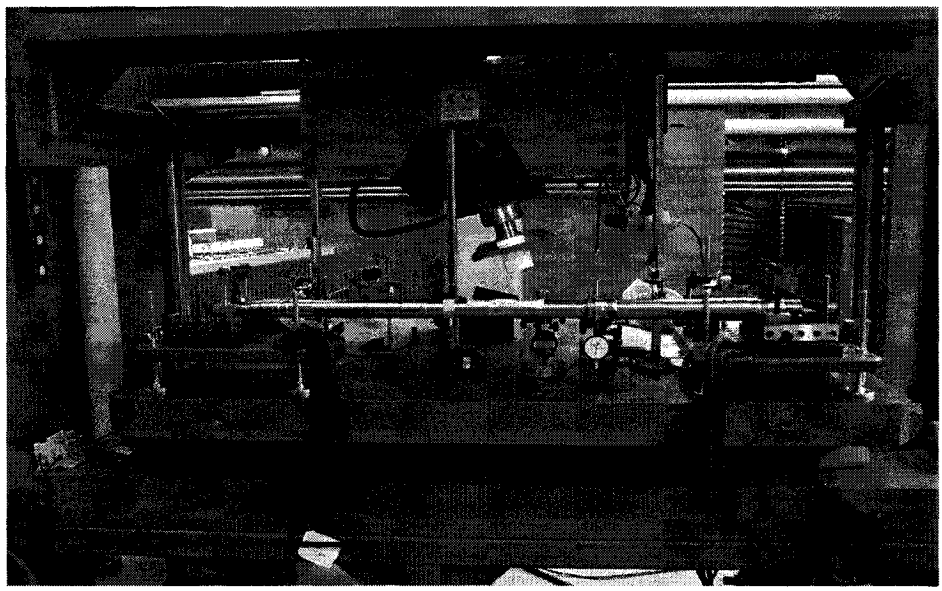

Figure 4.20 Setup shown on NRC's stir welding press

A punch was designed using the finite element results which showed that a length of 3.5 inch was ideal. Although the FEM results showed that a round shaped punch was to be used, the block shaped in a V(Vblock) (Figure 4.21 (1)) was used for the punch. This choice was done because the parts used for this preliminary experiment had different diameters, which made using a rounded shape punch to costly because it would require a different punch for each loaded diameter. The other advantage of using a Vblock is that a round shape could be added between the Vblock and the shaft for further experiments. The parts shown in Figure 4.21 (2) were designed by NRC to adapt the punch to their stir welding press.

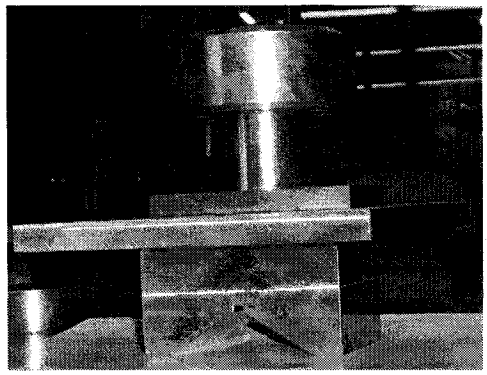

Figure 4.21 Punch adapted on the stir welding press

4.4.3 Supports

The supports length was chosen to be a 2 inch Vblock for the same reasons stated above for the press.

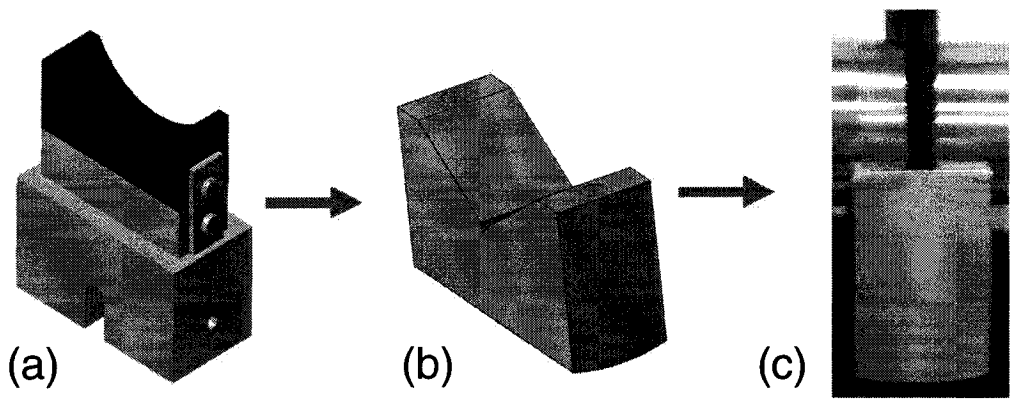

Figure 4.22 Design of the supports

The support was designed to insure that the shaft is least restrained in rotation which avoids stress concentration zones at the supports. The first design shown in Figure 4.22a was inspired by the equipments used on the market. It didn't restrain the shaft in rotation but it was a complicated system using over ten components. After studying the various other possible designs the support shown Figure 4.22b and c was the best solution because it was a one component easy to machine support. The supports were then produced at PWC (Figure 4.23).

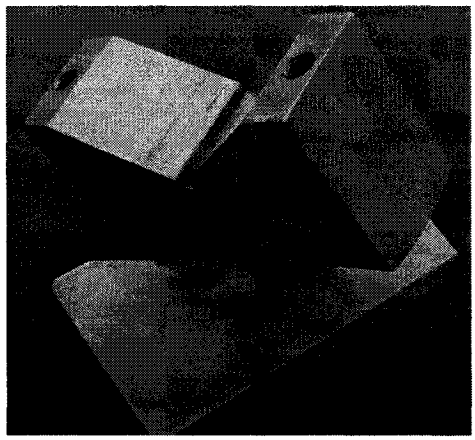

Figure 4.23 Machined supports

To ensure the shaft isn't restrained in rotation, the base of the supports is round. This allows the support to rotate when the shaft bends. The center of the round base is on the axis of the shaft so that there is not vertical movement of the center of the shaft at the supporting locations (Figure 4.24). This makes the analysis of measurements easier because the measures taken would be directly the deflection of the shaft without having to correct for vertical rigid body motion at the supports.

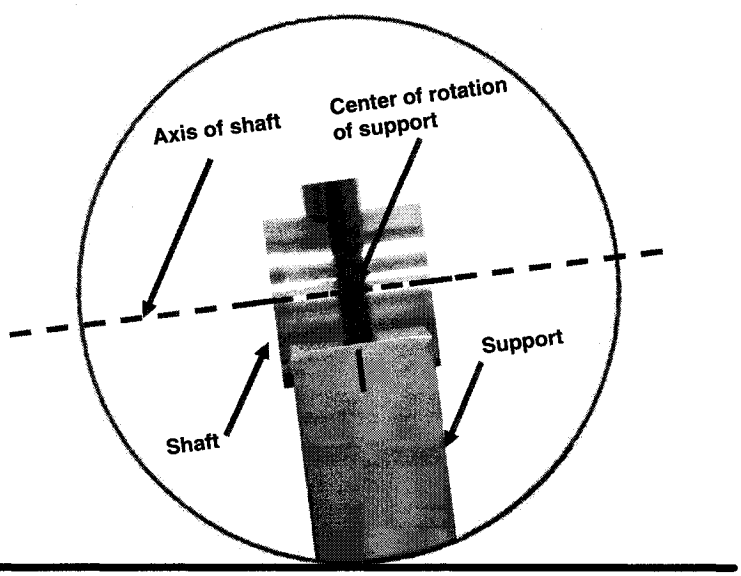

Figure 4.24 Center of rotation of the supports

The module shown in Figure 4.25 was assembled to control the lateral displacement of the supports as well as the shaft's rotation.

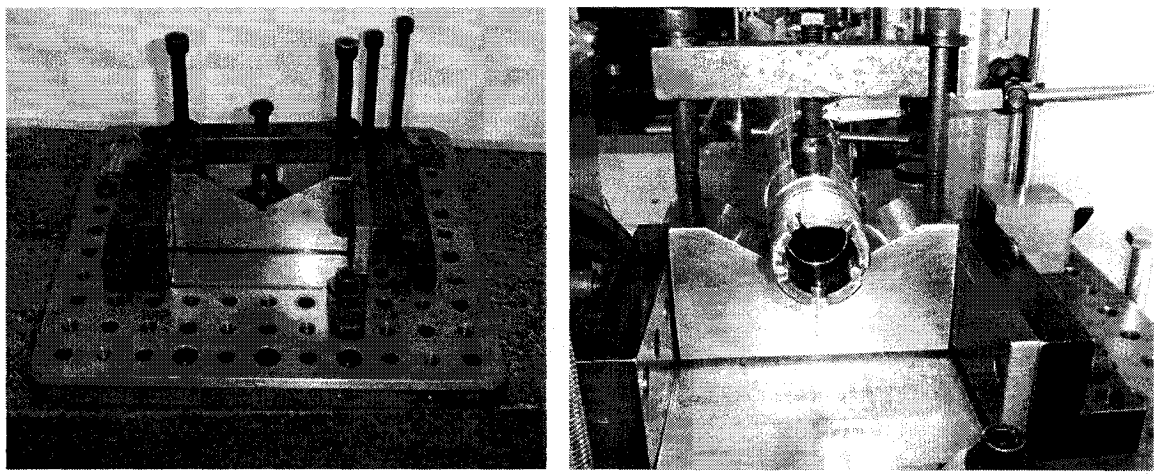

Figure 4.25 Module used to limit the support's lateral displacement and shaft's rotation.

4.4.4 Sensors

The sensors are used to measure the deflection during the loading and unloading process at different position along the shaft. For the prototype a first attempt done by NRC was to have a laser sensor (Figure 4.26a) mounted on a slider (Figure 4.26b). This solution was rejected because the accuracy we were looking for was better than the one of the laser and that the error generated by displacing the laser was too large.

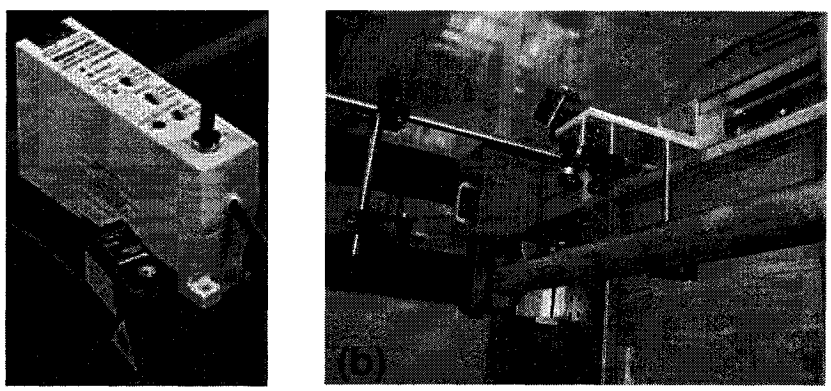

Figure 4.26 (a) Laser sensor (b) slider

The final setup (Figure 4.27) was to have a series of fixed gages including two runout gages from NRC and from PWC that had a resolution between 0.0001" and 0.0005" as well as two LVDT from PWC which had a resolution of 0.00001", which provided more accurate and repeatable results.

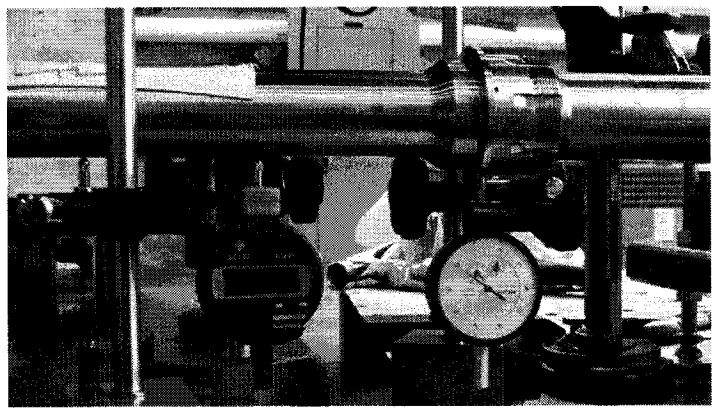

Figure 4.27 Fixed sensors

4.4.5 Observer

The observer is similar to the one developed by S.-C. Kim and S.-C. Chung (2000) [10] (Chapter 1.3). Its purpose is to predict the permanent deflection by drawing the load deflection curve during the loading of the shaft (Figure 4.28).

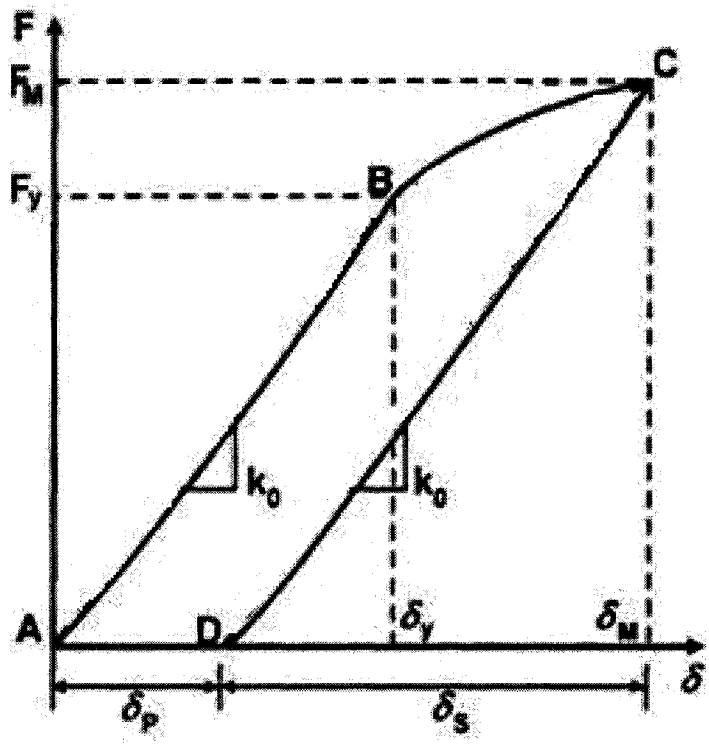

Figure 4.28 Load vs deflection curve for the prediction of permanent deflection

4.4.6 Measurement of the inner diameter eccentricity

Prior to straightening, the inner diameter eccentricity is measured at reference spot grinded positions along the length. For the prototype, the measures come from the ultrasound Saupal measuring system at Pratt & Whitney Canada (detailed description is found in chapter 4.4.5).

4.4.7 Database

The database is created using 10 different configuration of the position of the load and supports. Each position was carefully chosen so that the maximum bending stress appears under the loading point. This was controlled by creating an Excel application that gives the percentage of the stress at each critical section of the shaft for a defined position of the supports. By working with the finite element model it was noticed that if at the

maximum loading point, the shafts is stress axially by 1.33 * Se it will create enough permanent deflection to be able to straighten most shafts. Therefore for each configuration the stress at the critical sections must be at most 1/1.33 = 0.75= 75% of the stress at the loading point. Figure 4.29 is an example of an unacceptable configuration because the stress at the junction between the two holes (circled) will be more elevated then at the zone at which we want to load. Figure 4.30 is an example of an acceptable configuration because the stress at all the critical sections will be lower that the acceptable limit of 0.75.

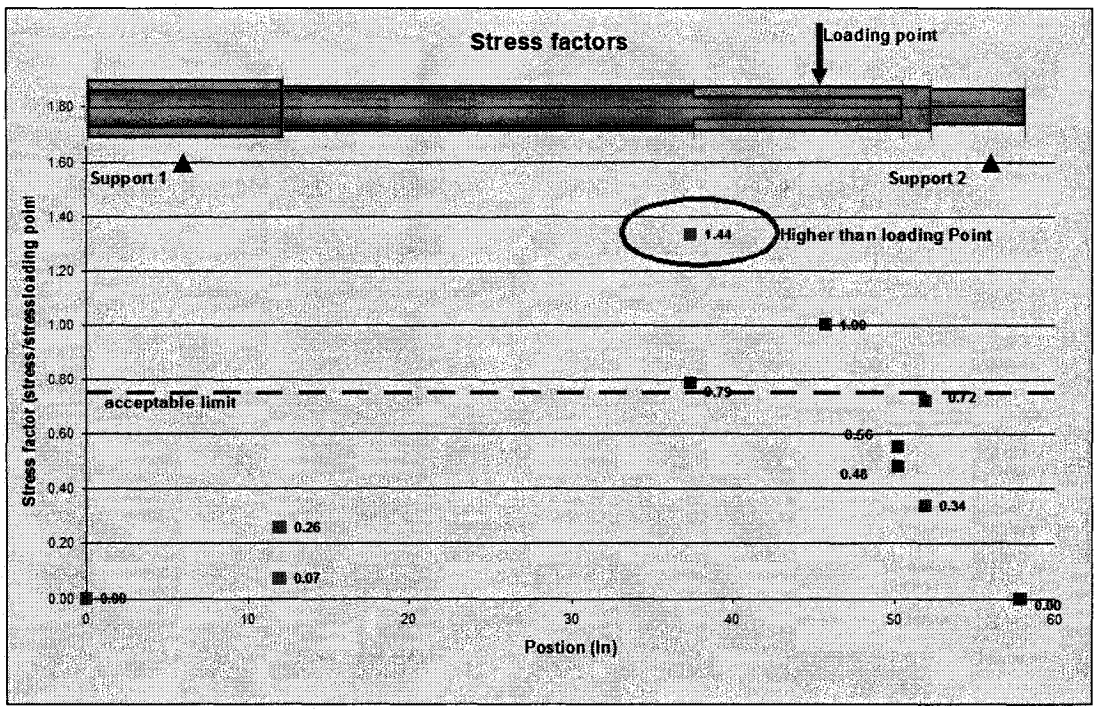

Figure 4.29 Unacceptable supporting condition

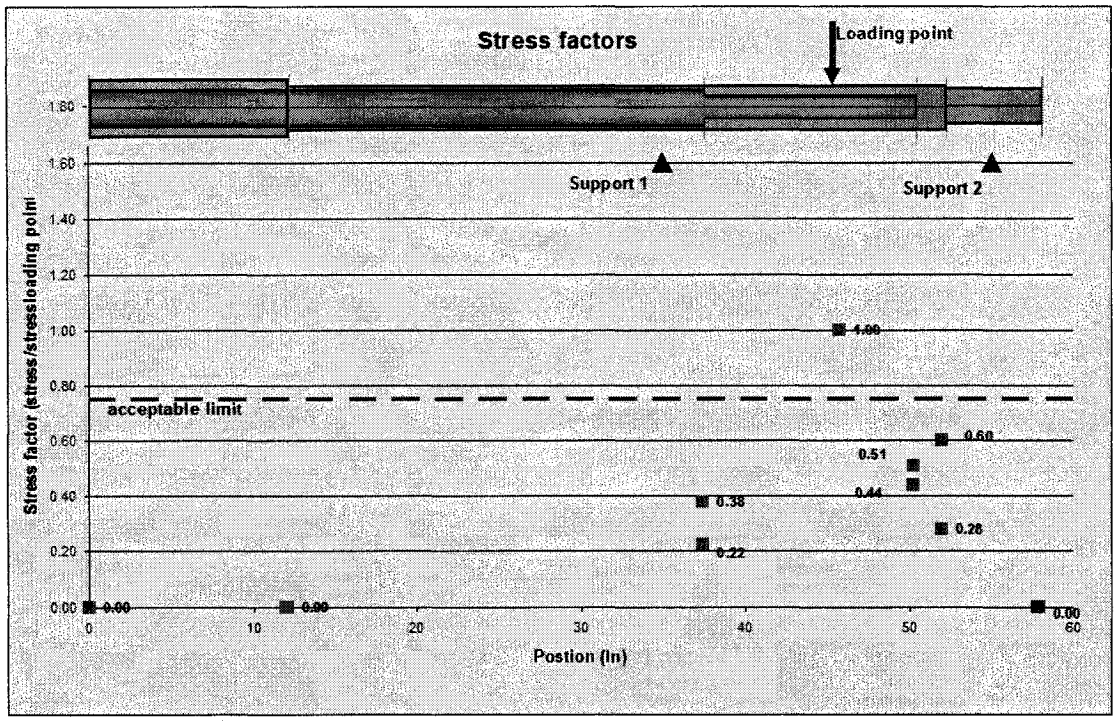

Figure 4.30 Acceptable supporting condition

For each configuration, the change ratios (CR) were predicted in the same manner as done by S.-C. Kim and S.-C. Chung (2000) [8], which is by considering the final shape being a triangle passing trough zero at the supports and at a maximum at the loading point. This error generated shown in Figure 4.31 is negligible because the only bent region is around the loaded region since the rest of the shaft acts as rigid bodies.

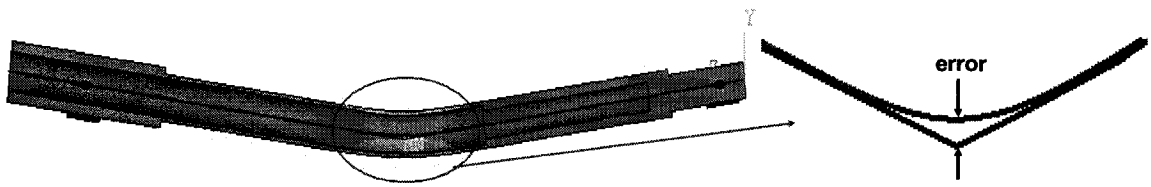

Figure 4.31 Error generate by using change ratios

The only difference with the method used by S.-C., Kim and S.-C. Chung (2000) [8] (Figure 4.32a), is that the change ratios are calculated as being the deflection at point (i)

divided by the deflection at a point independent of the loading point. This point is chosen so that there could always be a measurable amount of deflection there (Figure 4.32b).

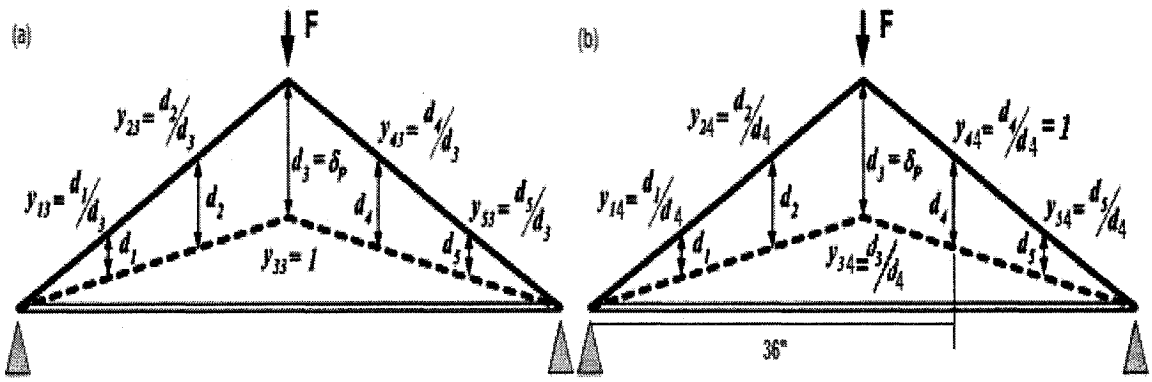

Figure 4.32 Change ratios (a) from S.-C. Kim and S.-C. Chung (2000) (b) modified

For each configuration, the change ratios (CR) could easily be evaluated by drawing a graph composed by two lines that pass through the following points:

CR = 0 at the position of the supports

CR of the two lines is equal at the loading position

CR = 1 of one line at the reference position

Figure 4.33 shows an example for two different configurations using a reference position of 25":

Configuration 1: Position of supports = 5"and 45", position of load= 15"

Configuration 2: Position of supports = 15"and 55", position of load= 35"

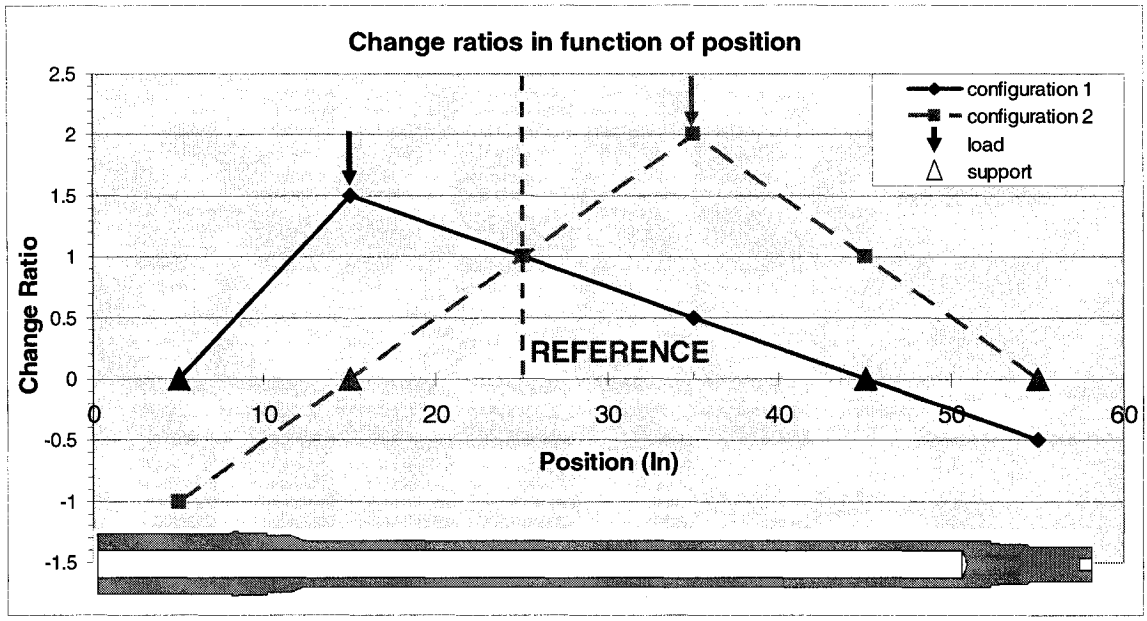

Figure 4.33 Examples of change ratios

The benefit of using the change ratios is that the permanent deflection created at any position "x" along the shaft can be calculated in function of the displacements of the reference point, independently of the geometric or material properties of the shaft.

For one configuration, Equation 4.4 defines the permanent deflection in function of "x":

$$D(X) = CR_1(X) \times Dref_1 \qquad \textit{Equation 4.4}$$

Where:

D(X) = Permanent deflection at axial distance "x"

$CR_1(X)$ = Change Ratio at axial distance "x"

$Dref_1$ = Permanent deflection of reference point

For two configurations, Equation 4.5 is to be used.

$$D(x) = CR_1(X) \times Dref_1 + CR_2(X) \times Dref_2 \qquad \textit{Equation 4.5}$$

And for n configurations, Equation 4.6 is to be used.

$$D(x) = CR_1(X)\ x\ Dref_1 + CR_2(X)\ x\ Dref_2 + \ldots + CR_{n-1}(X)\ x\ Dref_{n-1} + CR_n(X)\ x\ Dref_n \qquad \textit{Equation 4.6.}$$

The displacement at X1 could be written as in Equation 4.7.

$$[CR_1(X_1)\quad CR_2(X_1)\quad \ldots\quad CR_{n-1}(X_1)\quad CR_n(X_1)]\times\begin{bmatrix} Dref_1 \\ Dref_2 \\ \ldots \\ Dref_{n-1} \\ Dref_n \end{bmatrix} = [D(X1)] \qquad \textit{Equation 4.7.}$$

The database could also contain the acceptable limit if we want to straighten without stress relieving the part. These limits are obtained by studying the dynamic program that calculates the life of the shaft at its critical sections (2 of these sections are circled in Figure 4.34). It was observed that between the critical sections the shaft is over-dimensioned and therefore capable of supporting a certain amount of tensile residual stress. This over-dimensioned region could therefore be used to apply the load during a press straightening process.

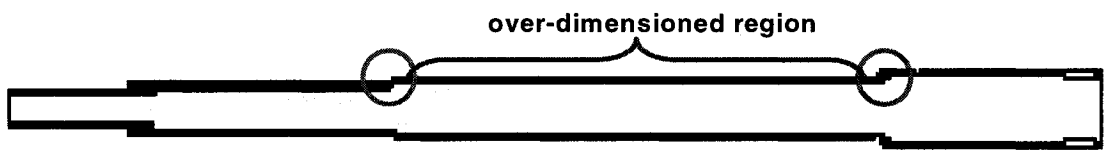

Figure 4.34 Over-dimensioned region between critical sections

Then the maximum residual stress could be evaluated to get a life factor close to one. Since the residual stress corresponds to a maximum deflection from the curve residual stress vs strain, the maximum authorized deflection for each configuration is found

All this study permits to produce a database of the form in Table 4.4.

Table 4.4 Database containing the change ratios per configuration

Pos support 1	Pos support 2	Pos force	CR1	CR2	CR3	CR4	CR5	CR6	CR7	CR8	CR9	CR10	CR11	CR12	MAX Deflection
(in)	(in)	(in)	2"	13.3"	19.3"	23"	27.8"	30"	35"	39.3"	40"	44.3"	49.3"	55.8"	(in)
2	27.8	19	0.0	-0.8	-1.2	-0.7	0.0	0.3	1.0	1.6	1.7	2.3	3.0	3.9	
2	27.8	23	0.0	-0.4	-0.5	-0.7	0.0	0.3	1.0	1.6	1.7	2.3	3.0	3.9	
2	44.3	19	0.0	1.8	2.8	2.3	1.8	1.5	1.0	0.5	0.5	0.0	-0.5	-1.2	
2	44.3	30	0.0	0.6	1.0	1.2	1.4	1.5	1.0	0.5	0.5	0.0	-0.5	-1.2	
2	55.8	19	0.0	1.2	1.8	1.6	1.3	1.2	1.0	0.8	0.8	0.6	0.3	0.0	
19.3	39.3	30	-3.5	-1.2	0.0	0.7	1.7	2.2	1.0	0.0	-0.2	-1.2	-2.3	-3.8	
19.3	55.8	30	-2.0	-0.7	0.0	0.4	1.0	1.2	1.0	0.8	0.8	0.6	0.3	0.0	
2	55.8	30	0.0	0.5	0.8	0.9	1.1	1.2	1.0	0.8	0.8	0.6	0.3	0.0	

4.4.8 Controller

The controller is going to calculate the optimal straightening parameters. These parameters are the configurations (positions of each support and of the loading) and the desired permanent displacement per configuration ($Dref_n$).

Equation 4.7 for "m" measuring points gives Equation 4.8.

$$\begin{bmatrix} CR_1(X_1) & CR_2(X_1) & \dots & CR_{n-1}(X_1) & CR_n(X_1) \\ CR_1(X_2) & CR_2(X_2) & \dots & CR_{n-1}(X_2) & CR_n(X_2) \\ \dots & \dots & \dots & \dots & \dots \\ CR_1(X_m) & CR_2(X_m) & \dots & CR_{n-1}(X_m) & CR_n(X_m) \end{bmatrix} \times \begin{bmatrix} Dref1 \\ Dref2 \\ \dots \\ Drefn-1 \\ Drefn \end{bmatrix} = \begin{bmatrix} D(X_1) \\ D(X_2) \\ \\ D(X_m) \end{bmatrix} \quad \textit{Equation 4.8}$$

By replacing the final displacements by the measured initial eccentricity [E(X)], we get Equation 4.9.

$$\begin{bmatrix} CR_1(X_1) & CR_2(X_1) & \dots & CR_{n-1}(X_1) & CR_n(X_1) \\ CR_1(X_2) & CR_2(X_2) & \dots & CR_{n-1}(X_2) & CR_n(X_2) \\ \dots & \dots & \dots & \dots & \dots \\ CR_1(X_m) & CR_2(X_m) & \dots & CR_{n-1}(X_m) & CR_n(X_m) \end{bmatrix} \times \begin{bmatrix} Dref1 \\ Dref2 \\ \dots \\ Drefn-1 \\ Drefn \end{bmatrix} = \begin{bmatrix} E(X_1) \\ E(X_2) \\ \\ E(X_m) \end{bmatrix} \quad \text{Equation 4.9}$$

$$(CR) \qquad X \quad (Dref) \quad = \quad (E)$$

Solving Equation 4.9 for Dref gives the optimal values to use for Dref using the configuration represented by the matrix CR (CR1 CR2 .. CRn) .

Dref is solved by using Equation 4.10.

$$Dref = Inverse(CR) \times E \qquad \textit{Equation 4.10}$$

Where:

CR = Change ratios matrix having as columns the attempted set of straightening Configurations (1 to n) and as column the change ratios evaluate at each measuring point (1 to m). ($CR_n(X_m)$ = change ratios of configuration n at measuring point m)

Dref = Displacement (inch) matrix where $Dref_n$ is the displacement of the reference point for configuration n.

E = Eccentricity (inch) matrix where E_m is the eccentricity at the measured point m.

The residual eccentricity (E_r) is then calculated using Equation 4.11.

$$Er = E - CR \times D \qquad \textit{Equation 4.11}$$

Equation 4.10 and 4.11 are solved for each possible combination of 1 to 5 straightening configurations.

If E_r is lower than the final desired precision the configuration set is retained only if the displacements Dref are lower than the allowable displacements. The solution having the minimal E_r is retained.

The controller was programmed using MATLAB 6.5 and its operation is shown in Figure 4.35.

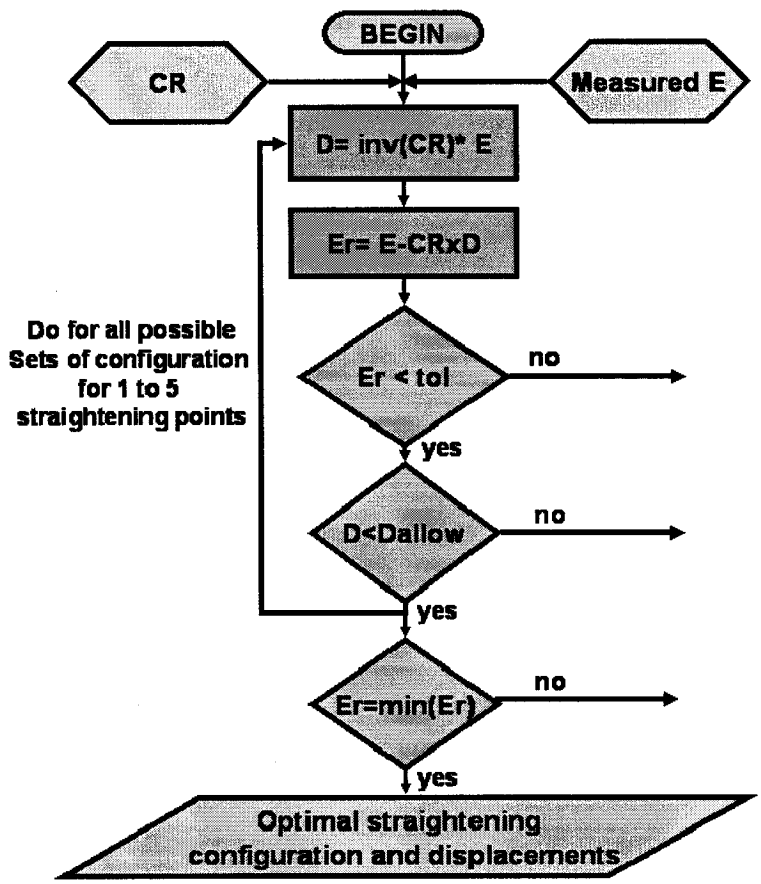

Figure 4.35 Controller's flow chart

4.5 Experiments

4.5.1 Objectives

A. Evaluate the finite element model precision by comparing it with the experimental results

B. Show that the process can be controlled and that the final deflection (after springback) can be predicted during the process

4.5.2 Description

The prototype was designed as cited previously and a series of test were done on scrapped shafts. Figure 4.36 shows the setup, as a shaft is loaded plastically.

Figure 4.36 Setup shown as the shaft is bent

4.5.3 Results of the press straightening experiments

To evaluate the finite element model the curves extracted from the experiments are compared with the ones extracted from the finite element model. For the test used to validate the finite element model the shaft is plastically loaded to 14000 lb at 31" and the supports are at 6" and 56" (Figure 4.37). Strain gages were also placed in the positions shown in Figure 4.38.

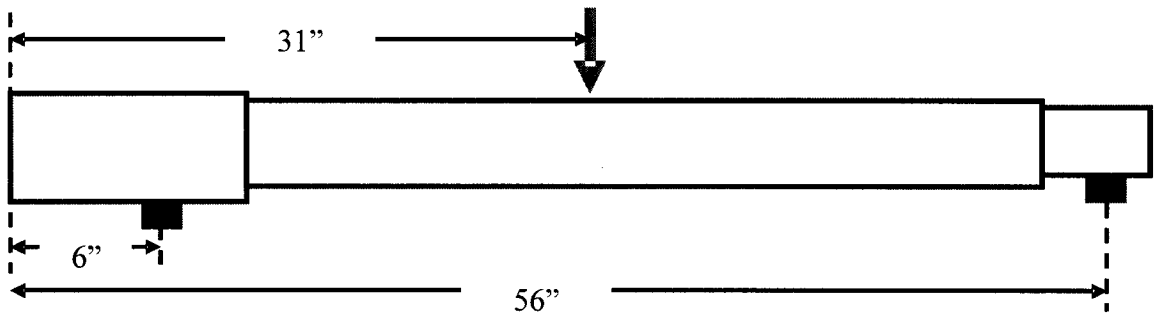

Figure 4.37 Position of supports and load used for tests

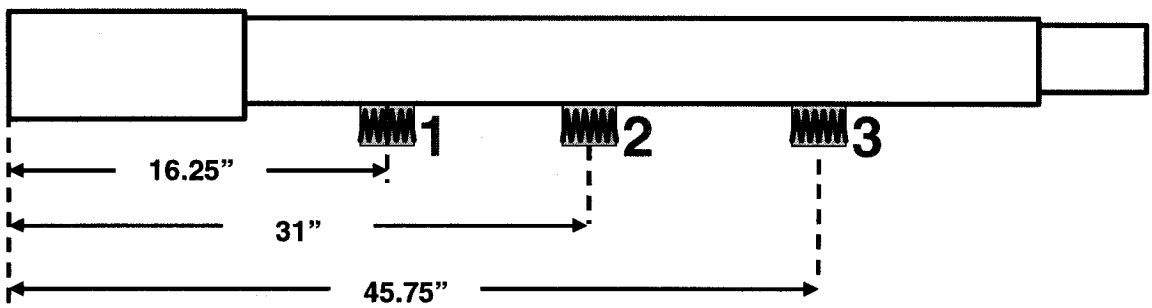

Figure 4.38 Position of strain gages

The finite element model used was the one described in chapter 4.1. Since the essential parameter of the model is the permanent deflection under the loading point, the final element model was loaded to get the same permanent deflection as the experimentally measured permanent deflection of 0.028".

The results compared are first the loaded and final deflection along the length of the shaft (Figure 4.39, Figure 4.40). In Figure 4.40, the experimental results for the permanent deflection are close to the FEM except for the two values encircled which errors are caused by the malfunction of gages.

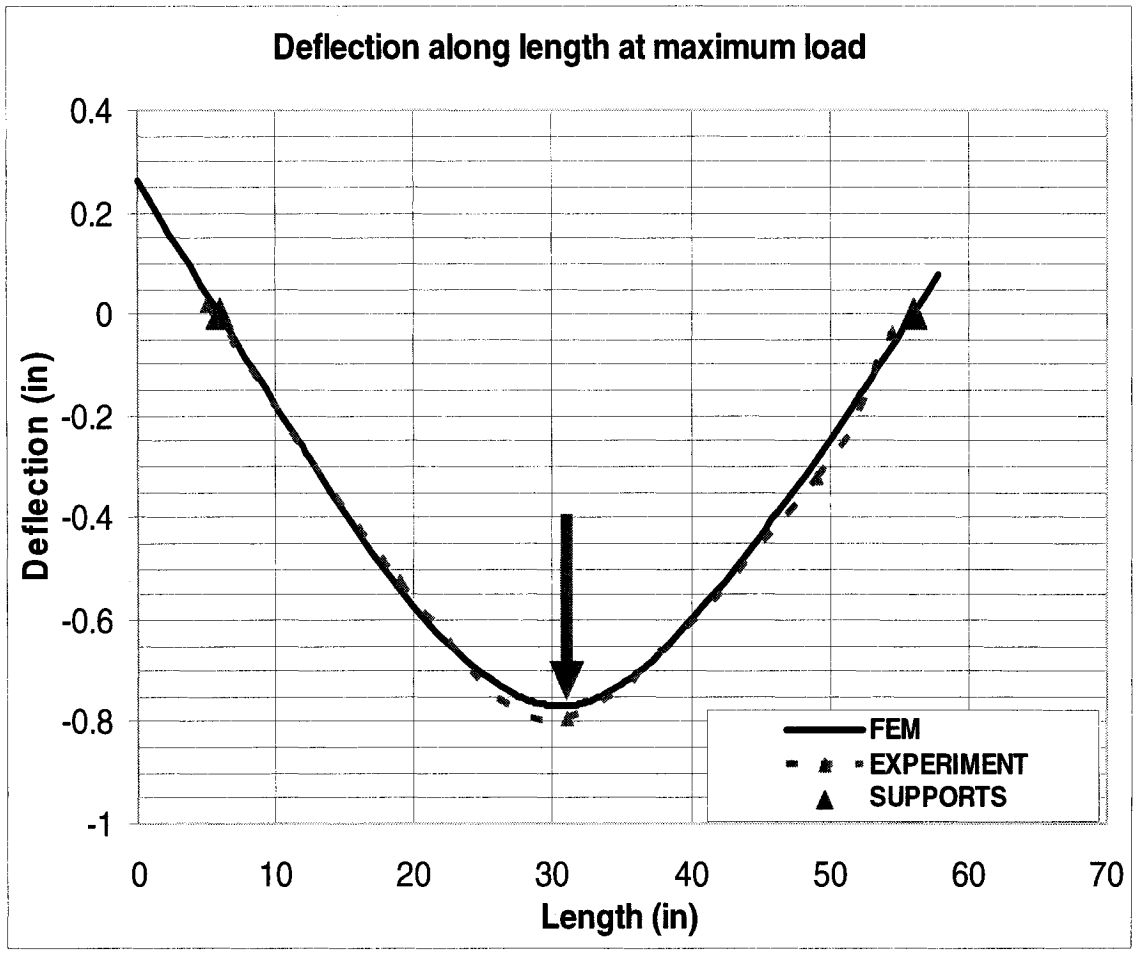

Figure 4.39 Deflection along length at maximum load

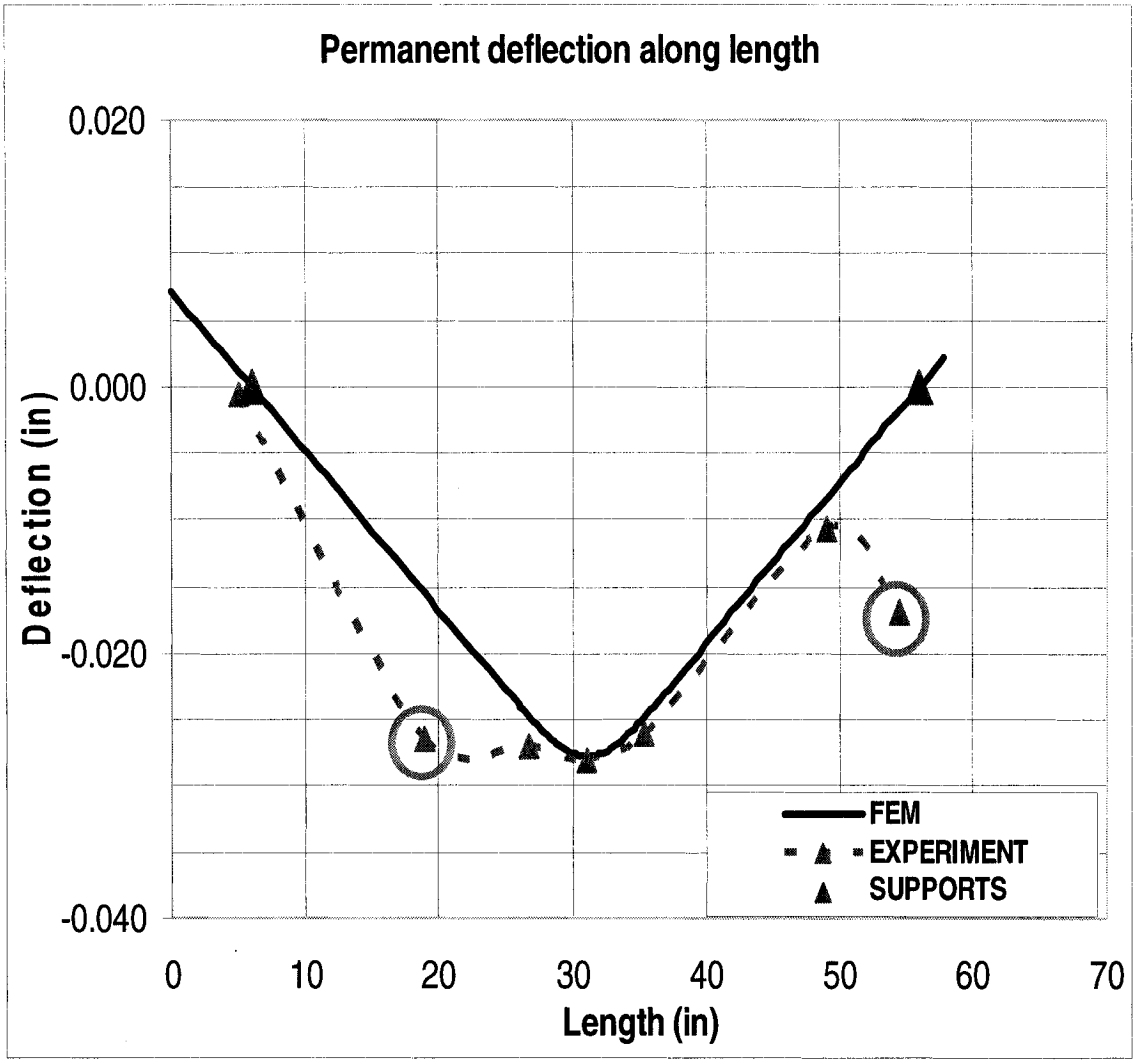

Figure 4.40 Permanent deflection along the length

The load and deflection as a function of the strain measured at 31" are plotted in Figure 4.41 and Figure 4.42 respectively. The results show that the modeled material isn't rigid enough because the slopes of the experimental results are higher than the ones of the FEM model.

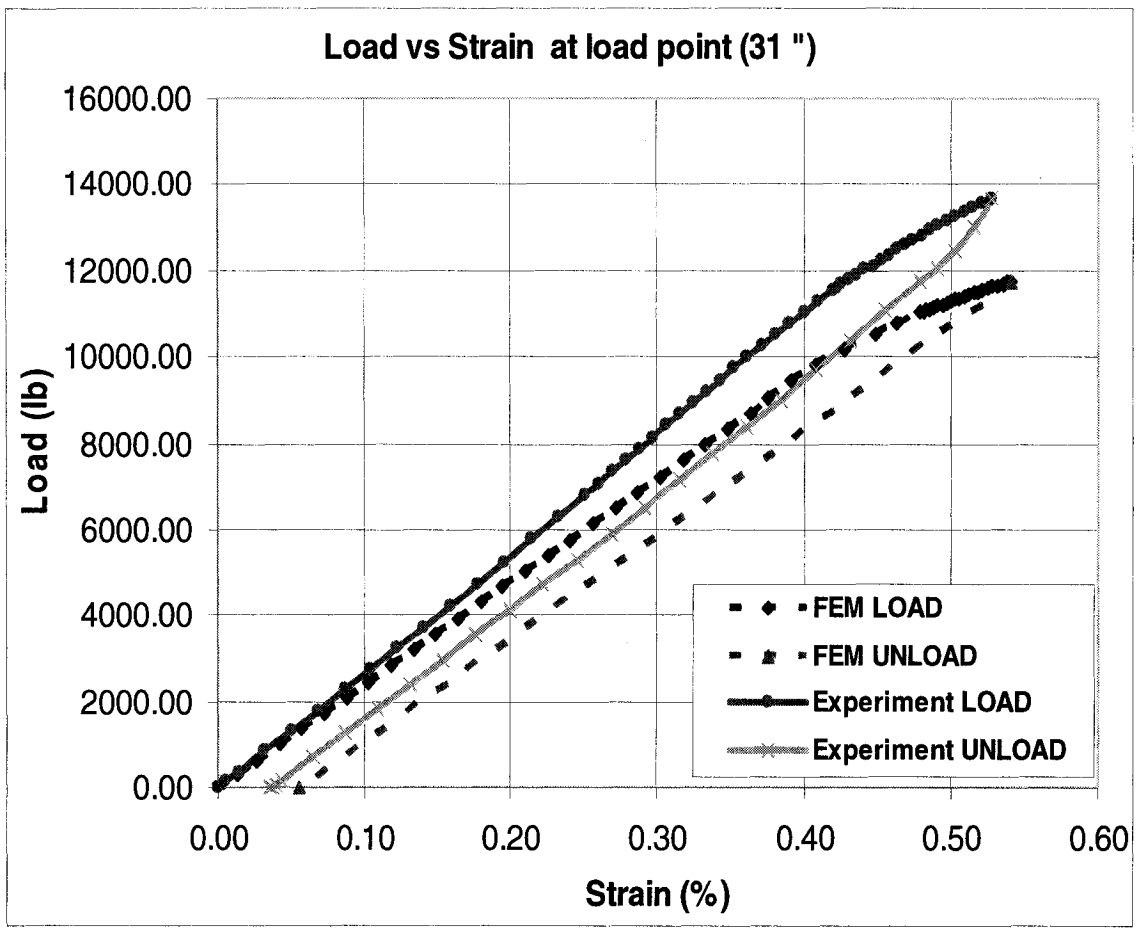

Figure 4.41 Load vs strain for the strain gauge at 31"

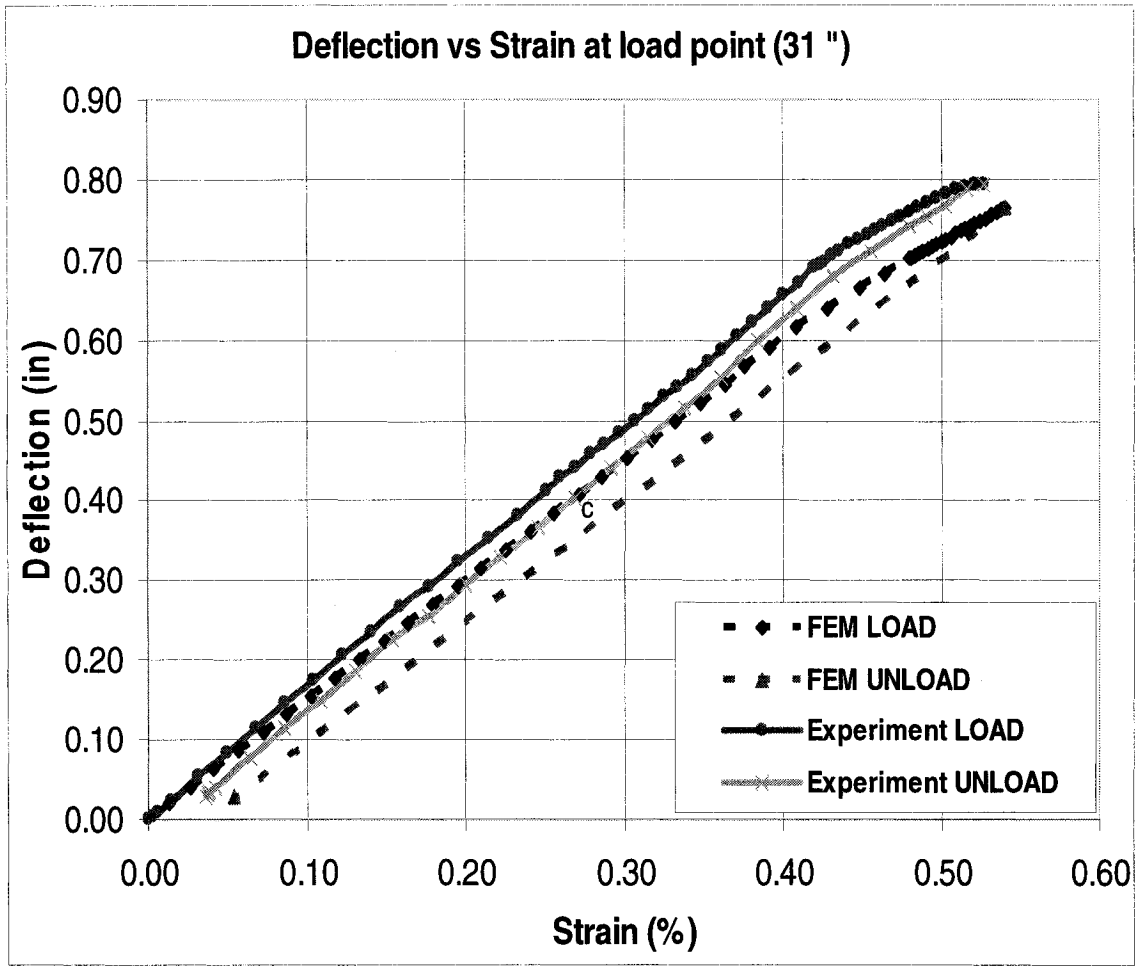

Figure 4.42 Deflection vs strain for the strain gauge at 31"

The deflection at 31" as a function of the strain at 16.25" (Figure 4.43) and 49" (Figure 4.44) are plotted. The results also show that the modeled material isn't rigid enough but it also shows that for all cases the final strain is zero at these locations.

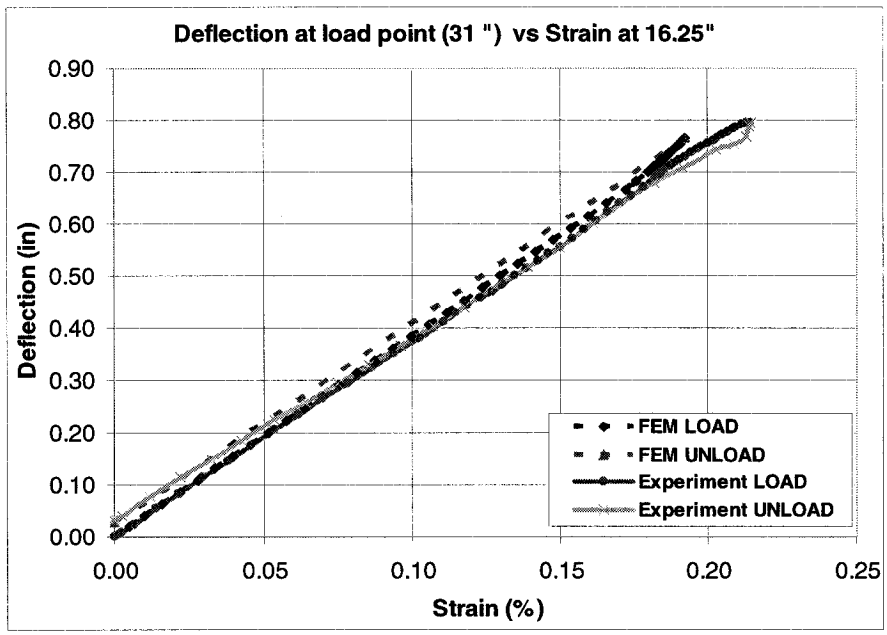

Figure 4.43 Deflection at 31" vs strain at 16.25"

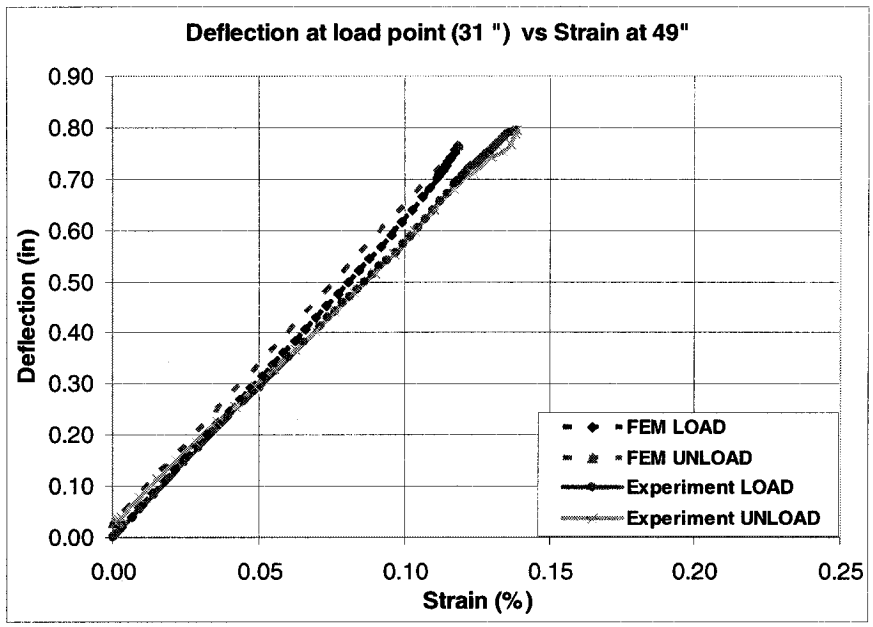

Figure 4.44 Deflection at 31" vs strain at 49"

Table 4.5 shows the percentage of error of the FEM with respect to the experimental results.

Table 4.5 Percentage of error of the FEM with respect to the experimental results

	Deflection	Strain 16.35"	Strain 31"	Strain 45"	Load
LOAD	-3.6	-10.2	2.6	-14.6	-14.0
UNLOAD	-2.0	N/A	52.1	N/A	N/A

The finite element model (FEM) overestimates the maximum plastic strain by over 50%. Since the residual stress is directly proportional to the plastic strain we could conclude that the residual stress is also overestimated by the same amount. This makes the use of the FEM safe because the maximum permissible deflection is directly proportional to the residual stress. This means that the overestimation of the residual stress by the FEM will give a lower acceptable permanent deflection limit.

4.6 Summary and conclusion

The finite element model uses the SOLID185 element type with:

- 12 divisions along the circumference;
- 2 divisions through the thickness;
- 1" length along the length;

and for a finely meshed region of 10" around the loading point:

- 8 divisions through the thickness;
- 0.5" length along the length;

This model gives results within 15% of the experimental ones, except for the plastic strain which is higher by 50% but still acceptable, since it overestimates the plastic strain and residual stress.

The design of the press straightening equipment is composed of the:

- Press: Stir welding press of NRC on witch a "V" shaped punch is mounted.
- Supports: Machined with a cylindrical base with its center on the shaft's axis.
- Sensors: Fixed gauges with a resolution under 0.001".
- Observer: Uses the load deflection curves to predict the permanent deflection.
- Measures: The inner diameter is measured by PWC Saupal ultrasound and the outer diameter by runout gauges .
- Database: Contain for different configurations, the relative deflection point "i" to deflection of a reference point (change ratios) and the maximum permanent deflection which avoids damaging the shaft.
- Controller: Using a MATLAB program the optimal straightening commands are chosen to straighten the shaft.

The only part of the designed equipment that needs more studying is the punch because when the shaft bends only the extremities of the punch stay in contact with the part and therefore generates undesirable stress concentrations at these regions.

Straightened shafts must be sent for post treatments to evaluate the effect of doing a stress relief and of machining the plastically deformed region. These results will be useful to better understand how to introduce a press straightening equipment in the PWC manufacturing process.

The advantages of the press straightening solution are that:

- equipments available on the market could be adapted to be used for precision shaft straightening;
- the process is predictable by the finite element model;
- the database is created by using the finite element model;
- the process is easily automated;
- the surface finish isn't affected.

The major inconvenient is that its use on the final part is restricted because it creates undesirable tensile residual stress on the surface.

Chapter V

Development of a precision peen straightening equipment for turbine engine shafts

5.1 Peen straightening and forming equipments

Peening equipments on the market are mostly shot peening equipments. These equipments are primarily used to enhance the fatigue life of rotating parts by inducing compressive surface residual stress. Shot peening was also used for forming process by S. Kittel, W. Linnemann, F. Wustefeld, R. Kopp [26] to curve thin plates.

For the straightening of shafts shot peening was put aside because the shafts are of relatively small diameter and sensor wouldn't have been able to get on-line measurements of the shafts deflection without risking damaging the sensor. Another disqualifying point is that with shot peening it's very difficult to get local residual stress regions and therefore get a good control of the shafts deflection.

The chosen peening tool for this study was an ultrasound peening machine. These types of equipments work by having cylindrical peens moved by an ultrasound vibrating membrane. The velocity of the peens is controlled by the frequency of the vibration of the membrane.

5.2 Design of prototype

The design of prototype (Figure 5.1) is almost identical to the one described for the press straightening in chapter 4, thus only the differences will be described below.

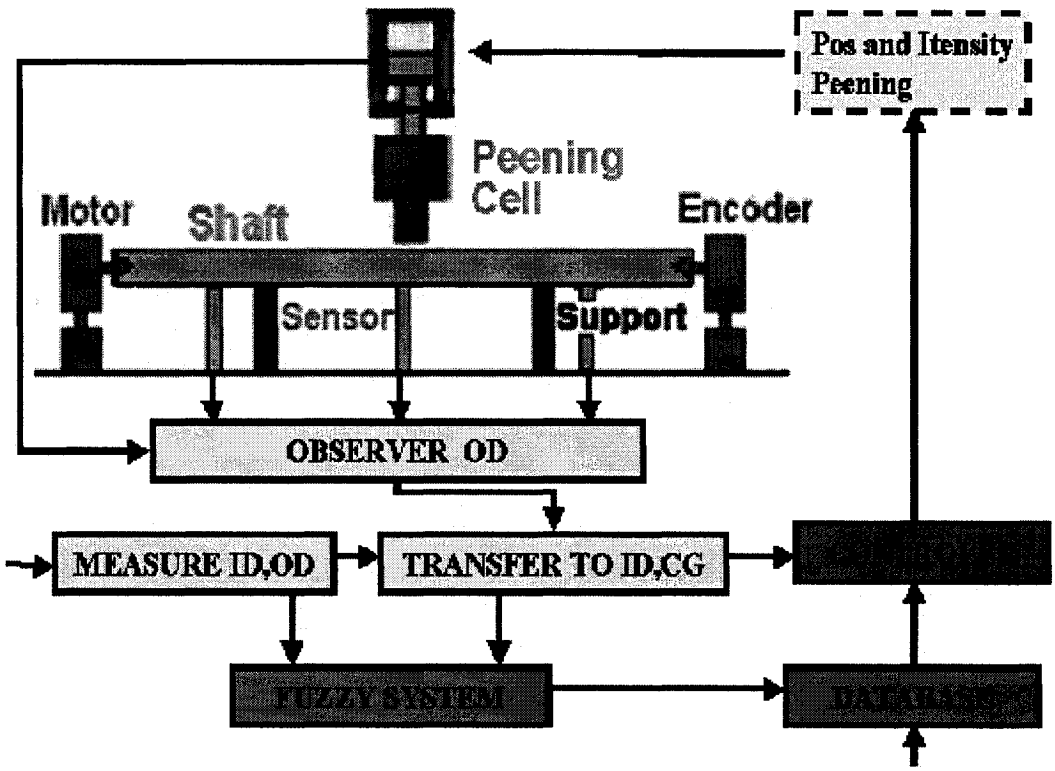

Figure 5.1 Design scheme of the peen straightening prototype

5.2.1 Peening

An ultrasound peening machine from Sonats (Figure 5.2) was used to create the surface residual stress necessary. The advantages of this peening equipment are that you can easily control the peening region and also assure a good coverage. The only disadvantage is that it is applied manually and therefore the intensity of the peening is variable.

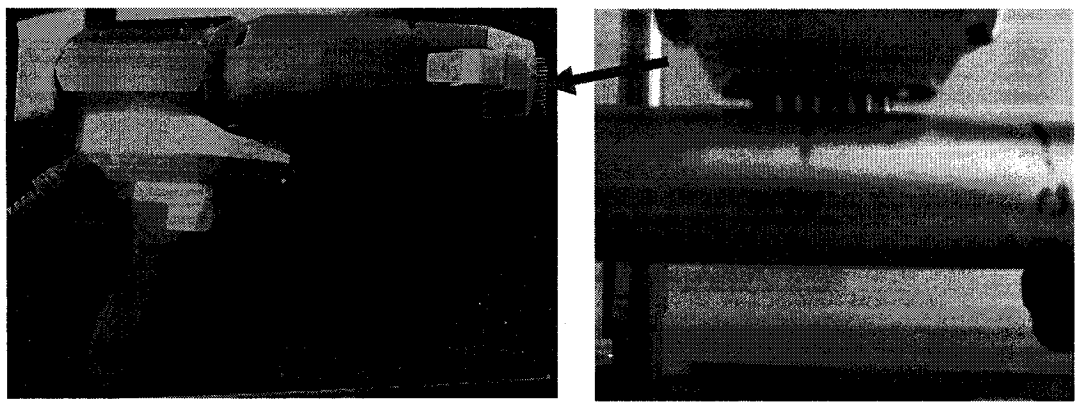

Figure 5.2 Sonats ultrasound peening gun

To obtain different final deflection the easiest peening parameters to modify is the length and width (area) of the peened region as well as the peening time. Test done at NRC to evaluate the effect of the peening area showed that the permanent deflection is almost directly proportional to the peened area. To get a better control on the peened area a rubber tape from PWC peening specialists delimited the desired peened area (Figure 5.3).

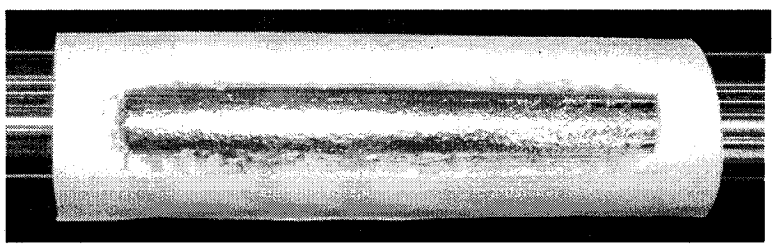

Figure 5.3 Protective rubber tape used to control the peening area

An Almen strip test was made to evaluate the intensity produced by ultrasound peening and to evaluate how much time we had to peen to get to saturation.

5.2.2 Supports

The supports rotation was fixed by a screw because the vibration altered the readings.

5.2.3 Sensors

A detailed description of the sensors is found in chapter 4.4.5.

5.2.4 Observer

The observer purpose is to control the permanent deflection (δ_p) by measuring the final deflection as a function of the peening parameters (I) (Figure 5.4). These parameters are the length and width (area) of the peened region as well as the peening time.

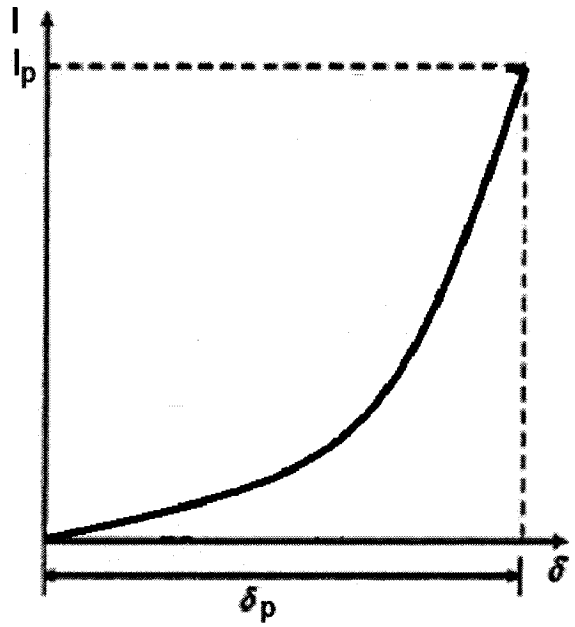

Figure 5.4 Peening parameters vs deflection for the prediction of permanent deflection

The permanent deflection is therefore easily measurable since the springback is negligible. The only difficulty is that the vibrations caused by the peening makes it impossible to measure the deflection during the peening. Therefore the peening has to be stopped to take the measurements. The difficulty is that the evaluation of how to modify

the peening parameters to get the desired permanent deflection is based mostly on experience.

5.2.5 Database

The database is also composed of the change ratios but for these change ratios the position of the supports is always at the extremities of the shaft. The maximum permanent deflection would only be limited by the roughness of the surface created and the amount of residual stress imputable to the surface. To get these limits a vast amount of experiments will be necessary. This could be part of a further study on the peen straightening process.

5.2.6 Controller

A detailed description of the controller is found in chapter 4.4.8.

5.3 Experiments

5.3.1 Objectives

The objectives of the experiments are to are to:

A. verify if the residual stress applied by shot peening is capable of creating sufficient deflection to straighten a deformed shaft.

B. evaluate the effect of peening on the shafts roundness and roughness

C. test if the permanent deflection created by this process is controllable and predictable.

5.3.2 Description

The setup shown in Figure 5.5 was used for the different experiments.

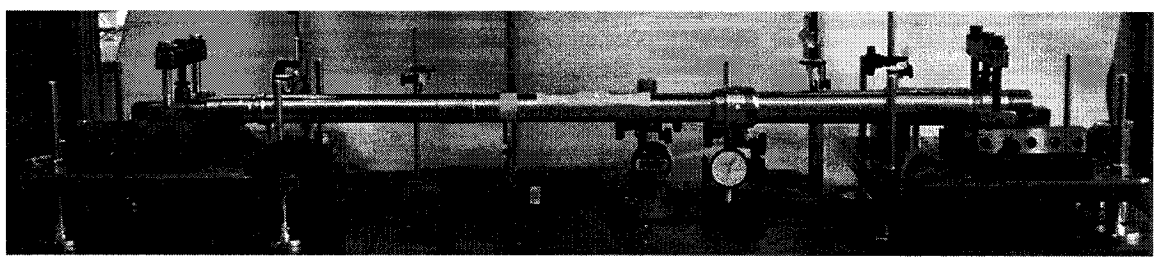

Figure 5.5 Peening experiments setup

5.3.3 Results

A. After a few experiments done on simple tubes, a first shaft was peened and the results showed that a permanent deflection of 0.012" was attained at two perpendicular planes giving a total permanent deflection of 0.016" between the two planes. This answered positively the objective by proving that an appreciable amount of permanent deflection was achievable.

B. The shaft was then brought to PWC to measure its roundness and roughness.

The measure of roundness in Figure 5.6 shows that some parts of the surface are elevated by about 0.0015".

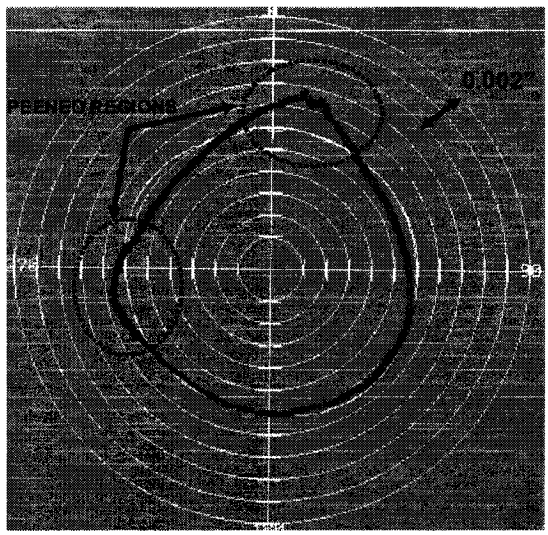

Figure 5.6 Roundness error created by peening

This is explained by the fact that the residual stresses created by peening are multidirectional. Since the residual stress generated in the circumferential direction distorts the roundness of the section, the peened area should be increased on the axial direction and decreased on the circumferential direction.

The measure of roughness in Figure 5.7 shows that the surface is indented by the peening and that the variation between the hills and valleys of these dents could be as much as 0.002".

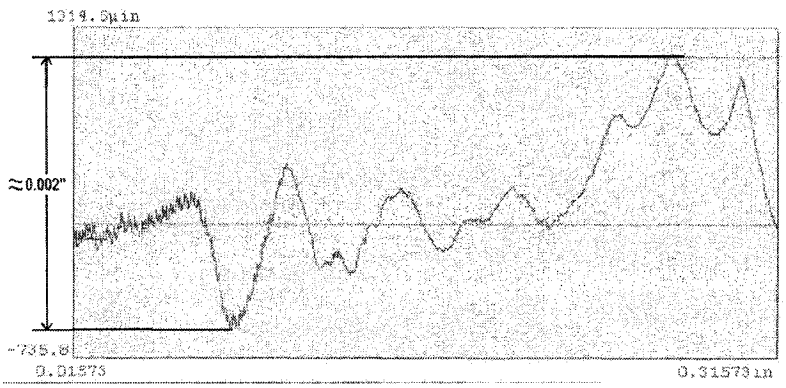

Figure 5.7 Dents created by ultrasound peening

C. To evaluate if the process was controllable and capable of straightening shafts, the ID and the OD were measured at 22 sections along the shaft (Figure 5.8). The ID eccentricity was measured using the ultrasound measuring machine described in chapter 3.1.1 and the OD runout was measured using a dial gauge.

Figure 5.8 Sections measured on the shaft

These measurements were used to evaluate the position of the center of gravity (COG) at each section (Figure 5.9). Then an attempt was made to straighten the shaft.

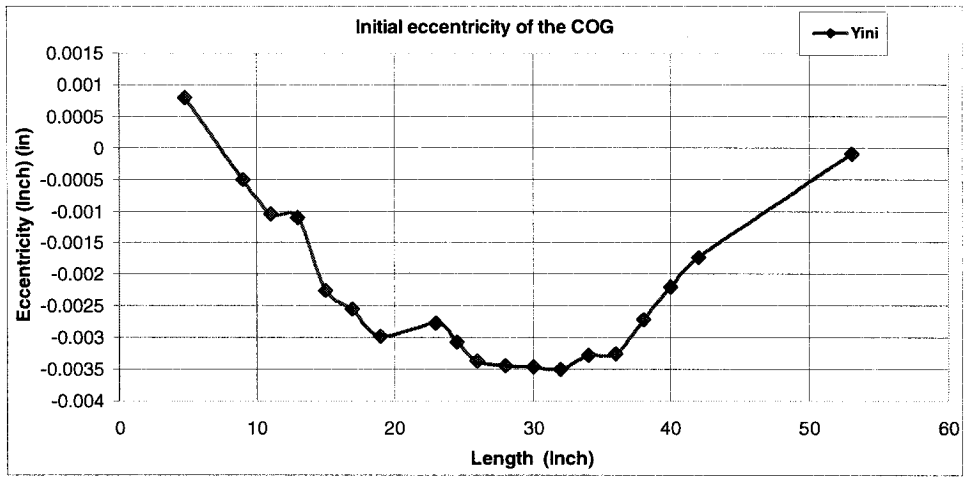

Figure 5.9 Measured eccentricity of the COG

The database was created using the point at 25" as the reference point. The database is tabulated in Table 5.1 where the first column and the first row are the positions in inches. The values of the rest of the table are the change ratios at the position in column (j) when the position in row (i) is peened.

Table 5.1 Change ratios used to create the database

PEENED POSITION (IN)	POSITION AT WHICH THE CHANGE RATIO IS EVALUATED (IN)																						
	5.25	7.75	9.5	11.5	13.5	15.5	17.5	19.5	21.5	23.5	25	26.5	28.5	30.5	32.5	34.5	36.5	38.5	40.5	42.5	47.5	53.5
5.3	1.65	1.57	1.51	1.44	1.38	1.31	1.25	1.18	1.12	1.05	1.00	0.95	0.88	0.82	0.75	0.69	0.62	0.56	0.49	0.42	0.26	0.06
7.8	1.06	1.57	1.51	1.44	1.38	1.31	1.25	1.18	1.12	1.05	1.00	0.95	0.88	0.82	0.75	0.69	0.62	0.56	0.49	0.42	0.26	0.06
9.5	0.83	1.23	1.51	1.44	1.38	1.31	1.25	1.18	1.12	1.05	1.00	0.95	0.88	0.82	0.75	0.69	0.62	0.56	0.49	0.42	0.26	0.06
11.5	0.66	0.97	1.19	1.44	1.38	1.31	1.25	1.18	1.12	1.05	1.00	0.95	0.88	0.82	0.75	0.69	0.62	0.56	0.49	0.42	0.26	0.06
13.5	0.54	0.79	0.97	1.17	1.38	1.31	1.25	1.18	1.12	1.05	1.00	0.95	0.88	0.82	0.75	0.69	0.62	0.56	0.49	0.42	0.26	0.06
15.5	0.44	0.66	0.80	0.97	1.14	1.31	1.25	1.18	1.12	1.05	1.00	0.95	0.88	0.82	0.75	0.69	0.62	0.56	0.49	0.42	0.26	0.06
17.5	0.37	0.55	0.68	0.82	0.96	1.10	1.25	1.18	1.12	1.05	1.00	0.95	0.88	0.82	0.75	0.69	0.62	0.56	0.49	0.42	0.26	0.06
19.5	0.32	0.47	0.58	0.70	0.82	0.94	1.06	1.18	1.12	1.05	1.00	0.95	0.88	0.82	0.75	0.69	0.62	0.56	0.49	0.42	0.26	0.06
21.5	0.27	0.40	0.49	0.60	0.70	0.80	0.91	1.01	1.12	1.05	1.00	0.95	0.88	0.82	0.75	0.69	0.62	0.56	0.49	0.42	0.26	0.06
23.5	0.23	0.35	0.42	0.51	0.60	0.69	0.78	0.87	0.96	1.05	1.00	0.95	0.88	0.82	0.75	0.69	0.62	0.56	0.49	0.42	0.26	0.06
25.0	0.21	0.31	0.38	0.46	0.54	0.62	0.70	0.78	0.86	0.94	1.00	0.95	0.88	0.82	0.75	0.69	0.62	0.56	0.49	0.42	0.26	0.06
26.5	0.21	0.31	0.38	0.46	0.54	0.62	0.70	0.78	0.86	0.94	1.00	1.06	0.99	0.91	0.84	0.77	0.69	0.62	0.55	0.47	0.29	0.07
28.5	0.21	0.31	0.38	0.46	0.54	0.62	0.70	0.78	0.86	0.94	1.00	1.06	1.14	1.06	0.97	0.89	0.80	0.72	0.63	0.55	0.33	0.08
30.5	0.21	0.31	0.38	0.46	0.54	0.62	0.70	0.78	0.86	0.94	1.00	1.06	1.14	1.22	1.12	1.02	0.93	0.83	0.73	0.63	0.39	0.09
32.5	0.21	0.31	0.38	0.46	0.54	0.62	0.70	0.78	0.86	0.94	1.00	1.06	1.14	1.22	1.30	1.19	1.07	0.96	0.85	0.73	0.45	0.11
34.5	0.21	0.31	0.38	0.46	0.54	0.62	0.70	0.78	0.86	0.94	1.00	1.06	1.14	1.22	1.30	1.38	1.25	1.12	0.98	0.85	0.52	0.13
36.5	0.21	0.31	0.38	0.46	0.54	0.62	0.70	0.78	0.86	0.94	1.00	1.06	1.14	1.22	1.30	1.38	1.46	1.31	1.15	1.00	0.61	0.15
38.5	0.21	0.31	0.38	0.46	0.54	0.62	0.70	0.78	0.86	0.94	1.00	1.06	1.14	1.22	1.30	1.38	1.46	1.54	1.36	1.18	0.72	0.17
40.5	0.21	0.31	0.38	0.46	0.54	0.62	0.70	0.78	0.86	0.94	1.00	1.06	1.14	1.22	1.30	1.38	1.46	1.54	1.62	1.40	0.86	0.21
42.5	0.21	0.31	0.38	0.46	0.54	0.62	0.70	0.78	0.86	0.94	1.00	1.06	1.14	1.22	1.30	1.38	1.46	1.54	1.62	1.70	1.04	0.25
47.5	0.21	0.31	0.38	0.46	0.54	0.62	0.70	0.78	0.86	0.94	1.00	1.06	1.14	1.22	1.30	1.38	1.46	1.54	1.62	1.70	1.90	0.46
53.5	0.21	0.31	0.38	0.46	0.54	0.62	0.70	0.78	0.86	0.94	1.00	1.06	1.14	1.22	1.30	1.38	1.46	1.54	1.62	1.70	1.90	2.14

The eccentricity was the entered in the controller (Matlab program) which gave the position of the peening region as well as their respective necessary permanent deflection at the reference point (25").

Figure 5.10 shows the curves corresponding to the three selected peening region as well as the sum of the three curves.

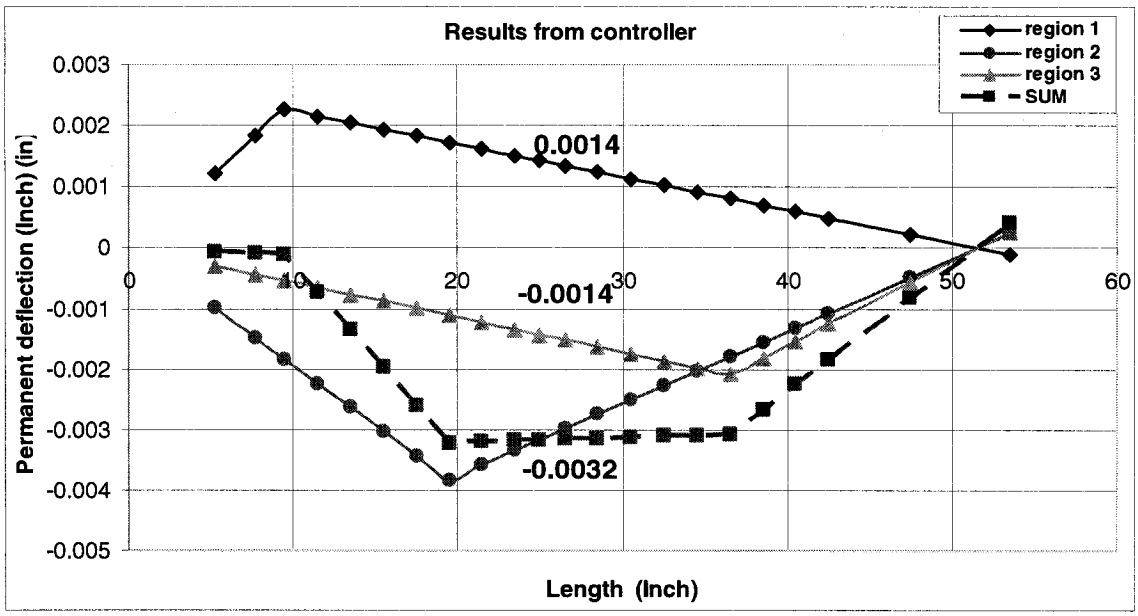

Figure 5.10 Chosen peening position and corresponding permanent deflections at 25"

To obtain the desired permanent deflection at each peened position a small region was peened and based on the results the size of the necessary region was defined since the generated deflection is directly proportional to the peened region.

Figure 5.11 shows that the correction done straightened the shaft to a maximum deflection at each section lower than 0.0005" from an initial maximum value of 0.0035".

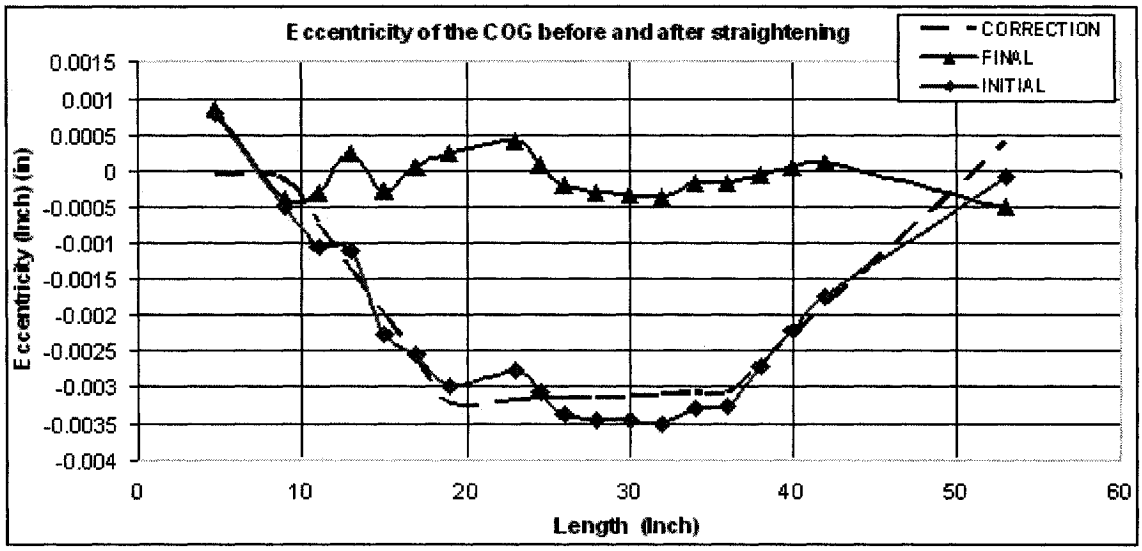

Figure 5.11 Actual, correction and final result

In addition to having a final runout well under the tolerance of 0.004", the shaft is more balanced because the COG"s of each section is distributed around the axis of rotation that goes through 0 in Figure 5.11.

5.4 Summary and conclusion

The design of the peen straightening equipment is composed of the:

- Peener: Sonats Ultrasound peening gun .
- Supports: Machined with a cylindrical base, so it will rotate with the shaft.
- Sensors: Fixed gauges with a resolution under 0.001".
- Observer: Measures the permanent deflection, but bases on experiences to get desired permanent deflection
- Measures: The inner diameter is measured by PWC Saupal ultrasound and the outer diameter by runout gauges .
- Database: Contain the for different configurations, the relative deflection point "i" to deflection of a reference point (change ratios) and the maximum permanent deflection which avoids damaging the shaft.
- Controller: Using a MATLAB program the optimal straightening commands are chosen to straighten the shaft.

The results from the experiments show that :

A. It is possible to generate by ultrasound peening enough permanent deflection to straighten turbine engine shafts.

B. Peening creates undesirable surface roughness and distorts the roundness of the shafts.

C. The peening process is controllable because a shaft's COG was straighten to a final maximum runout under 0.001" from an initial maximum of 0.007".

The major advantage of peen straightening is that its use improves the shafts resistance because it creates compressive residual stress on the surface.

The disadvantages are that:

- the roundness of the shaft is affected
- the surface finish is deteriorated
- the residual stress could relax at high temperatures, therefore re-bending the shaft
- the peening parameters are evaluated based on experiments

The improvements on the shot peening solution would be to:

- Peen the inside of the shaft instead of the outside. This gets ride of the surface finish issue.
- Add a fuzzy controller to help the observer chose the peening parameters.
- Restrict the peening to regions where the temperature is low enough to avoid relaxation of the residual stress.

Chapter VI

Patent for a precision low plasticity burnishing straightening method and equipment for hollow shafts

6.1 Description of the technology

This technology is similar to peen straightening except that it uses the low plasticity burnishing (LPB) process, instead of a peening process, to induce the residual stress which will curve the shaft in a manner to straighten it.

This method uses the low plasticity burnishing process (Figure 6.1) developed and patented by Paul S. Prevey. This process consists in a smooth free-rolling spherical ball that is pressed against and rolled along the surface of the workpiece to be burnished. The ball is hard and has a high modulus of elasticity and high yield strength. To ensure free rolling, the ball is supported in a spherical-socket fluid bearing. The force with which the ball is pressed against the surface is made large enough to deform a surface layer of material into a state of compression. This residual compression will create, in the same manner as for peen straightening, a bending moment bends the shaft to its straightened shape (Figure 6.1).

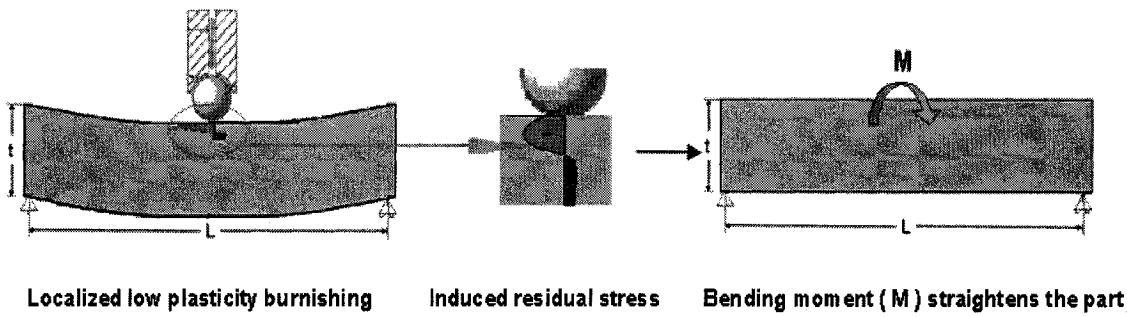

Figure 6.1 Residual stress and bending moment generated by LPB

The advantages of LPB is that by the use of the positioning capability of a computer numerically controlled (CNC) machine tool, the ball could be moved along the surface where the residual stress is required, and by controlling the pressure, the desired permanent deflection could be achieved.

6.2 Design of equipment

A draft design of equipment using LPB to straighten shafts is shown in Figure 6.2.

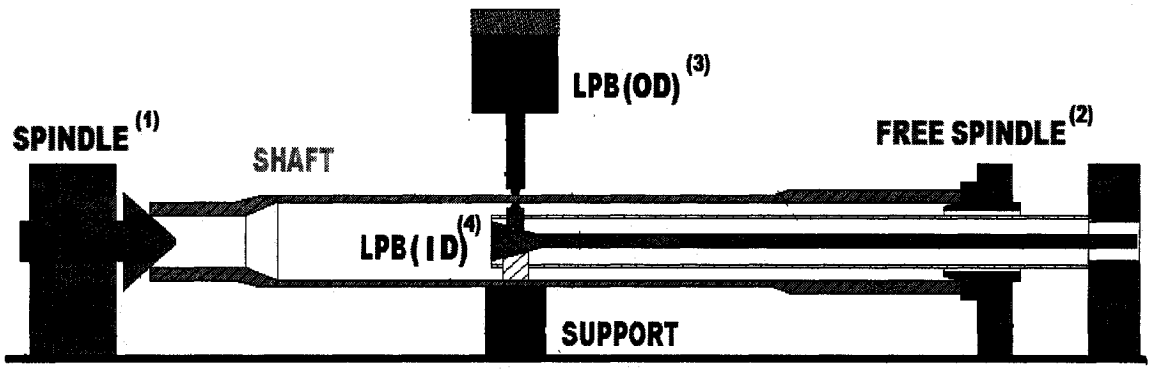

Figure 6.2 LPB Shaft straightening equipment

The shaft is supported by two spindle (1) and (2), spindle (1) is controlled by a motor and spindle (2) is free to follow. A first LPB (3) applies a residual stress on the OD and another LPB (4) applies a residual stress on the ID.

The use of an LPB on the OD and ID permits to generate the residual stress configuration shown in Figure 6.3.

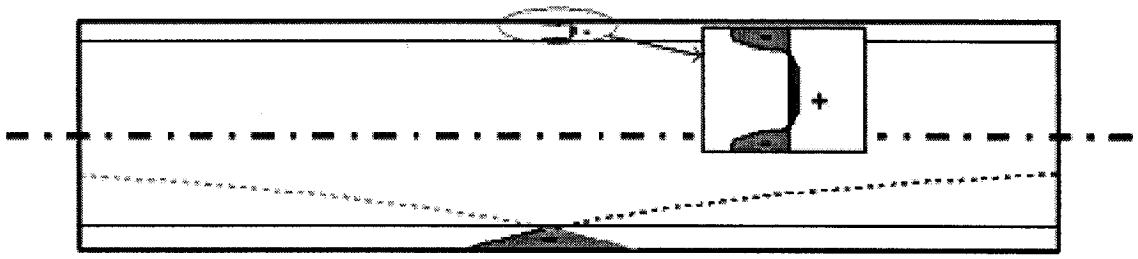

Figure 6.3 Shape of residual stress created when straightening by burnishing

The advantages of LPB are that it;

- produces minimal cold work, giving the generated residual stress a resistance to thermal relaxation at high temperature.

- is controllable in position and amplitude of induced stress,

- gives a good surface finish,

- is easy to control in any desired path across the surface, as in a typical multi-axis CNC.

Conclusion

Two solutions were studied to correct the straightness and concentricity of turbine engine shafts: press straightening and peen straightening. A study on a third solution, straightening by low plasticity burnishing (LPB), was also initiated.

Press straightening

For press straightening the shaft is pressed against supports to create a plastically deformed region, this generates a permanent deflection were the shaft needs to be corrected. A finite element model (FEM) helped understand the phenomenon and design the prototype. Test done on shafts with the prototype were in accordance with the FEM.

Peen straightening

For peen straightening the shaft surface is peened to create a residual compressive stress, this generates a permanent deflection where the shaft need to be corrected

The results from the experiments show that :

(a) It's possible to generate by ultrasound peening enough permanent deflection to straighten turbine engine shafts.

(b) Peening creates undesirable surface roughness and distorts the roundness of the shafts.

(c) The peening process is controllable because a shaft's COG was straightened to a final maximum runout under 0.001" from an initial maximum of 0.007".

Straightening by low plasticity burnishing

The method is similar to peen straightening except that it uses the low plasticity burnishing (LPB) process, instead of a peening process, to induce the residual stress.

This method is in its early design process and is very promising because of all the known advantages of this method of inducing residual stress that where studied and described by Paul S. Prevey (200) [23].

Advantages and Disadvantages

The advantages and disadvantages of each method are described in Table 7.1

Table 6.1 Advantages and disadvantages of the proposed methods

	ADVANTAGES	DISADVANTAGES
P R E S S	-Equipments available on the market could be adapted -Predictable by the FEM -Database is created by using the FEM -Easily automated. -The surface finish isn't affected	- Restricted use on final part because it creates undesirable tensile residual stress on the surface.
P E E N	-Induces compressive residual stress -Benefit effect on material properties	-FEM Model complicated -Bad surface finish -Roundness affected -Stress relaxes at high temperatures - observer based on experiments
L P B	-Produces minimal cold work -Resists to thermal relaxation at high temperature. -Controllable in position and amplitude of induced stress - Good surface finish - controllable in any desired path across the surface	

Proposed process

As shown in Figure 7.1, a combination of press straightening and peen straightening would give the best results. The press straightening could be used only at the beginning of the process because of the induced tensile residual stress and the peen straightening could be used to refine the straightening on the finished shaft.

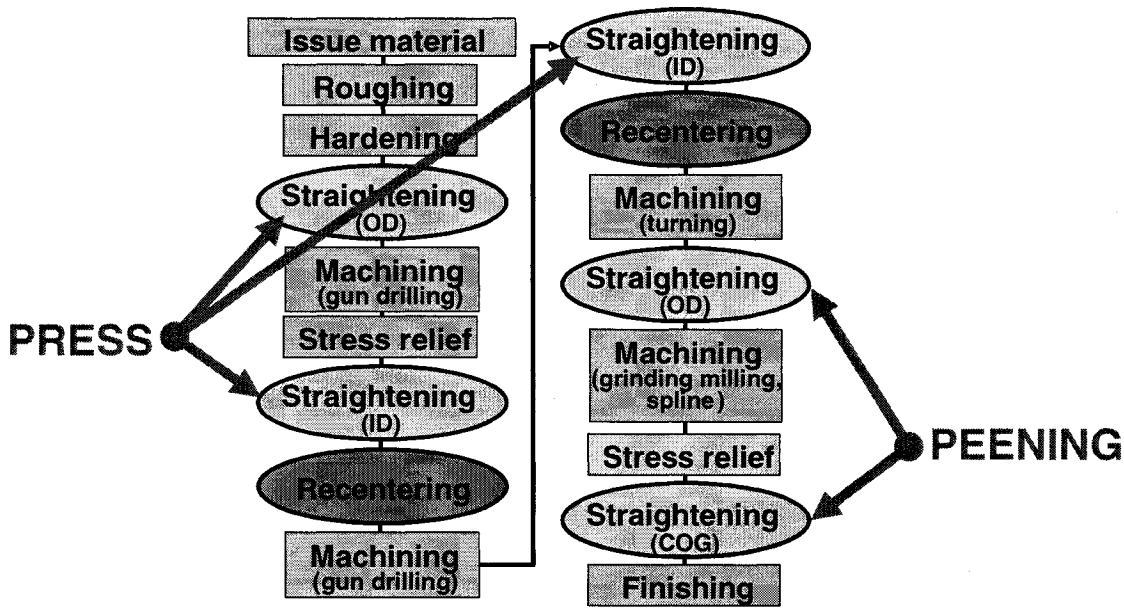

Figure 7.1 Proposed manufacturing process of shafts with straightening

Future developments

Press straightening

The punch should be improved because when the shaft bends only the extremities of the punch stay in contact with the part and therefore generates undesirable stress concentrations at these regions. Possible solutions are:

- using a deformable material between the shaft and the punch
- splitting the punch in many component that could adjust to the bending of the shaft

Straightened shafts were sent for post treatments to evaluate the effect of doing a stress relief and of machining the plastically deformed region. These results will be useful to better understand how to introduce a press straightening equipment in the PWC manufacturing process.

Shot peening

To improvements on the shot peening solution would be to:

- Peen the inside of the shaft instead of the outside. This gets ride of the surface finish issue.
- Adding a fuzzy controller to help the observer choOse the peening parameters.
- Restrict the peening to regions where the temperature is low enough to avoid relaxation of the residual stress.

Straightening by LPB

A prototype as well as a finite element model should be put together. Test similar to the ones on peen and press straightening, should be done. If the experiments show that straightening by low plasticity burnishing gives better results that peen straightening then the proposed process shown in Figure 7.1 should use LPB instead of peen straightening.

Bibliography

1. BENSON, Tom. 2004. Gas turbine propulsion. In. *Glenn Research Center web site.* [On line]. http://www.lerc.nasa.gov/WWW/K-12/airplane/turbine.html (Consulted the 26th July 2004)

2. PRATT & WHITNEY U.S.2004. How engines work. In. *Pratt & Whitney U.S. web site.* [On line]. http://www.pratt-whitney.com/how.htm (Consulted the 26th July 2004)

3. RUDD, P., HETHERINGTON, L. 1989. "Advances in precision hole making". Manufacturing Engineering. 102. 82-89.

4. CHIN, J.-H., HSIEH, C.-T., LEE, L.-W. 1996. "The shaft behavior of BTA deep hole drilling tool". International journal of mechanical science.38:5. 461-482.

5. KARL, D. P., MORISETTE, J., TAAM, W. 1994. "Some Applications of a Multivariate Capability Index in Geometric Dimensioning and Tolerancing". Quality Engineering. 6:4. 649-667.

6. PILLET, M., ROCHON, S., DUCLOS, E. 1998. "SPC -- Generalization of Capability Index Cpm: Case of Unilateral Tolerances". *Quality Engineering.* 10:1. 171-177.

7. MINITAB INC. 2000. *Minitab.* Version 14.12.0. [Logiciel]. Montréal : la Cie. Program File (10 Mo).

8. BENEX CORP.2003. Straightening solutions. In. *Benex Corp's web site.* [On line]. http://www.benexcorp.com/html/solution.html (Consulted the 22nd June 2003)

9. EITEL PRESSES.2003. Eitel Straightening Presses. In. *Eitel Presses web site.* [Online]. http://www.eitelpresses.com/ (Consulted the 2nd July 2003)

10. KIM, S.-C., CHUNG, S.-C. 2002. "Synthesis of the multi-step straightness control system for shaft straightening processes". *Mechatronics.* 12. 139-156.

11. HAN, K., OWEN, D.R.J., PERIC, D. 2002. "Combined finite/discrete element and explicit / implicit simulations of peen forming process". *Engineering Computations.* 19:1. 92–118.

12. HAN, K., OWEN, D.R.J., Crook, A.J.L, PERIC, D. 2000. "A combined finite / discrete element simulation of shot peening processes Part I: studies on 2D interaction laws". *Engineering Computations.* 17:5. 593-619.

13. HAN, K., OWEN, D.R.J., PERIC, D., yu, j. 2000. "A combined finite / discrete element simulation of shot peening processes Part II: 3D interaction laws ". Engineering Computations. 17:6. 680-702.

14. AL-HASSANI, S.T.S., KORMI, K., WEBB, D.C.. 1999. "Numerical simulation of multiple shot impact". International Conference on Shot Peening. 7. 217-227.

15. MEGUID, S.A., SHAGAL, G., STRANART, J.C., Daly, J. 1999. "Three-dimensional dynamic finite element analysis of shot-peening induced residual stresses". Finite Elements in Analysis and Design. 31. 179–191.

16. PHYSIQUE & INDUSTRIE. 2003. Residual stress. In. *physique &industrie web site.*

[On line]. http://www.physiqueindustrie.com/residual_stress.htm
(Consulted the 30th August 2003)

17. WATANABE, Y., HASEGAWA, N. 1996. "Simulation of residual stress distribution on shot peening". International Conference of Shot Peening. 6. 530-535.

18. PREVÉY, Paul S., HORNBACH, Douglas J., 1996. "The effect of prior cold work on tensile residual stress development in nuclear weldments". Journal of Materials Engineering and Performance. 5:1. 51-56.

19. MULLER, E. 1999. "The development of residual stresses at bending specimens under the influence of setting and stress peening". *International Conference on* Shot Peening. 7. 88-95.

20. WICK, A., CHULZE, V., VOHRINGER, O. .1999. "Influence of the shot peening temperature on the relaxation behavior of residual stresses during cyclic bending". International Conference on Shot Peening. 7. 102-109.

21. WANG, C. H., LIU, Q. . 2002. "Predictive models for small fatigue cracks growing through residual stress fields". In. galaxy scientific *'s web site.* [On line]. http://www.galaxyscientific.com/agingaircraft2002/Sessions/2/2A4_Wang_doc.PDF
(Consulted the 13th September 2003)

22. PREVÉY, Paul S., TELESMAN, Jack, GABB, Timothy, KANTZOS, Peter .2000. "Fod resistance and fatigue crack arrest in low plasticity burnished IN718". National Turbine Engine High Cycle Fatigue Conference. 5. 1-12.

23. PREVÉY, Paul S. .2000. "The effect cold work on thermal stability of residual compression in surface enhanced IN718".*ASM Materials Solutions Conference &* Exposition. 20. 1-9.

24. LEVASSEUR, GUy . 2002. The growth factor. In. *Metal finishing news web site.* [On line]. http://www.mfn.li/article.php?id=110 (Consulted the 13th June 2003)

25. LIDA, K. .1984. "Dent and affected layer produced by shot peening". International Conference on Shot Peening. 2. 283-292.

26. KITTEL,S., LINNENAN, W., WÜSTFELD, F., KOPP, R. .1999. "Tight tolerance peen forming with on-line shape control". International Conference on Shot Peening. 7. 301-307.

27. LE GUERNIC, Y., ECKERSLEY, J. .1996. "Peenstress software selects shot peening parameters".International Conference on Shot Peening. 6. 481-492.

28. FUCHS, H. O., HUTCHINSON, E. R. .1958. "Shot peening, designer's guide to the process, it's applications, its effects, and how and where to specify it.". *Machine Design.* 30. 116-125.

29. CHAMPAIGNE, J. . 2001. "Shot peening overview". In. *shotpeener.com's web site.* [On line]. http://www.shotpeener.com/learning/spo.pdf (Consulted the 13th September 2003)

30. HARRRISON, Howard L, MILLS, Blake D. .1951. "Effects of light peening on the yielding of steel".*Welding Journal.* 30:5. 251-253.

31. LEGHORN, George, .1957. "The story of shot peening". *A.S.N.E. Journal* . 653-666.

32. CHAMPAIGNE, J. . 2001. "The little book on shot peening" . In. *shotpeener.com's web site.* [On line]. http://www.shotpeener.com/learning/tlb.pdf (Consulted the 13th September 2003)

33. BAZERGUI, A. 2002, « Résistance des matériaux ». Presses internationales Polytechnique